Arch Computat Methods Eng (2018) 25:397–435
https://doi.org/10.1007/s11831-016-9202-3

ORIGINAL PAPER

Smoothed Finite Element Methods (S-FEM): An Overview and Recent Developments

W. Zeng[1] · **G. R. Liu**[2]

Received: 27 October 2016 / Accepted: 4 November 2016 / Published online: 21 November 2016
© CIMNE, Barcelona, Spain 2016

Abstract The smoothed finite element methods (S-FEM) are a family of methods formulated through carefully designed combinations of the standard FEM and some of the techniques from the meshfree methods. Studies have proven that S-FEM models behave softer than the FEM counterparts using the same mesh structure, often produce more accurate solutions, higher convergence rates, and much less sensitivity to mesh distortion. They work well with triangular or tetrahedral mesh that can be automatically generated, and hence are ideal for automated computations and adaptive analyses. Some S-FEM models can also produce upper bound solution for force driving problems, which is an excellent unique complementary feature to FEM. Because of these attractive properties, S-FEM has been applied to numerous problems in the disciplines of material mechanics, biomechanics, fracture mechanics, plates and shells, dynamics, acoustics, heat transfer and fluid–structure interactions. This paper reviews the developments and applications of the S-FEM in the past ten years. We hope this review can shed light on further theoretical development of S-FEM and more complex practical applications in future.

✉ W. Zeng
zengwe@mail.uc.edu; zeng.work@gmail.com

[1] Thayer School of Engineering, Dartmouth College, Hanover, NH 03755, USA

[2] Department of Aerospace Engineering and Engineering Mechanics, University of Cincinnati, 2851 Woodside Dr., Cincinnati, OH 45221, USA

1 Introduction

1.1 Motivation

As one of the most successful numerical methods, the finite element method (FEM) [1–3] has been widely accepted and used for solving mechanics problems in science and engineering. During the 1950s, Turner [4] proposed and generalized the direct stiffness method (DSM) as an efficient approach for structural design in aerospace industry, which may be regarded as the embryonic stage of the FEM. Since early 1960s, both the theoretical explorations and engineering applications of FEM, have gained substantial momentum. The FEM is now regarded as the one of best methodologies for solving practical problems efficiently in almost all areas of engineering and physical sciences, including structural analysis, mechanical and aeronautical engineering, material science, fluid flow, thermodynamics, biomechanics, soil mechanics, electromagnetism, etc..

The key idea of the FEM was mainly established over 1950s–1970s. Since then it has been found that the standard FEM has some limitations or drawbacks during its intensive applications, including [1–3, 5–7]:

- Poor accuracy when linear triangular and tetrahedral mesh (T-mesh) is used. This is due to its overly-stiff behavior, rooted at the fully compatible Galerkin weak formulation. These elements, however, are the only types of elements which can be generated automatically for solids and structures with complicated geometries.
- FEM demands for high quality mesh of quadrilateral (Q4) and hexahedral (H8) elements, leading to difficulties in automatic mesh generation, especially for geometry of irregular 3D shapes. Mapping procedures

must be used in the FEM to ensure the compatibility along the interfaces of these Q4 and H8 elements. When an element is distorted, the Jacobin matrix becomes bad conditioned, leading to poor solutions or even breakdown during the computation process. For this reason, most commercial FEM software packages need a sophisticated pre-processor. The analysts have to be well-trained to use the FEM software properly and effectively. Failing to meet some of the rules can lead to serious computational consequences.

- Much less accurate solution in stresses on the element interfaces.
- The solution is always a lower bound (for force-driving problems) in the energy norm measure. The lack of upper bound solution, leads to difficulty to quantify the errors in the numerical solutions.
- Volumetric locking phenomenon: The error of the solution increases significantly when the Poisson's ratio approaches to 0.5 (incompressible solids), due to the fully enforced compatibility with assumed displacements, which allows the bulk modulus (that is infinite for incompressible solids) to dominate the energy in the entire system.

These issues are attributed to the nature of the fully compatible displacement approach following the standard variational principle [5, 7], in which all the operations are confined within the elements. Many numerical strategies such as hybrid FEM techniques [8] and meshfree methods [5], have sought to resolve these issues. These remedial methods are able to treat some of these issues. However, most of the critical issues have not been effectively addressed yet. For hybrid FEM, there is no effective formulation for triangular/tetrahedral elements so far, and its operation is still confined within the elements. The meshfree methods operate beyond the elements and have achieved remarkable progresses (a recent review of meshfree methods for solid mechanics problems can be found in [9]). However, the programming efforts and costs of computing in meshfree methods can be much more expensive than the FEM.

1.2 Background of Smoothed Finite Element Methods

To stabilize the nodal integrated Galerkin meshfree methods, Chen et al. [10] proposed a stabilized conforming nodal integration (SCNI) scheme, using the strain smoothing technique. On the other front in the development of FE techniques, Liu et al. [11–36] have applied the strain smoothing technique to the finite element settings, and proposed a class of smoothed finite element methods (S-FEMs or S-FEM), through a number of creative fashions to construct the smoothing domains. In the past few years, the S-FEM has been proven to be a valuable combination of meshfree techniques with the standard FEM, which effectively addresses almost all the above mentioned limitations of FEM, through the use of some meshfree concepts and techniques. A generalized gradient smoothing (GGS) technique [17] was further proposed as an extension of the strain smoothing technique to discontinuous functions. The GGS allows the utilization of a class of nodal shape functions created by the point interpolation method (PIM [6]) for creating novel numerical models. Based on the GGS, Liu established the G space theory and the so-called weakened weak (W^2) formulation for various types of problems [37–45]. The W^2 formulation offers fresh possibilities for developing a wide new class of compatible and incompatible (uniformly) "soft" models with attractive properties such as conformability, volumetric locking free, superconvergence, upper or lower bound, and ultra-accuracy. Typical W^2 models are the recent smoothed point interpolation methods (S-PIMs or S-PIM) that can use both polynomial and radial basis functions (RBFs) to construct nodal shape functions using irregularly distributed nodes. Essentially, the S-FEMs is a simplified linear version of S-PIMs with most of their properties. The general idea of the S-FEM is to utilize a standard FE mesh (often but not limited to the T-mesh) to improve the performance of FEM without increasing the degrees of freedoms and much of the computational efforts [38, 41, 45–49]. It modifies the compatible strain field through smoothing the derivatives of the field functions by creating various types of smoothing domains on top of the element mesh. The earliest type of S-FEM models uses smoothing domains that are located within the quadrilateral elements, which is now termed as the cell-based FEM or CS-FEM [11–14, 50]. Only the shape function values (not the gradients or derivatives) at points on the boundaries of the smoothing cells are involved in the computation of the stiffness matrices in CS-FEM. This simplifies the computation, in which the mapping procedure in standard FEM is not required, and hence the Jacobian matrices are no longer involved. This also allows the use of elements of poor quality and enables severe mesh distortion during large deformation. The smoothing domains can also be constructed crossing element interface and over elements around a node, an edge or a face, which brings in the information from the adjacent elements, for desirable "smoothing effects". Typical S-FEM models include the node-based S-FEM (NS-FEM) for both 2D and 3D problems [20, 40, 51], edge-based S-FEM (ES-FEM) for 2D and 3D [21–24, 52], and face-based S-FEM (FS-FEM) for 3D [27, 28]. In addition, hybrid types of smoothing domains can also be designed [16, 29, 32–35, 53–61], such as the αFEM [18, 25, 26, 53, 54] and βFEM [36].

Many studies have been conducted on the numerical aspects of S-FEMs in stability, convergence, accuracy, and efficiency. Each of these different S-FEM models has been found with different features or properties, and has been applied to solve a wide class of practical mechanics problems for desirable solutions, such as elastic–plastic analysis [23, 62], visco-elastoplastic analysis [24, 28, 51], contact analysis [55, 56, 63, 64], crystal plasticity modeling [36, 65], plates and shells [19, 59, 66–104], composites [79, 82, 83, 85–88, 90, 91, 95, 98, 102, 105–115], limit and shakedown analysis [116–120], fatigue and fracture mechanics [31, 32, 34, 121–141], stochastic analysis [142, 143], vibration and dynamic analysis [14, 52, 53, 68, 76–78, 80–83, 88, 89, 93, 99, 100, 103, 105, 144–153], structural acoustics [154–169], impact problems [170], adaptive analysis [56, 120, 134, 171, 172], heat transfer and thermo-mechanical problems [173–185], piezoelectricity and photonic devices [186–193], fluid–structure interaction [30, 194–203], hyperelasticity and applications in biomechanics [35, 61, 204–210]. Generally, some important features and properties of S-FEM found so far include:

- S-FEM models can be created using any given FEM mesh including the T-mesh, without introducing additional degrees of freedom to the system.
- The existed S-FEM models utilize the simplicial linear PIM shape functions for assuming the displacement field without isoparametric mapping, and the stiffness matrix can be computed using only the shape functions themselves (not the derivatives).
- The stability of a S-FEM model for static problems is ensured by proper smoothing domain creation and by satisfying the condition of a minimum number of linearly independent smoothing domains [45].
- Compared with the standard FEM, S-FEMs are more robust in dealing with mesh distortion and with extremely large deformation [35–37], because no mapping procedure is performed.
- Because of the "softening effect", S-FEM models alleviate the overestimation of stiffness in the compatible FEM [42–44, 211]. As such, they often show higher accuracy and higher convergence rates in displacement, especially in stress solutions [13, 42, 49].
- S-FEM allows the use of elements of general shape, such as n-sided polygonal elements and even brick elements [15].
- A smoothing domain in S-FEM models may involve parts of adjacent elements. It has more supporting nodes for the smoothing domain than the nodes of an element. Hence, the bandwidth of the stiffness matrix of a S-FEM model is larger than those in the FEM counterpart, which may lead to higher computational cost for the same mesh structure. However, for a given computational cost, the S-FEM models can be more accurate and achieve higher efficiency [20, 22, 27].
- Some S-FEM models show unique properties, such as upper bound in strain energy, and free from volumetric locking, which is suitable for incompressible materials.
- As a class of displacement-like models similar to FEM, many existing algorithms of FEM are compatible or can be easily modified and applied to S-FEM [13].

In this work, the S-FEM will be comprehensively reviewed for the first time in both methodology and applications. The rest of the paper is organized as follows: In Sect. 2, the formulations of S-FEM are briefly introduced; Sect. 3 covers the classification of main S-FEM models and their major properties; several important aspects of the fundamental theories are discussed and summarized in Sect. 4; in Sect. 5, we examine the major applications of S-FEM models to various problems. The final section provides a summary and some concluding remarks.

2 S-FEM Formulations

2.1 Basics of Gradient Smoothing Operation

For S-FEM models, the numerical implementations related to the evaluation of stiffness matrix are based on smoothing domains (or cells for CS-FEM), which can be performed within elements but more often beyond the elements. The smoothed strains can be computed via curves for 2D (or surfaces for 3D) integrations along the boundary of the smoothing domains, using the assumed displacement values and the normal components on the boundary. The procedure is as follows.

Consider a solid mechanics problem whose problem domain is divided into a set of elements as in the standard FEM. On top of the element mesh, the domain is further divided into a set of non-overlapping and non-gap representative smoothing domains $\Omega_k^s (k = 1, 2, \ldots, N_s)$ with boundary Γ_k^s for each, such that $\Omega \approx \bigcup_{k=1}^{N_s} \Omega_k^s$ and $\Omega_i^s \cap \Omega_j^s = \emptyset$ for $i \neq j$, in which N_s is the number of all the smoothing domains. The smoothed strain at a point $\mathbf{x}_C$ in a smoothed domain can be computed by

$$\begin{aligned} \bar{\boldsymbol{\varepsilon}}_k(\mathbf{x}_C) &= \int_{\Omega^h} \boldsymbol{\varepsilon}^h(\mathbf{x}) \Phi_k(\mathbf{x} - \mathbf{x}_C) \mathrm{d}\Omega \\ &= \int_{\Omega^h} \underbrace{\mathbf{L}_d \mathbf{u}^h(\mathbf{x})}_{\boldsymbol{\varepsilon}^h(\mathbf{x})} \Phi_k(\mathbf{x} - \mathbf{x}_C) \mathrm{d}\Omega \end{aligned} \tag{1}$$

where $\boldsymbol{\varepsilon}^h(\mathbf{x})$ is the compatible strain that is obtained using the assumed strain by differentiation, $\mathbf{L}_d$ is a matrix of

differential operators with following format for 2D and 3D cases respectively

$$\mathbf{L}_d = \begin{bmatrix} \partial/\partial x & 0 \\ 0 & \partial/\partial y \\ \partial/\partial y & \partial/\partial x \end{bmatrix} \quad \text{and}$$
$$\mathbf{L}_d = \begin{bmatrix} \partial/\partial x & 0 & 0 \\ 0 & \partial/\partial y & 0 \\ 0 & 0 & \partial/\partial z \\ \partial/\partial y & \partial/\partial x & 0 \\ 0 & \partial/\partial z & \partial/\partial y \\ \partial/\partial z & 0 & \partial/\partial x \end{bmatrix} \tag{2}$$

In Eq. (1), $\Phi_k(\mathbf{x}-\mathbf{x}_C)$ is an assumed smoothing function which satisfies at least the positivity and unity properties:

$$\Phi_k(\mathbf{x}-\mathbf{x}_C) \geq 0 \quad \text{and} \quad \int_{\Omega_k^s} \Phi_k(\mathbf{x}-\mathbf{x}_C)\mathrm{d}\Omega = 1 \tag{3}$$

The Heaviside-type piecewise constant function is the mostly popular adopted smoothing function, which can be defined as

$$\Phi_k(\mathbf{x}-\mathbf{x}_C) = \begin{cases} 1/V_k^s \text{ or } 1/A_k^s, & \mathbf{x} \in \Omega_k^s \\ 0, & \mathbf{x} \notin \Omega_k^s \end{cases} \tag{4}$$

where $V_k^s = \int_{\Omega_k^s} \mathrm{d}\Omega$ is the volume (for 3D) or $A_k^s = \int_{\Omega_k^s} \mathrm{d}\Omega$ is the area (for 2D) of the smoothing domain Ω_k^s. If we substituting Eq. (4) into Eq. (1) and introduce the divergence theorem, it then yields the following form of smoothed strains

$$\underbrace{\bar{\boldsymbol{\varepsilon}}_k}_{\text{constant in } \Omega_k^s} = \frac{1}{V_k^s}\int_{\Omega_k^s} \mathbf{L}_d\mathbf{u}^h(\mathbf{x})\mathrm{d}\Omega = \frac{1}{V_k^s}\int_{\Gamma_k^s} \mathbf{n}_k^s(\mathbf{x})\mathbf{u}^h(\mathbf{x})\mathrm{d}\Gamma \tag{5}$$

where V_k^s can be replaced by A_k^s for 2D smoothing domains, $\mathbf{n}_k^s(\mathbf{x})$ is a matrix containing the components of the unit outward normal on the boundary Γ_k^s, defined as

$$\mathbf{n}_k^s(\mathbf{x}) = \begin{bmatrix} n_{kx}^s & 0 \\ 0 & n_{ky}^s \\ n_{ky}^s & n_{kx}^s \end{bmatrix} \quad \text{for 2D,} \quad \text{or}$$
$$\mathbf{n}_k^s(\mathbf{x}) = \begin{bmatrix} n_{kx}^s & 0 & 0 \\ 0 & n_{ky}^s & 0 \\ 0 & 0 & n_{kz}^s \\ n_{ky}^s & n_{kx}^s & 0 \\ 0 & n_{kz}^s & n_{ky}^s \\ n_{kz}^s & 0 & n_{kx}^s \end{bmatrix} \quad \text{for 3D} \tag{6}$$

where n_{kx}^s and n_{ky}^s and n_{kz}^s represent the unit outward normal components on Γ_k^s projected on, respectively, the x-, y-, and y-axis. It is seen from the LHS of Eq. (5) that the strain is now computed using integration rather than differentiation, which is a weak formulation at the stage of strain evaluation.

Note also that when the smoothing domain shrinks to zero, while keeping the center at $\mathbf{x}_C$, we have

$$\bar{\boldsymbol{\varepsilon}}_k = \lim_{\Omega_k^s \to 0} \frac{1}{V_k^s}\int_{\Omega_k^s} \boldsymbol{\varepsilon}^h(\mathbf{x})\mathrm{d}\Omega = \boldsymbol{\varepsilon}^h(\mathbf{x}_C) \tag{7}$$

which means that the smoothed strain becomes the compatible strain at the center of the smoothing domain.

2.2 Techniques for Strain Smoothing

In Eq. (5), we need the value of the assumed displacements $\mathbf{u}^h(\mathbf{x})$. It can be approximated through the similar manner as in the FEM, by using the nodal shape functions, for which we use a finite element mesh. However, one does not have to generate the shape function in S-FEM. The art of S-FEM starts with smoothing domain creation, which works as follows.

It first creates the smoothing domains based on the elements in a background mesh. For example, in the CS-FEM, we may use quadrilateral elements with 4 nodes (Q4). In this case, typical smoothing domains can be created as shown in Fig. 1, where one Q4 elements can be divided into 1, 2, 3, 4, 8, or 16 smoothing domains. Each of the smoothing domains has a quadrilateral shape bounded by four boundary segments, and it is supported by the same Q4 element with 4 nodes.

When an FEM mesh of triangular elements with 3 nodes (T3 or Tr3) are used, one may create smoothing domains based on edges, leading to an ES-FEM-T3 (or ES-FEM-Tr3) model, as shown in Fig. 2a for 2D problems. In this case a smoothing domain in the interior of the domain is

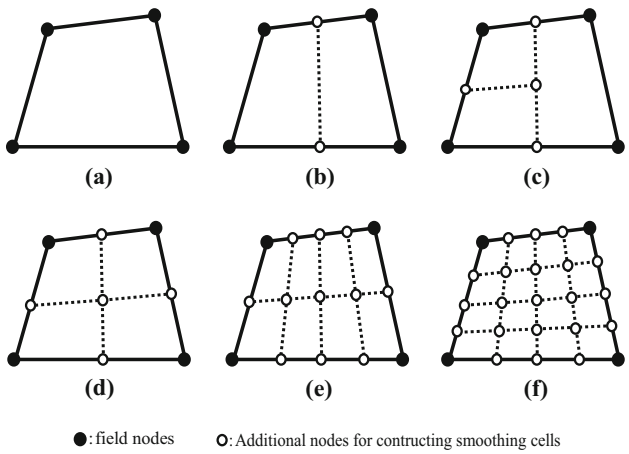

Fig. 1 Schematic illustration of cell-based smoothing domains, e.g., division of a quadrilateral element into smoothing cells (SCs) by connecting the mid-segment-points of opposite segments of smoothing domains [36]: **a** $n_{SC} = 1$, **b** $n_{SC} = 2$, **c** $n_{SC} = 3$, **d** $n_{SC} = 4$, **e** $n_{SC} = 8$, and **f** $n_{SC} = 16$ (from [142])

supported by two elements and bounded by four boundary segments to shape a quadrilateral. Each of the segments connects a node to the center of the involved T3 element. The smoothing domains on boundary edges are triangular and bounded by three edge segments (one of which is the boundary edge), and it is supported only by one element.

Alternatively, one may create smoothing domains based on nodes, as shown in Fig. 3a. In this case, a smoothing domain is generally a polygon bounded by multiple straight boundary segments, each of which connects the midpoint of an edge to a center of the T3 element. For the shaded node-based smoothing domain, it is supported by five elements and is bounded by 10 segments of straight lines.

The similar approach can be extended to 3D problems, where the smoothing domains will be constructed upon 3D mesh with boundary surfaces. For example, if the linear tetrahedral elements with 4 nodes (T4 or Te4) are adopted, the smoothing domains can be created based upon the

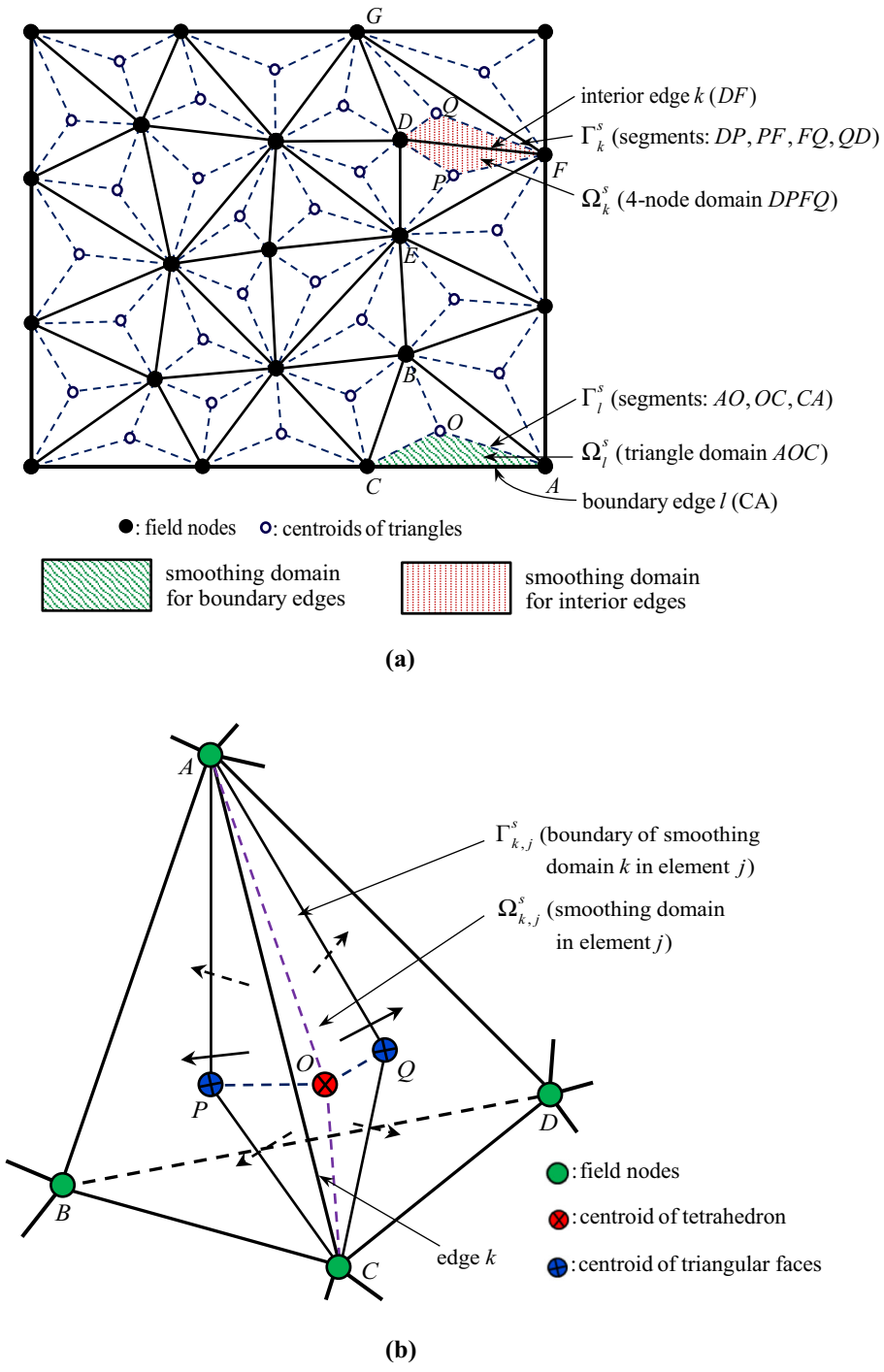

Fig. 2 Schematic illustration of edge-based smoothing domains based on triangular or tetrahedral elements: **a** the smoothing domain Ω_l^s is a triangle AOC for a boundary edge l and the smoothing domain Ω_k^s is the four-sided convex polygon $DPFQ$ for an interior edge k and **b** the sub-smoothing domain $\Omega_{k,j}^s$ for edge k in the element j is a double tetrahedron $ACPOQ$

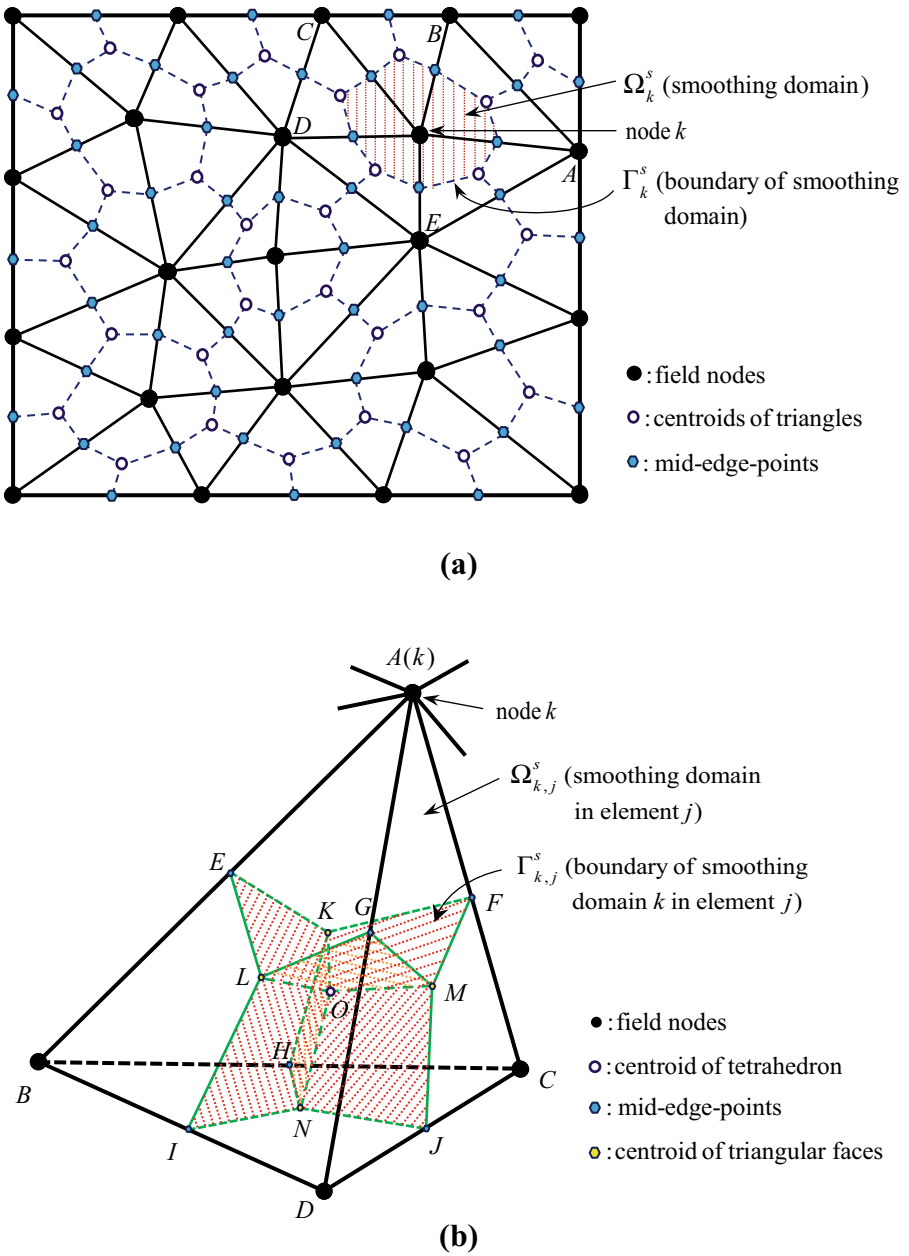

Fig. 3 Schematic illustration of node-based smoothing domains based on triangular or tetrahedral elements: **a** the smoothing domain Ω_k^s for node k is a polygon with $2n_k^e$ sides (where n_k^e is the number of elements surrounding node k) and **b** the sub-smoothing domain $\Omega_{k,j}^s$ for node k in the element j is a polyhedron *AELGMFKO*

edges of elements and formulated as an ES-FEM-T4 (or ES-FEM-Te4) model, as shown in Fig. 2b. Similarly, we can create NS-FEM-T4 by creating smoothing domains based on the nodes, as shown in Fig. 3b. One may also create smoothing domains associated with the faces of the T4 element, known as the FS-FEM-T4 model. As shown in Fig. 4, the face-based smoothing domain Ω_k^s is created by connecting three nodes of the face (A, B, C) to the centers of the two neighboring elements (P, Q). Several representative smoothing domains are summarized in Table 1. More detailed procedure for constructing the smoothing domains can be found in [45].

Once the smoothing domains are created, we know exactly the relationship between the smoothing domain boundaries and their supporting elements and nodes. The values of shape functions of all the nodes at any point on a segments can be easily calculated via simple point interpolation method (PIM) [6, 45]. For example, the values of the four nodal shape functions at the 12 Gauss points on the boundary of four smoothing domains of a Q4 element (shown in Fig. 5a) can be computed by simple point interpolation, as listed in the Table 2. Similar point interpolations can be easily implemented for the six-sided polygonal element (see Fig. 5b), and the results are listed

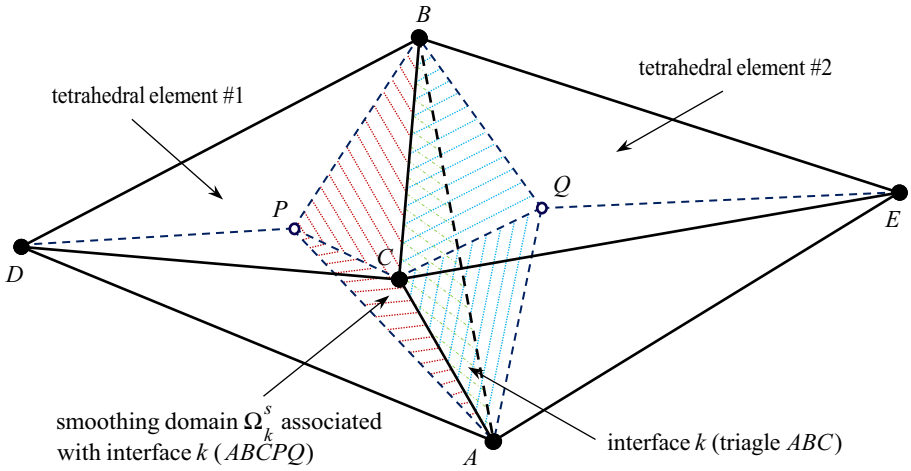

Fig. 4 Schematic illustration of face-based smoothing domains based on tetrahedral elements: a face-based smoothing domain Ω_k^s created from two adjacent tetrahedral elements based upon their interface k

Table 1 Typical existing types of smoothing domains (SD's)

Type[a]	Method for creation and number of SD's (N_s)	S-FEM models	Dimension of problem
Cell-based SD (CSD)	SD's or smoothing cells (SC's) are divided from and located within the elements ($N_s = \sum_{i=1}^{N_e} n_{sc}^i$, $n_{sc}^i = 1, 2, 3, 4, \ldots$)	CS-FEM *n*CS-FEM	1D, 2D, 3D
Edge-based SD (ESD)	SD's are created based on edges by connecting portions of the surrounding elements sharing the associated edge ($N_s = N_{edge}$)	ES-FEM	2D, 3D
Node-based SD (NSD)	SD's are created based on nodes by connecting portions of the surrounding elements sharing the associated node ($N_s = N_{node}$)	NS-FEM	1D, 2D, 3D
Face-based SD (FSD)	SD's are created based on faces by connecting portions of the surrounding elements sharing the associated face ($N_s = N_{face}$)	FS-FEM	3D

[a] There are S-FEM models that use combinations of different types of SDs, such as αFEM, and βFEM

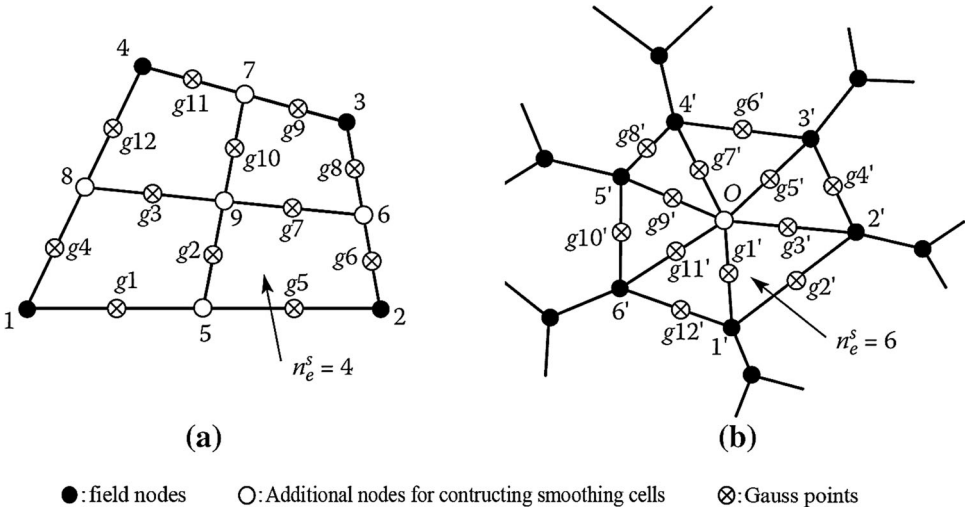

Fig. 5 Positions of Gauss points at mid-segment-points on segments of smoothing domains. **a** Four quadrilateral smoothing domains in a Q4 element and **b** six triangular smoothing domains in a six-sided polygonal element (from [45])

in Table 3. The point here is that it is not required to explicitly generate the shape functions.

Now, we can rewrite the assumed displacement $\mathbf{u}^h(\mathbf{x})$ in Eq. (5) using the values of shape functions $\mathbf{N}_I(\mathbf{x})$ and the nodal displacements $\mathbf{d}_I$ for all the elements and their nodes that support the smoothing domain:

$$\bar{\boldsymbol{\varepsilon}}_k = \sum_{I \in S_k^n} \bar{\mathbf{B}}_{Ik} \mathbf{d}_{Ik} \tag{8}$$

Table 2 Values of 4 nodal shape functions at different points within a Q4 element [45] (shown in Fig. 5a)

Point	N_1	N_2	N_3	N_4	Description
1	1.0	0	0	0	Field node
2	0	1.0	0	0	Field node
3	0	0	1.0	0	Field node
4	0	0	0	1.0	Field node
5	1/2	1/2	0	0	Side midpoint
6	0	1/2	1/2	0	Side midpoint
7	0	0	1/2	1/2	Side midpoint
8	1/2	0	0	1/2	Side midpoint
9	1/4	1/4	1/4	1/4	Intersection of two bi-medians
$g1$	3/4	1/4	0	0	Gauss point (mid-segment point of $\Gamma^s_{k,p}$)
$g2$	3/8	3/8	1/8	1/8	Gauss point (mid-segment point of $\Gamma^s_{k,p}$)
$g3$	3/8	1/8	1/8	3/8	Gauss point (mid-segment point of $\Gamma^s_{k,p}$)
$g4$	3/4	0	0	1/4	Gauss point (mid-segment point of $\Gamma^s_{k,p}$)
$g5$	1/4	3/4	0	0	Gauss point (mid-segment point of $\Gamma^s_{k,p}$)
$g6$	0	3/4	1/4	0	Gauss point (mid-segment point of $\Gamma^s_{k,p}$)
$g7$	1/8	3/8	3/8	1/8	Gauss point (Mid-segment point of $\Gamma^s_{k,p}$)
$g8$	0	1/4	3/4	0	Gauss point (mid-segment point of $\Gamma^s_{k,p}$)
$g9$	0	0	3/4	1/4	Gauss point (mid-segment point of $\Gamma^s_{k,p}$)
$g10$	1/8	1/8	3/8	3/8	Gauss point (mid-segment point of $\Gamma^s_{k,p}$)
$g11$	0	0	1/4	3/4	Gauss point (mid-segment point of $\Gamma^s_{k,p}$)
$g12$	1/4	0	0	3/4	Gauss point (mid-segment point of $\Gamma^s_{k,p}$)

Table 3 Values of six nodal shape functions at different points within a 6-sided polygonal element [45] (shown in Fig. 5b)

Point	$N_{1'}$	$N_{2'}$	$N_{3'}$	$N_{4'}$	$N_{5'}$	$N_{6'}$	Description
$1'$	1.0	0	0	0	0	0	Field node
$2'$	0	1.0	0	0	0	0	Field node
$3'$	0	0	1.0	0	0	0	Field node
$4'$	0	0	0	1.0	0	0	Field node
$5'$	0	0	0	0	1.0	0	Field node
$6'$	0	0	0	0	0	1.0	Field node
O	1/6	1/6	1/6	1/6	1/6	1/6	Centroid point
$g1'$	7/12	1/12	1/12	1/12	1/12	1/12	Gauss point (mid-segment point of $\Gamma^s_{k,p}$)
$g2'$	1/2	1/2	0	0	0	0	Gauss point (mid-segment point of $\Gamma^s_{k,p}$)
$g3'$	1/12	7/12	1/12	1/12	1/12	1/12	Gauss point (mid-segment point of $\Gamma^s_{k,p}$)
$g4'$	0	1/2	1/2	0	0	0	Gauss point (mid-segment point of $\Gamma^s_{k,p}$)
$g5'$	1/12	1/12	7/12	1/12	1/12	1/12	Gauss point (mid-segment point of $\Gamma^s_{k,p}$)
$g6'$	0	0	1/2	1/2	0	0	Gauss point (mid-segment point of $\Gamma^s_{k,p}$)
$g7'$	1/12	1/12	1/12	7/12	1/12	1/12	Gauss point (mid-segment point of $\Gamma^s_{k,p}$)
$g8'$	0	0	0	1/2	1/2	0	Gauss point (mid-segment point of $\Gamma^s_{k,p}$)
$g9'$	1/12	1/12	1/12	1/12	7/12	1/12	Gauss point (mid-segment point of $\Gamma^s_{k,p}$)
$g10'$	0	0	0	0	1/2	1/2	Gauss point (mid-segment point of $\Gamma^s_{k,p}$)
$g11'$	1/12	1/12	1/12	1/12	1/12	7/12	Gauss point (mid-segment point of $\Gamma^s_{k,p}$)
$g12'$	1/2	0	0	0	0	1/2	Gauss point (mid-segment point of $\Gamma^s_{k,p}$)

where S_k^n is the set of supporting nodes of the elements supporting Ω_k^s, and the smoothed strain–displacement matrix can be computed by

$$\bar{\mathbf{B}}_{Ik} = \frac{1}{A_k^s}\int_{\Gamma_k^s} \mathbf{n}_k^s(\mathbf{x})\mathbf{N}_I(\mathbf{x})\mathrm{d}\Gamma = \begin{bmatrix} \bar{b}_{Ikx} & 0 & \bar{b}_{Iky} \\ 0 & \bar{b}_{Iky} & \bar{b}_{Ikx} \end{bmatrix}^T \tag{9}$$

where

$$\bar{b}_{Ikh} = \frac{1}{A_k^s}\int_{\Gamma_k^s} N_I(\mathbf{x}) n_{kh}^s(\mathbf{x})\mathrm{d}\Gamma, \quad h = x, y \tag{10}$$

Consider the ES-FEM for 2D problem as an example. In this case, the (shaded) edge-based smoothing domain *DPFQ* shown in Fig. 2 is supported by 4 nodes *D*, *E*, *F*, *G* of two elements *DEF* and *DFG*. The smoothed strain–displacement matrix for the whole smoothing domain Ω_k^s can be written as

$$\bar{\mathbf{B}}_k = \begin{bmatrix} \bar{\mathbf{B}}_{Dk} & \bar{\mathbf{B}}_{Ek} & \bar{\mathbf{B}}_{Fk} & \bar{\mathbf{B}}_{Gk} \end{bmatrix} \tag{11}$$

It is noted that in Eq. (10) the derivatives of the shape functions N_I are not required. If we use the 1-point Gauss quadrature for the numerical integration along each segment $\Gamma_{k,t}^s$ of the boundary Γ_k^s, the Eq. (10) becomes

$$\bar{b}_{Ikh} = \frac{1}{A_k^s}\sum_{t=1}^{n_\Gamma^s} N_I\left(\mathbf{x}_t^{GP}\right) n_{kh,t} l_{k,t}, \quad h = x, y \tag{12}$$

where n_Γ^s is the total number of the boundary segments $\Gamma_{k,t}^s \subset \Gamma_k^s$, with $n_\Gamma^s = 3$ for smoothing domain of a boundary edge, and $n_\Gamma^s = 4$ for smoothing domain of an interior edge (Fig. 2a). For this ES-FEM-T3 model, only one Gauss point is needed for the numerical integration along any of the boundary segments, because the shape function changes linearly along it and the unit normal vector components is a constant on a segment.

For T3 elements, the area of a smoothing domain can be calculated using the areas of the elements supporting the smoothing domain:

$$A_k^s = \int_{\Omega_k^s} d\Omega = \frac{1}{3}\sum_{j=1}^{n_k^e} A_j^e \tag{13}$$

where n_k^e is the number of elements attached to the edge and A_j^e is the area of a supporting element.

The above equations show the standard way to compute the smoothed strain–displacement matrix $\bar{\mathbf{B}}_{Ik}$ for a node *I* of a smoothing domain *k*, which can be coded without much difficulty. An alternative way to compute $\bar{\mathbf{B}}_{Ik}$ is to use directly the $\mathbf{B}_j^e$ obtained by the *j*th element associated with the edge *k*. The FE $\mathbf{B}_j^e(\mathbf{x})$ for the node *I* in an element is given by

$$\mathbf{B}_{Ie}(\mathbf{x}) = \mathbf{L}_d \mathbf{N}_I(\mathbf{x}) \tag{14}$$

where the entries of matrix $\mathbf{B}_j^e$ are constants for linear triangle elements. The equation can be derived using the divergence theorem reversely to convert the line integral along Γ_k^s to an area integration over Ω_k^s:

$$\begin{aligned} \bar{\mathbf{B}}_{Ik} &= \frac{1}{A_k^s}\int_{\Gamma_k^s} \mathbf{n}_k^s(\mathbf{x})\mathbf{N}_I(\mathbf{x})\mathrm{d}\Gamma = \frac{1}{A_k^s}\int_{\Omega_k^s} \mathbf{L}_d \mathbf{N}_I(\mathbf{x})\mathrm{d}\Omega \\ &= \frac{1}{A_k^s}\int_{\Omega_k^s} \mathbf{B}_I(\mathbf{x})\mathrm{d}\Omega \end{aligned} \tag{15}$$

It is apparently from the above equation that the smoothed **B** matrix is the weighted average of the standard compatible **B** matrices in the smoothing domain. For the ES-FEM-T3 model, as an example, we have:

$$\bar{\mathbf{B}}_I = \frac{1}{A_k^s}\sum_{j=1}^{n_k^e}\left[\frac{1}{3}A_j^e \mathbf{B}_j^e\right] \tag{16}$$

where $\mathbf{B}_j^e = \sum_{I\in S_j^e} \mathbf{B}_I$, and the summation stands for assembly or more precisely "node-matched summation" at the strain–displacement matrix level for all the elements in the supporting set S_j^e. For example in Fig. 2a, elements *DEF* and *DFG* support the red shaded smoothing domain Ω_k^s. However, element *DFG* does not contribute to node *E*, and hence when $\bar{\mathbf{B}}_E$ is computed, it has only 1/3 contribution of $\mathbf{B}_E$ for the matched node *E* from element *DEF*. Likewise, when $\bar{\mathbf{B}}_G$ is computed, it has only 1/3 contribution of $\mathbf{B}_G$ from element *DFG*. When $\bar{\mathbf{B}}_D$ or $\bar{\mathbf{B}}_F$ is computed, however, it has a sum contribution (of $\mathbf{B}_D$ or $\mathbf{B}_F$) from both elements, as they all have matched nodes *D* and *F*. The smoothed strain matrix for the whole smoothing domain Ω_k^s can be written as

$$\bar{\mathbf{B}}_k = \left[\underbrace{\frac{1}{3}\mathbf{B}_{De\_DEF} + \frac{1}{3}\mathbf{B}_{De\_DFG}}_{\bar{\mathbf{B}}_D} \quad \underbrace{\frac{1}{3}\mathbf{B}_{Ee\_DEF}}_{\bar{\mathbf{B}}_E} \quad \underbrace{\frac{1}{3}\mathbf{B}_{Fe\_DEF} + \frac{1}{3}\mathbf{B}_{Fe\_DFG}}_{\bar{\mathbf{B}}_F} \quad \underbrace{\frac{1}{3}\mathbf{B}_{Ge\_DFG}}_{\bar{\mathbf{B}}_G}\right] \tag{17}$$

It has to be noted that Eqs. (11) and (17) are identical, if T3 elements (linear PIM) are used. For other strain smoothing techniques, they follow a quite similar fashion of smoothing

operation as illustrated above to evaluate the smoothed strain–displacement matrix $\overline{\mathbf{B}}_I$.

Once the smoothed **B** matrices are obtained, following a similar assembling procedure of the FEM, the components of the local stiffness matrices of smoothing domains can be assembled to a global stiffness matrix for generating a global equation system. The smoothed global stiffness matrix $\bar{\mathbf{K}}$ can be assembled from the contributions of stiffness from all the individual smoothing domains, in which its entries reads

$$\begin{aligned}\bar{\mathbf{K}}_{IJ} &= \int_{\Omega} \bar{\mathbf{B}}_I^T \mathbf{c} \bar{\mathbf{B}}_J \mathrm{d}\Omega = \sum_{k=1}^{N_s} \left[\int_{\Omega_k^s} \bar{\mathbf{B}}_{Ik}^T \mathbf{c} \bar{\mathbf{B}}_{Jk} \mathrm{d}\Omega \right] \\ &= \sum_{k=1}^{N_s} \underbrace{\bar{\mathbf{B}}_{Ik}^T \mathbf{c} \bar{\mathbf{B}}_{Jk} A_k^s}_{\mathbf{K}_{IJk}} \end{aligned} \tag{18}$$

where the summation is a node-matched summation at the stiffness matrix level. The derivation of the above equation is essentially the same as that performed in the FEM. The difference is that FEM is element-based, while the S-FEM is now smoothing domain based. When I and J are "far" apart, $\bar{\mathbf{K}}_{IJ}$ will vanish, and hence the global stiffness matrix $\bar{\mathbf{K}}$ is a sparse, and banded when the numbering of the nodes are proper. It is a symmetric positive definite (SPD) matrix, after (sufficient) essential boundary conditions are imposed [3, 45]. The bandwidth (assuming optimized node numbering) of $\bar{\mathbf{K}}$ depends on the types of S-FEM model. For CS-FEM, it is the same as the FEM. For ES-FEM-T3, the bandwidth of $\bar{\mathbf{K}}$ is about 30% larger than the FEM counterpart and it is about double for NS-FEM-T3.

3 Major S-FEM Models and Their Properties

In the past decade, considerable effort has been devoted to developing these smoothing techniques based FEM, a broad classification of these S-FEM models so far can be based upon the element types used in the models:

- Quadrilateral or hexahedral elements (e.g., Q4 or H8) based models: a typical cell-based S-FEM model constructed upon Q4 or H8 mesh.
- Triangular or tetrahedral elements (e.g., T3 or T4) based models: this type of S-FEM models usually conduct the smoothing operation beyond elements and bring in the information from the neighboring elements, including the node-based and edge-based S-FEM models. It is important to note that simplex elements (triangles or tetrahedrons) have much flexibility to create high quality mesh and they are the only elements to automatically generate mesh for objects with arbitrary shapes, though they are not recommended in the standard FEM due to undesired features.
- n-sided polygonal or polyhedral elements based models: The problem domain can be discretized by a set of polygons or polyhedrons with an arbitrary number of sides. The cell-based smoothing technique is employed within this type of elements, known as nCS-FEM models [15, 150, 212–214]. However, the smoothing domain can also be constructed upon edges [215] or nodes [20] to obtain different models (e.g., nES-FEM).

Based on the types of smoothing domains, the S-FEM models are generally classified into: Cell-based S-FEM (CS-FEM), Node-based S-FEM (NS-FEM), Edge-based S-FEM (ES-FEM), Face-based S-FEM (FS-FEM), Selective S-FEM, alpha FEM (αFEM), beta FEM (βFEM), and other variations. This classification is more convenient for discussions of properties of the S-FEM models, since the properties are largely determined by the smoothing effect that is mainly affected by the smoothing domain type(s).

3.1 Cell-Based S-FEM (CS-FEM)

As the earliest S-FEM model, the CS-FEM [11] creates smoothing cells/domains located inside the Q4 elements (Fig. 1). The numerical implementation of CS-FEM is very similar to that of the FEM, and the bandwidth of stiffness matrix of CS-FEM is as same as that of FEM. The smoothing operations are implemented inside the elements, i.e., without crossing element manipulations, thus the CS-FEM can be realized via user-defined subroutines in some commercial finite element software packages, including ABAQUS user-defined elements (UEL [216] or VUEL).

The CS-FEM has been extended to free and forced vibration analysis [14], general n-sided polygonal element (or nCS-FEM) [15], volumetric locking problems [16], plate/shell analysis [66, 67, 76, 77], and coupling with the extended finite element method (X-FEM) [49]. The idea of cell-wise strain smoothing was also formulated with 3D hexahedral elements in [49] and [50] and higher order elements [217]. Through extension of CS-FEM for triangular elements combined with the stabilized DSG technique or Mindlin plate element, a number of applications have been presented for static and dynamic analysis of plates and shells [77–93, 95–103]. The major features of the CS-FEM can be summarized as:

1. Due to the transformation of area (volume for 3D) integration into the line (surface for 3D) integration [11, 13], the integrations for computing the strain matrix can be implemented along the boundary of the smoothing cells. Thus the strain is computed in a weak fashion without coordinate transformation or isoparametric mapping involved, which helps the CS-FEM have better performance than standard FEM when elements are distorted.

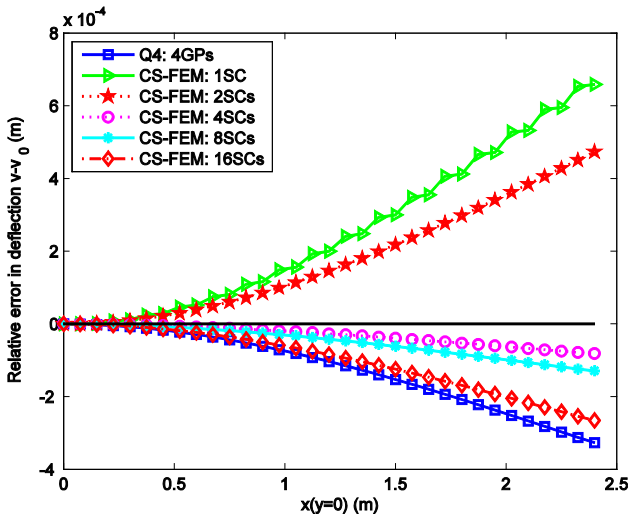

Fig. 6 Comparison of the relative errors of displacement between CS-FEM using different number of smoothing cells ($n_{SC} = 1, 2, 4, 8, 16$) and standard FEM. A softer S-FEM model can be created using less smoothing domains

2. When single smoothing cell ($n_{SC} = 1$) is used in Q4 or H8 elements, the solution of CS-FEM is the same as the FEM with reduced integration. While for $n_{SC} \to +\infty$, it approaches the standard FEM with full integration. Compared with the exact solutions, there exists some optimal number of smoothing cells to obtain the best accuracy (generally $n_{SC} = 4$ for Q4 elements [13] and $n_{SC} = 8$ for H8 elements). Figure 6 shows the comparisons of relative errors of the deflection along centerline for a cantilever beam under a downward loading at the tip [142]. It is clearly shown that a softer S-FEM model can be created using less (but larger) smoothing domains.
3. For CS-FEM, the convergence rates were found higher than FEM in both displacement and energy norms and the error is smaller than that of FEM ($n_{SC} = 4$).

3.2 Edge-Based S-FEM (ES-FEM)

The ES-FEM evaluates the weak form based on edge-based smoothing domain, which are constructed associated with edges of T-elements (T3 for 2D and T4 for 3D), as illustrated in Fig. 2. The ES-FEM is applicable to other shapes of element, including the general polygonal or polyhedral elements. So far the work on ES-FEM has been focused on T-elements, since it has advantages in automatic mesh generation and for adaptive mesh rezoning. As a most popular S-FEM model, intensive applications of ES-FEM lead to the major findings as follows:

1. The ES-FEM-T3 has a close-to-exact stiffness and often offers super-convergent and very accurate solutions, which may be often better than the standard FEM using Q4 elements with the same sets of nodes.
2. It is always temporally stable and works well with poor quality mesh, and hence ideal for dynamic analysis, and eigenvalue analysis.
3. To deal with volumetric and/or bending locking, special treatments have been implemented in ES-FEM, including the use of bubble functions [33, 218, 219], enrichment of drilling rotations [220], and $\bar{F}$-bar aided technique ($\bar{F}$-barES-FEM-T4) [208].
4. For acoustic analysis, the ES-FEM is less sensitive to the wave number for solving the Helmholtz equation, which can provide much accurate frequency response for a wide range of wave numbers [21, 155, 157, 158].
5. The ES-FEM equipped with stabilized discrete shear gap (DSG) technique can effectively avoid the shear locking in the analyses of Reissner–Mindlin plates [69, 70].

3.3 Node-Based S-FEM (NS-FEM)

The NS-FEM was initially inspired by the linear conforming point interpolation method (LC-PIM) [221–223], and the linearly conforming radial point interpolation method (LC-RPIM) when the RBFs are included later [224]. The strain smoothing in NS-FEM is performed over the smoothing domain that cover the nodes (see Fig. 3). Numerical applications have shown that the NS-FEM has the following properties:

1. The NS-FEM is even softer than the ES-FEM, which is also known as "overly soft" or underestimation property. Because of this unique property, it can produce upper-bound solutions in strain energy (for force driving problems) and it is so far the only displacement model that can offer upper bound solution. This is because the number of smoothing domains used in an NS-FEM model is much smaller than that of the ES-FEM counterpart, due to the fact that the number of nodes is always less than that of edges in a T-mesh. Based on the W^2 formulation theory, a S-FEM model is in general softer when the number of smoothing domain is less, and vice versa. The similar phenomenon was observed in Fig. 6 for the CS-FEM.
2. The NS-FEM can alleviate effectively the volumetric locking for nearly incompressible materials. However, the accuracy of the NS-FEM may not be ideal for some problems. To improve the accuracy, it has been combined with the ES-FEM, known as NS/ES-FEM, in a "selective" formulation for hyperelastic materials undergoes extremely large deformation [35, 115, 172, 205–208]. It has been pointed out that NS-FEM (or NS/ES-FEM) is not fully locking-free for idealized fully incompressible materials. Improvements by

including bubble functions have been made in ES-FEM for handling idealized purely incompressible materials [33].

3. It is able to produce very accurate and often super-convergent stress solutions, measured in energy norm.
4. The stress at nodes can be calculated directly from the nodal displacements without any post-processing process [51].
5. The NS-FEM is usually less efficient computationally. This is due to the larger bandwidth in the stiffness matrix caused by the use of more supporting elements (hence nodes) for node-based smoothing domains.
6. Though it is proven spatially stable, the NS-FEM may be "temporally" unstable. This is because for dynamic problems, we have additionally the mass matrix in addition to the stiffness matrix. Therefore, there is a competition between the eigenvalues of the stiffness matrix and the mass matrix. In NS-FEM models, the stiffness is reduced quite significantly due to the overly-soft behavior, and hence the eigenvalues for some modes could be (relatively) lower than that of the mass matrix. Such modes are observed as the *non-zero-energy* spurious modes. Thus without special treatments, it is not preferred to use NS-FEM for dynamic problems [204]. Some stabilization techniques [144, 151, 165, 185] (e.g., squared-residual) were recently proposed to cure the temporal instability of the NS-FEM. Note that the use of such a stabilization technique may result in the loss of upper bound property of NS-FEM. It is recommended that the NS-FEM should be used only when we are interested in obtaining an upper bound solution, or for nearly incompressible materials.

3.4 Face-Based S-FEM (FS-FEM)

The ES-FEM has been further extended for 3D problems to form the so-called face-based S-FEM (FS-FEM), which creates smoothing domains associated with the faces of tetrahedral elements as shown in Fig. 4. Similar to ES-FEM, the FS-FEM is significantly more accurate than FEM using same T4 mesh for dynamic [162] and both linear and nonlinear problems (e.g., visco-elastoplastic analysis [28]). As a 3D S-FEM model, the FS-FEM is very attractive for practical applications. For example, Duong [225, 226] has integrated the FS-FEM into the open source software *Code Aster* for large scale nonlinear applications, including biomedical problems.

3.5 Selective S-FEM

The idea of selective S-FEM schemes was first introduced in [16] with cell-based smoothing technique to eliminate volumetric locking, and to improve numerical performance at the same time. A typical selective scheme of S-FEM applies two different types of smoothing domains, i.e., edge/face-based and node-based domains, selectively for two different material "part" [45] (e.g., deviatoric part and volumetric part). For the volumetric or hydrostatic part, the node-based scheme is used to "soften" the large bulk modulus to avoid locking issues [55, 56, 205–207]. The edge or face-based scheme will be utilized for the deviatoric part for good accuracy. Both the high accuracy and locking-free features of selective S-FEM have been verified by many examples of nearly incompressible materials. It already has some and will have more potential applications in biomechanics of soft biomaterials [35, 115, 205, 207] with properties of micromechanical incompressibility.

3.6 Alpha FEM (αFEM)

To avoid the spurious non-zero energy modes existed in NS-FEM for dynamic problems, Liu et al. [18] presented an effective way to formulate a numerical method with "right" stiffness, which is named as the alpha finite element method (αFEM). In αFEM, nearly exact solution for a given problem can be obtained by scaling the gradient of strains in the physical coordinates and/or Jacobian matrices via an adjustable factor "α". [18, 25, 26]. Several versions of αFEM have also been developed, including Aα-DSG3 method with approximation of displacements and rotations by FEM and bending, geometrical and shear strains by NS-FEM [74, 107]. As the αFEM can alleviate the locking issues and performs well for dynamic problems, it is widely applied in vibration and acoustic problems [53, 154, 164, 167, 168], and plate analysis [74, 107]. These methods are proven to be stable and convergent. However, a αFEM may or may not be variationally consistent, depending how it is formulated [54].

3.7 Beta FEM (βFEM)

Inspired by the idea of αFEM, a more general, versatile and ultra-accurate smoothed βFEM was developed by Zeng et al. [36, 227]. In the βFEM, the stiffness matrix is computed utilizing strains smoothed over the smoothing domains constructed by both the edges/faces and nodes of T-meshes. Figure 7 shows the creation of smoothing domain for βFEM: the node-based smoothing domains [the domain surrounding a node, e.g., node B as shown in Fig. 7a and node $A(q)$ in (b)] and the edge/face-based smoothing domains. Exact solution in strain energy can be approached by a proper adjustable parameter β, due to the fact that the exact solution is within the narrow interval bounded by the solutions of NS-FEM and ES/FS-FEM. The effectiveness of

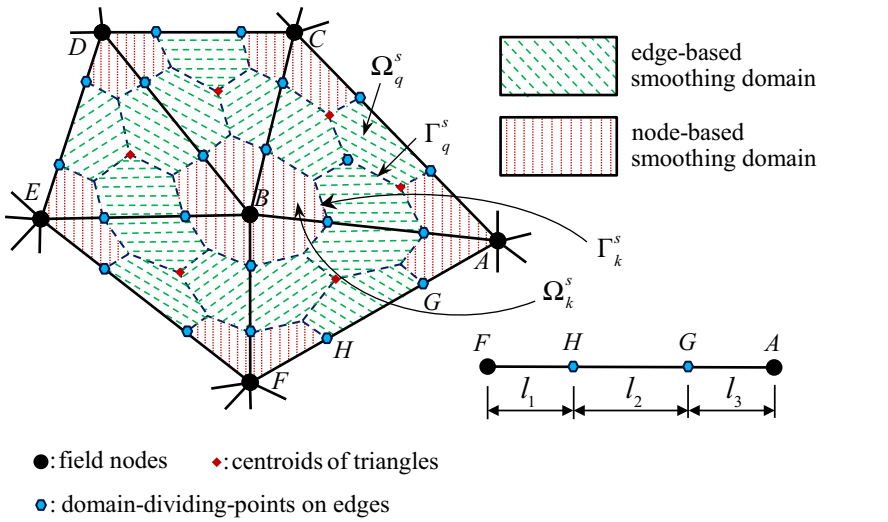

(a)

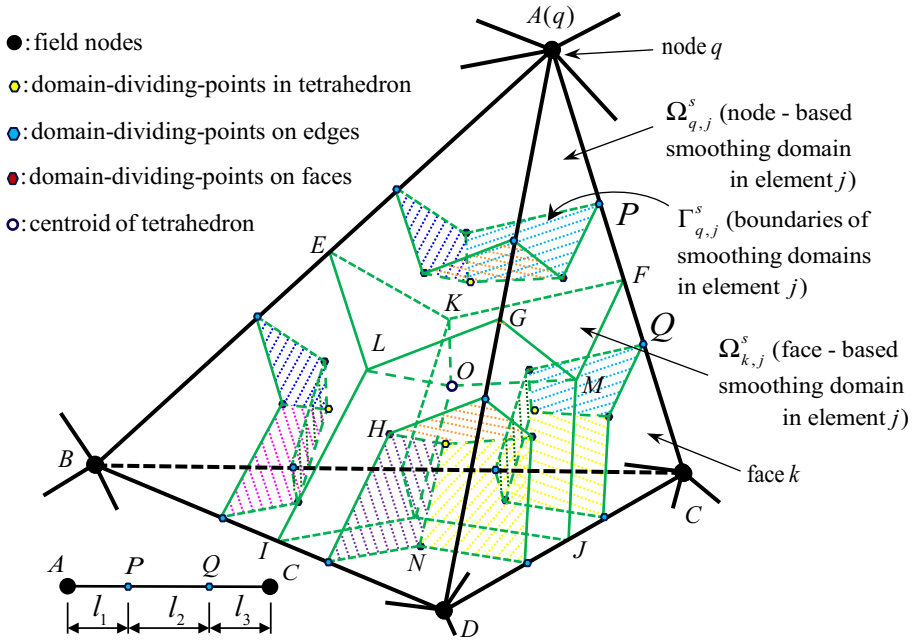

(b)

Fig. 7 Schematic illustration of the βFEM with sub-smoothing domains discretized by node-based and edge/face-based smoothing techniques: **a** 2D βFEM and **b** 3D βFEM

the βFEM has already been demonstrated in some numerical applications including crystal plasticity modeling and vibration analysis. The method is found to be temporal stable, insensitive to mesh distortion and immune from volumetric locking. The good performance is attributed to its key features inherited from both NS-FEM and ES/FS-FEM.

3.8 Other Variations

In order to resolve issues or drawbacks in standard FEM or even some S-FEM models, a few variations of smoothing technique based FEM models have been proposed in the past several years. For example, to solve fracture mechanics problems, some smoothed singular elements have been formulated with ES-FEM [121, 123–128, 130–132, 134, 140, 141], NS-FEM [122] or X-FEM [31, 32, 122, 129, 133, 138] to capture a proper order of singularity near the crack-tip. The stabilized node-based smoothed finite element method (sNS-FEM) [144, 151, 165, 185] can eliminate the spurious non-zero energy modes that exist in NS-FEM for vibration analysis. The *F*-bar aided ES-FEM (*F*-barES-FEM-T4) inherits the

shear locking-free property of ES-FEM and volumetric locking-free property of the *F*-bar method, which is able to relax the corner locking issue and suppress the pressure oscillation in nearly incompressible materials [208]. In [219], a bubble-enhanced ES-FEM was performed to analyze volume-constrained problems in 2D linear elasticity. A hybrid smoothed extended finite element/level set method incorporated with the interfacial energy effect [58] was proposed to model nanoscale inhomogeneities without remeshing involved in interface geometry changes. In [213], the polyhedral elements combined with cell-based smoothing technique were developed for treating non-matching interfaces between dissimilar hexahedral meshes.

$$\mathbb{G}_h^1(\Omega) = \left\{ \begin{array}{l} v|\, v(\mathbf{x}) = \mathbf{N}(\mathbf{x})\mathbf{d}, \\ v \in \mathbb{L}^2(\Omega), \\ \sum\limits_{n=1}^{N_s} \left(\int_{\Gamma_n^s} v(s) n_i \mathrm{d}s \right)^2 > 0 \Leftrightarrow v \neq c \in \mathbb{R}, \quad i = 1, \ldots, d \end{array} \quad \forall \mathbf{d} \in \mathbb{R}^{N_n} \right\} \tag{19}$$

4 Theoretical Aspects of S-FEM: G Space and W^2 Formulation

Numerous numerical examples have demonstrated that all these models mentioned above are stable and converge to the exact solution when the mesh is refined. Special properties for different S-FEM models have also been observed in a large number of numerical examinations. However, it is still important to theoretically prove the stability, convergence, convergence rate and the predictable properties since it is not possible to exhaust all the possible problems via numerical tests. Therefore, the safest way is to prove in theory for general settings with a set of conditions, and then test with numerical examples under the same conditions. Theoretical study on S-FEM has two paths. The first path is the most general one and it uses the G space theory [5, 43, 44]. The second path uses the standard variational principle, prove the orthogonality of the smoothed strain field, and then show that the smoothed Galerkin weak form is variationally consistent. Finally, we argue from the fact that when the number of the smoothing domain approach infinite and the size of the smoothing domain approaches to zero, the smoothed strain field approaches the compatible strain field. Because the FEM can converge to the exact solution, and the S-FEM uses also compatible displacements, the S-FEM shall also converge to the exact solution when the mesh is refined. This proof is rather straightforward, and is detailed in [42] and in the Sect. 4.7 of [45], which we will not repeat here. Instead, we now summarize the first path of the proof as below, since it is more general. As a set of stand-alone theorems, it is also applicable to the S-PIM models [6].

4.1 G Space Theory

A detailed discussion on G space theory can be found in the Chap. 3 of [5] and also in [37]. Here we only brief the necessary part of the theory for this review article. A $\mathbb{G}_h^1$ space is of finite dimension established for a discretized problem domain with nodes. It can be defined as:

where $\mathbf{d} = \{ d_1 \quad d_2 \quad \cdots \quad d_{N_n} \}^{\mathrm{T}}$ is the vector of nodal function values, and $\mathbf{N}(\mathbf{x})$ is the matrix of nodal shape functions of arbitrary order constructed using the element-based method in FEM, or a meshfree method such as PIM and radial PIM (or RPIM for short), and can be written as

$$\mathbf{N}(\mathbf{x}) = [N_1(\mathbf{x}) \quad N_2(\mathbf{x}) \quad \cdots \quad N_{N_n}(\mathbf{x})] \tag{20}$$

For creating functions in $\mathbb{G}_h^1$ spaces, we do not restrict on how these shape functions are created, as long as they satisfy the following conditions:

1. *Linearly independency condition* all these nodal shape functions are linearly independent over the problem domain and hence are capable to form a basis. Naturally, the FEM shape functions satisfy this condition. The simple PIM (e.g., Tables 2, 3) also satisfies this condition, because of the independent local nature of the interpolations performed.
2. *Bound condition* all the functions constructed using these shape functions must be square integrable over the problem domain. This is to ensure the convergence of a numerical model to be created. The shape functions of FEM, PIM and RPIM all satisfy this condition.
3. *Positivity conditions* there exists a division of Ω_i^s such that $\sum_{n=1}^{N_s} \left(\int_{\Gamma_n^s} v(s) n_i \mathrm{d}s \right)^2 > 0$, if and only if $v \neq c \in \mathbb{R}$, $\forall \mathbf{d} \in \mathbb{R}^{N_n}$ and $i = 1, \ldots, d$. It (together

Table 4 Minimum number of smoothing domains $N_s^{\min}$ for problem domain discretized with n_t total nodal unknowns

Dimension of the problem	Minimum number of smoothing domains (for solid mechanics problems)
1D	$N_s^{\min} = n_t$
2D	$N_s^{\min} = 2n_t/3$
3D	$N_s^{\min} = 3n_t/6 = n_t/2$

with the linearly independent condition) is to ensure the stability of a numerical model to be created. This condition can be satisfied when the number of the smoothing domains exceeds that given in Table 4.

As in the standard FEM we require the shape functions satisfy the basic properties of partitions of unity [228], Delta function property and (local) linear consistency [6].

The major difference between a $\mathbb{G}_h^1$ space and FEM $\mathbb{H}_h^1$ space is that the $\mathbb{H}_h^1$ space requires both the function and its first gradient of the function square integrable, but in the $\mathbb{G}_h^1$ space we require only the function itself square integrable. Therefore, the requirement on function is now further weakened upon the already weakened requirement for functions in a $\mathbb{H}_h^1$ space. Hence a $\mathbb{G}_h^1$ space can be viewed as space of a set of functions with weakened weak (W^2) requirements on continuity. In a $\mathbb{H}_h^1$ space, the bound condition is achieved by imposing the smoothness upon the first derivatives of the function to be square integrable. Therefore, in an FEM model, we typically require the nodal shape functions to be continuous over the problem domain. The stability is automatically ensured for functions in a $\mathbb{H}_h^1$ space as long as the smoothness is satisfied, due to the Poincare-Friedrichs inequality. In the $\mathbb{G}_h^1$ space, the smoothness requirement is only on the function being square integrable. The stability in the $\mathbb{G}_h^1$ space, however, is ensured by imposing the positivity condition, which needs to be ensured by proper construction of the smoothing domains.

Because a member in a $\mathbb{G}_h^1$ space is also a member of a $\mathbb{L}^2$ space, therefore a $\mathbb{G}_h^1$ space is a subspace of $\mathbb{L}^2$ space: $\mathbb{G}_h^1(\Omega) \subset \mathbb{L}^2(\Omega)$. Note that any function created using FEM shape functions satisfies the above mentioned three conditions, it belongs to a $\mathbb{G}_h^1$ space, as long as the condition given in Table 4 are met. The proof on this is a little lengthy, but can be found in [37, 229]. Therefore, all the theorems proven for functions in $\mathbb{G}_h^1$ space also applies to $\mathbb{H}_h^1$ space: $\mathbb{H}_h^1 \subseteq \mathbb{G}_h^1$. Finally, we note $\lim_{\substack{N^s\to\infty \\ \Omega^s\to 0}} \mathbb{G}_h^1 \to \mathbb{H}_h^1$, which is due to Eq. (7).

The displacement (vector) field, we require the components all in the $\mathbb{G}_h^1$. The associated inner product as

$$(\mathbf{w},\mathbf{v})_{\mathbb{G}^1(\Omega)} = (\mathbf{w},\mathbf{v})_{\mathbb{L}^2(\Omega)} + \sum_{n=1}^{N_s} A_n^s \bar{\boldsymbol{\varepsilon}}^T(\mathbf{w})\bar{\boldsymbol{\varepsilon}}(\mathbf{v}) \tag{21}$$

The associated $\mathbb{G}_h^1$ semi-norm is defined as

$$|\mathbf{w}|^2_{\mathbb{G}^1(\Omega)} = \sum_{n=1}^{N_s} A_n^s \bar{\boldsymbol{\varepsilon}}^T(\mathbf{w})\bar{\boldsymbol{\varepsilon}}(\mathbf{w}) \tag{22}$$

and the $\mathbb{G}_h^1$ full norm becomes

$$\|\mathbf{w}\|^2_{\mathbb{G}^1(\Omega)} = \|\mathbf{w}\|^2_{\mathbb{L}^2(\Omega)} + |\mathbf{w}|^2_{\mathbb{G}^1(\Omega)} \tag{23}$$

We finally define a space for functions that are fixed on the Dirichlet boundaries and hence the functions cannot "float"

$$\mathbb{G}^1_{h,0} = \left\{\mathbf{w} \in \mathbb{G}_h^1(\Omega) | \mathbf{w} = 0 \text{ on } \Gamma_u\right\} \tag{24}$$

4.2 Key Inequalities for Functions in $\mathbb{G}_h^1$ Spaces

4.2.1 The 0th Inequality

Based on the definition, we have the most basic inequality:

$$|w|_{\mathbb{G}^1(\Omega)} \le \|w\|_{\mathbb{G}^1(\Omega)}, \quad \forall w \in \mathbb{G}_h^1 \tag{25}$$

which means that the $\mathbb{G}_h^1$ full norm is always larger than the $\mathbb{G}_h^1$ semi-norm.

4.2.2 The 1st Inequality

Functions in a $\mathbb{G}_h^1$ space satisfy the 1st inequality

$$\|\mathbf{d}\|_{\mathbb{L}^2(\Omega)} \ge c^f_{dw}\|w\|_{\mathbb{G}^1(\Omega)}, \quad \forall w \in \mathbb{G}_h^1 \tag{26}$$

or equivalently

$$\|w\|_{\mathbb{G}^1(\Omega)} \ge c^f_{wd}\|\mathbf{d}\|_{\mathbb{L}^2(\Omega)}, \quad \forall w \in \mathbb{G}_h^1 \tag{27}$$

where c^f_{dw} and c^f_{wd} are nonzero positive constant independent of w and $\mathbf{d}$. This means that the full $\mathbb{G}_h^1$ norm of a function is equivalent to the L^2 norm of the nodal values of the function. A proof for these inequalities is given in [43].

4.2.3 The 2nd Inequality

If at least a minimum number of linearly independent smoothing domains are used in a S-FEM model to evaluate the $\mathbb{G}_h^1$ norms, it should have

$$|w|_{\mathbb{G}^1(\Omega)} \ge c^s_{wd}\|\mathbf{d}\|_{\mathbb{L}^2(\Omega)}, \quad \forall w \in \mathbb{G}^1_{h,0}(\Omega) \tag{28}$$

or equivalently

$$\|\mathbf{d}\|_{\mathbb{L}^2(\Omega)} \ge c^s_{dw}|w|_{\mathbb{G}^1(\Omega)}, \quad \forall w \in \mathbb{G}^1_{h,0}(\Omega) \tag{29}$$

This means that the semi-norm $|w|_{\mathbb{G}^1(\Omega)}$ and the norm $\|\mathbf{d}\|_{\mathbb{L}^2(\Omega)}$ is equivalent. The proof on this is uses a positivity relay, which is lengthy and given in [43].

4.2.4 The 3rd Inequality

When a minimum number of independent node-based smoothing domains are used to evaluate the $\mathbb{G}_h^1$ norms, there exists a positive nonzero constant c_G such that,

$$c_G\|w\|_{\mathbb{G}^1(\Omega)} \le |w|_{\mathbb{G}^1(\Omega)}, \quad \forall w \in \mathbb{G}_{h,0}^1 \tag{30}$$

meaning that the $\mathbb{G}_h^1$ full norm and the $\mathbb{G}_h^1$ semi-norm of any function in a $\mathbb{G}_h^1$ space are equivalent. This is a generalized Poincare–Friedrichs inequality for a finite $\mathbb{G}_h^1$ space. It is fundamentally important for stability of weakened weak formulation based on G spaces. A detailed proof on this norm equivalence theorem in G space theory requires the 1st and 2nd inequalities, and the details are given in [43, 229], when the FEM and PIM shape functions are used.

4.3 Weakened Weak (W^2) Form

4.3.1 Essential Chain Inequality

Combination of the 0th and 3rd inequalities, it provides the following chain inequalities.

$$c_G\|w\|_{\mathbb{G}^1(\Omega)} \le |w|_{\mathbb{G}^1(\Omega)} \le \|w\|_{\mathbb{G}^1(\Omega)}, \quad \forall w \in \mathbb{G}_{h,0}^1 \tag{31}$$

It essentially says that the semi-norm of any function in a $\mathbb{G}_h^1$ space can be bounded from both sides by its full norm; it can only be zero if and only if the function is zero everywhere, and it is finite as long as the function is finite. This chain inequality is essential and fundamentally important to ensure the stability and convergence of a W^2 formulation that uses smoothed derivatives to construct the stiffness matrix of a model.

4.3.2 Cauchy–Schwarz Inequality

The $\mathbb{G}_h^1$ inner product defined in Eq. (21) has the Cauchy–Schwarz inequality:

$$(w,v)_{\mathbb{G}^1(\Omega)} \le \|w\|_{\mathbb{G}^1(\Omega)} \cdot \|v\|_{\mathbb{G}^1(\Omega)} \tag{32}$$

To show this, we first observe its symmetry: because swapping places for w and v will not change the value of the inner product. Second, it is positive definite, because of the positivity of the $(w,v)_{\mathbb{L}^2(\Omega)}$ and semi-positivity of $(\bar{\varepsilon}(w),\bar{\varepsilon}(v))_{\mathbb{L}^2(\Omega)}$. Finally, it is bilinear, because of the bilinear property of $(w,v)_{\mathbb{L}^2(\Omega)}$ and $(\bar{\varepsilon}(w),\bar{\varepsilon}(v))_{\mathbb{L}^2(\Omega)}$.

The Cauchy–Schwarz inequality is fundamentally important for the continuity of the W^2 formulation.

4.3.3 Bilinear Forms in $\mathbb{G}_h^1$ Spaces for Solid Mechanics

Consider again a stable solid (with symmetric positive definite or SPD material constant matrix $\mathbf{c}$) defined in a problem domain that is discretized with a set of elements. We require also that at least the minimum number of linearly independent smoothing domains is used (Table 4) [43, 44]. The smoothed bilinear form is then defined as:

$$\bar{a}_D(\mathbf{w},\mathbf{v}) = \sum_{k=1}^{N_s} \bar{\boldsymbol{\varepsilon}}_k^T(\mathbf{w})\mathbf{c}\boldsymbol{\varepsilon}_k(\mathbf{v})A_k^s \tag{33}$$

where $\bar{\boldsymbol{\varepsilon}}_i$ is the vector of the smoothed strains in the smoothed domain Ω_i^s [see Eq. (5)]:

$$\bar{\boldsymbol{\varepsilon}}_i(\mathbf{w}) = \frac{1}{A_i^s}\int_{\Gamma_i^s} \mathbf{L}_n\mathbf{w}(\mathbf{x})\mathrm{d}\Gamma \tag{34}$$

We noticed that L^2 norm of the strain vector is the $\mathbb{G}_h^1$ semi-norm:

$$|\mathbf{w}|_{\mathbb{G}^1(\Omega)} = \|\bar{\boldsymbol{\varepsilon}}\|_{L^2}, \quad \forall \mathbf{w} \in \mathbb{G}_{h,0}^1 \tag{35}$$

which is useful in proving important properties in the following sections. We shall also immediately have the following inequality.

4.3.4 The 4th Inequality

$$c_G\|\mathbf{w}\|_{\mathbb{G}^1(\Omega)} \le \|\bar{\boldsymbol{\varepsilon}}\|_{\mathbb{L}^2}, \quad \forall \mathbf{w} \in \mathbb{G}_{h,0}^1 \tag{36}$$

which is equivalent to the 2nd Korn's inequality for functions in a $\mathbb{H}_h^1$ space.

Combining the 0th inequality and Eq. (35), we have the following chain inequality:

$$c_G\|\mathbf{w}\|_{\mathbb{G}^1(\Omega)} \le \|\bar{\boldsymbol{\varepsilon}}\|_{\mathbb{L}^2} \le \|\mathbf{w}\|_{\mathbb{G}^1(\Omega)}, \forall \mathbf{w} \in \mathbb{G}_{h,0}^1 \tag{37}$$

Theorem 1 (Ellipticity with respect to G semi-norm) *For solids of stable materials, there exists a nonzero positive constant c_{aw}^s independent of* $\mathbf{w}$*, such that*

$$\bar{a}_D(\mathbf{w},\mathbf{w}) \ge c_{aw}^s|\mathbf{w}|_{\mathbb{G}^1(\Omega)}^2, \quad \forall \mathbf{w} \in \mathbb{G}_{h,0}^1. \tag{38}$$

The proof needs to use smallest eigenvalue of the material constant matrix $\mathbf{c}$ that is SPD, L^2 norm definition by inner product, and that the L^2 norm of the strain vector is the same as the semi-norm. Finally, we have this inequality and the detailed proof can be found in the Sect. 5.4 of [5].

Theorem 2 (Ellipticity or coercivity: 5th inequality) *For solids of stable materials, there exists a nonzero positive constant* c^f_{aw} *such that*

$$\bar{a}_D(\mathbf{w},\mathbf{w}) \geq c^f_{aw}\|\mathbf{w}\|^2_{\mathbb{G}^1(\Omega)}, \quad \forall \mathbf{w} \in \mathbb{G}^1_{h,0} \tag{39}$$

which implies the ellipticity or coercivity of bilinear forms.

This is the outcome of the 3rd inequality and Theorem 1. It is important because it ensures the existence (and hence the uniqueness) and consequently stability of the solution of a W^2 formulation.

Theorem 3 (Continuity: 6th inequality) *For solids of stable materials, there exists a nonzero positive constant* c^f_{awv} *such that*

$$\bar{a}_D(\mathbf{w},\mathbf{v}) \leq c^f_{awv}\|\mathbf{w}\|_{\mathbb{G}^1(\Omega)}\|\mathbf{v}\|_{\mathbb{G}^1(\Omega)}, \quad \forall \mathbf{w} \in \mathbb{G}^1_h, \quad \forall \mathbf{v} \in \mathbb{G}^1_h \tag{40}$$

The proof needs the largest eigenvalue of the SPD matrix **c**, the Cauchy–Schwarz inequality, the fact that an L^2 norm preservation property of the unitary matrix, Eq. (35), and the 0th inequality. The detailed proof can be found in Sect. 5.4 of [5].

Theorem 3 ensures that the bilinear from is continuous. Together with the ellipticity, it ensures the stability of the solution of a W^2 formulation.

4.3.5 The 7th Inequality: Softened Model

For stable solid materials and any $\mathbf{w} \in \mathbb{H}^1_h$ the smoothed bilinear form is smaller than the standard bilinear form used in FEM:

$$\bar{a}_D(\mathbf{w},\mathbf{w}) \leq a(\mathbf{w},\mathbf{w}), \quad \forall \mathbf{w} \in \mathbb{H}^1_h \tag{41}$$

The proof can be found in the Chap. 4 of [5] and a more general inequality than Eq. (41) can be found in [17]. The 7th inequality implies that a model established based on the smoothed bilinear form will be "softer" than that of bilinear form, which was initially revealed in [223].

4.3.6 Monotonic Convergence Property: 8th Inequality

Consider a division D_1 that divides domain Ω into a set of smoothing domains $\boxed{\Omega} = \cup_{i=1}^{N_s} \boxed{\Omega}^s_i$ where the box stands for enclosed domain. If a new division D_2 is performed by sub-dividing a smoothing domain in D_1 into n_{sd} sub-smoothing-domains: $\boxed{\Omega}^s_i = \cup_{j=1}^{n_{sd}} \boxed{\Omega}^s_j$, then the following inequality stands

$$\bar{a}_{D_1}(\mathbf{w},\mathbf{w}) \leq \bar{a}_{D_2}(\mathbf{w},\mathbf{w}) \tag{42}$$

This is known as the 8th inequality first presented in [223]. It implies that the "softening" effect in a W^2 formulation will be reduced monotonically with the increase of the number of smoothing domains in a nested manner. Based on this inequality, one knows how to reduce or increase the stiffness or softness of a W^2 model. Arguing along this line, we can expect that $\lim_{\substack{N^n\to\infty \\ \Omega^s\to 0}} \bar{a}(\mathbf{w},\mathbf{w}) \to a(\mathbf{w},\mathbf{w})$. In other word, the S-FEM approaches to an FEM model at the limit that the dimension of all the smoothing domains approaches to zero. We can also say that an FEM model is a special case of S-FEM at such a limit. This limit property is also rooted at Eq. (7).

4.3.7 A Weakened Weak (W^2) Statement

We are now ready to express the W^2 statement for solid mechanics problems. An approximated solution $\bar{\mathbf{u}} \in \mathbb{G}^1_{h,0}$ satisfies the following weakened weak (W^2) form:

$$\bar{a}_D(\mathbf{w},\bar{\mathbf{u}}) = f(\mathbf{w}), \forall \mathbf{w} \in \mathbb{G}^1_h \tag{43}$$

where $f(v)$ is a *linear functional* defined as

$$f(\mathbf{w}) = (\mathbf{w},\mathbf{t})_{\Gamma_N} + (\mathbf{w},\mathbf{b})_{\Omega} \tag{44}$$

in which **t** and **b** are the traction force applied on the natural boundary of the problem domain and the body force applied over the problem domain, respectively.

It is noted that the linear functional $f(\mathbf{w})$ is exactly the same as that in the standard FEM. The Eq. (43) is also called the generalized smoothed Galerkin weak from.

If we substitute $\bar{\mathbf{u}} = \sum_{J=1}^{N_n} \mathbf{N}_J(\mathbf{x})\bar{\mathbf{d}}_J$ as the trial function, and set $\mathbf{N}_I(\mathbf{x}), I = 1, \ldots, N_n$, as the test function **v** into the W^2 statement, it becomes the following system of N_n equations.

$$\bar{a}_D(\mathbf{w},\bar{\mathbf{u}}) = \sum_{k=1}^{N_s}\left[\bar{\boldsymbol{\varepsilon}}^T_k(\mathbf{N}_I)\mathbf{c}\boldsymbol{\varepsilon}_k(\bar{\mathbf{u}})A^s_k\right] = \sum_{k=1}^{N_s}\left[\underbrace{\bar{\mathbf{B}}^T_{Ik}\mathbf{c}\bar{\mathbf{B}}_{Jk}A^s_k}_{\mathbf{K}_{IJk}}\bar{\mathbf{d}}_{Jk}\right], \quad I = 1,\ldots,N_n \tag{45}$$

which yields Eq. (18).

Theorem 4 (W^2 solution in $\mathbb{H}^1_h$ spaces: variationally consistent) *If the solution is sought from a* $\mathbb{H}^1_h$ *space, the* W^2 *statement Eq. (43) is variationally consistent in the standard weak formulation and hence the solution will be stable, unique and convergent to the exact solution of the strong statement when* $h \to 0$ (*therefore* $\Omega^s_i \to 0$).

The proof for this theorem needs two ingredients. First, it is that the smoothed strain is an orthogonal projection (the Theorem 4.1 in [5]) of the compatible strain and hence is variationally consistent. The W^2 solution is thus stable and convergent. Second, the discretized FEM space

is a subspace of the continuum Hilbert space. When $h \to 0$ (and $\Omega_i^s \to 0$), the solution shall approach to the exact solution of the corresponding strong form PDE. More discussion on this topic can be found in the Chap. 5 of [5].

Theorem 5 (W^2 solution in $\mathbb{G}_h^1$ spaces: convergence to the exact solution) *For solids of stable materials, the solution of the W^2 statement Eq. (43) is stable, unique and convergent to the exact solution of the strong statement when $h \to 0$ ($\Omega_i^s \to 0$).*

Proof: We need here three key pieces in this proof: (1) the ellipticity of the bilinear form, (2) the continuity of the bilinear form, and (3) the convergence of the solution to the exact solution. The ellipticity has already been given by Theorem 2, and the continuity is given by Theorem 3. Based on the Lax–Milgram theorem, Theorems 2 and 3 ensures that a W^2 formulation has a stable and unique solution for any given discrete model. However, we do not know where the solution converges to, when the mesh of the model is refined. We need to show that the solution of the W^2 formulation converges to the exact solution. To this end, we present the following arguments:

1. First, in any of the smoothing domains we see that the smoothed strain field is constant in each and every smoothing domain. Such a constant strain field fully satisfies the strong form equation (in its homogeneous form) in each and every smoothing domain; this means the *complementary* energy principle is satisfied in all these smoothing domains. There are energy leaks.
2. Second, on all the interfaces of the smoothing domains the displacement field is continuous (compatible); therefore, any discrepancy on (smoothed) stresses on the interface will not generate any work, and hence no leak of energy. The work done by the external forces (body forces and tractions on the boundary, the linear form in the W^2 statement) are counted via the *potential* energy principle (the W^2 formulation does not change the linear functional), and thus there is no leak of energy, either. In addition, all these displacement (essential) boundary conditions are satisfied in a S-FEM model. Since the potential energy principle is satisfied on all these places (except within the smoothing domains), there is no energy leak there either.
3. Therefore, when the mesh (background cells together with the smoothing domains) is refined, all the strong form equations will be better satisfied at every point in all these smoothing domain, and the external forces are balanced by the potential energy principle with compatible displacements. There will be no energy leaks at any places in the problem during the process. The solution will surely converge to the exact solution at any point in the problem domain.

In the numerical tests, we have confirmed that all these S-FEM models pass the linear patch test to machine accuracy [5]. This implies that as long as the exact solution of a problem is at least of linear consistency, a S-FEM model may approach the exact solution when the mesh is refined enough. This partially verifies Theorem 5.

The above "argument" proof offers a critical insight to be understanding of a S-FEM model. It is, in fact, a very special "space-hybrid" model that satisfies both the complimentary energy principle and the potential energy principle. The former is satisfied within all smoothing domains, and the latter is satisfied on the rest of places in the model. On one hand, a S-FEM model is a "partial" compatible model (that obeys the total potential energy principle), because it satisfies: (1) the displacement conditions, (2) the displacements are continuous on the interfaces of all the smoothing domains, and (3) the measure of the work done by the external forces. However, the S-FEM is not a fully compatible model, since the differential stain-displacement condition is not satisfied within the smoothing domains, due to the use of the smoothing strains. This partial compatibility makes the S-FEM model "stiffer". On the other hand, the S-FEM is a partially equilibrium model (that obeys the total complimentary energy principle), because the equilibrium conditions are satisfied within all the smoothing domains, but the stress boundary conditions are not satisfied at the points on the stress boundary and on the interfaces of the smoothing domains. This partial equilibrium feature makes the S-FEM model "softer". Therefore, a S-FEM model is equipped with a very important "knob" to tune the softening effects, enabling us to build softer model (NS-FEM) for upper bound solutions, stiffer model (ES-FEM) for mostly lower bound with very accurate solutions, and right-stiffness model (αFEM and βFEM) for close to exact or nearly exact solutions. The art of the S-FEM is that is gives creative ways to construct smoothing domains or performing the strain smoothing operations [5].

Theorem 6 (Upper bound to the FEM solution) *The strain* energy *of the S-FEM solution $\bar{\mathbf{u}} \in \mathbb{H}_{h,0}^1$ is no less than that of the FEM solution $\tilde{\mathbf{u}} \in \mathbb{H}_{h,0}^1$, when the same mesh is used for creating the numerical models.*

$$U(\tilde{\mathbf{u}}) \leq \bar{U}(\bar{\mathbf{u}}) \tag{46}$$

The proof is lengthy and can be found in [17] by variational formulation and in [223] by energy principle formulation. Although we will not repeat the proof here, we will provide an intuitive physical understanding of Theorem 6. From the 7th inequality, we know that a S-FEM model is always softer than

its FEM counterpart. Therefore, the displacement field obtained from the model should be "larger" and so is the strain field. The strain energy obtained using such a "larger" strain field should also be "larger" compared to that of the FEM model. In other words, the upper bound property is the consequence of the fact that an S-FEM model is always "softer" than its FEM counterpart.

4.3.8 Upper Bound to the Exact Solution: Special Cases

The strain energy of a S-FEM solution $\bar{\mathbf{u}}$ is no less than that of the exact solution $\mathbf{u}$, if $\bar{\mathbf{u}}$ is found from a $\mathbb{H}^1$ space that contains the exact solution:

$$\bar{U}(\mathbf{u}) \leq \bar{U}(\bar{\mathbf{u}}) \tag{47}$$

When the $\mathbb{H}_h^1$ space contains the exact solution, the FEM model will reproduce the solution [3] and Eq. (46) becomes (47).

We noted that the S-FEM will produce the exact solution if it is linear. Although the solution space may contain the exact solution, if a finite division of smoothing domain is used, the S-FEM will not necessarily reproduce the exact solution. It produces an approximated solution that approaches to the exact solution when the dimension of the smoothing domains approaches zero.

It is worth emphasizing that Eq. (47) has only theoretical significance, because generally it is difficult to assume a space that contains the exact solution, unless the exact solution has a very simple form. Even if it can be done, one can simply use the FEM to produce the exact solution, and there is no need for any other form of solution method.

4.3.9 Upper Bound to the Exact Solution: Usual Occurrences

The strain energy of the solution $\bar{\mathbf{u}} \in \mathbb{G}^1$ of a sufficiently large S-FEM model is no less than that of the exact solution $\mathbf{u}$, when the smoothing domains are properly chosen for sufficient smoothing effects:

$$U(\mathbf{u}) \leq \bar{U}^D(\bar{\mathbf{u}}) \tag{48}$$

Precise proof for this property is difficult due to the challenge in quantifying the exceptions. This important upper bound property was found always true when NS-FEM models are used with not too small number of elements in any of the dimensions. An intuitive explanation and "proof" by numerical examples can be found in [17, 222, 223, 230]. A discussion can also be found in the Chap. 8 of [5]. The upper bound property is practically important because it implies that a sufficiently large S-FEM model can provide upper bound to the exact solution in energy norm by properly chosen smoothing domains. Here we emphasis how the smoothing domains are constructed rather than how many smoothing domain is used in an actual S-FEM model.

4.3.10 Rate of Convergence

Once a model is confirmed to be stable and convergent, the error in the solution will depend on the error in the interpolation of the displacement and the approximation of the strains. Therefore, the rate of convergences can be analyzed via the errors during the displacement interpolation and strain approximations. On the rate of convergence for the displacement solution (in L^2 norm), some theoretical studies have shown that it is largely the same for S-FEM and its FEM counterpart [43, 44]. Numerical tests frequently found the rate of S-FEM is often higher.

On the rate of convergence of solutions in stresses (in energy norm), we know that the linear FEM is 1.0 [1, 7]. The S-FEM is usually found to be much higher and Liu [43] has proven an ideal rate of around 1.5 for the NS-FEM. In many numerical examples, S-FEM can achieve a rate of larger than 1.5. The precise proof on this is not yet available. Intuitively, we know that the smoothing operation has helped a great deal to improve the rate of convergence. We know the low rate convergence of the FEM is the compatible formulation, which does not influence the derivatives of the assumed function. When the solution error is measured in H^1 norm, it loses 1 order. It can also be argued that the stresses on the interfaces of the FEM elements jumps, which naturally reduce the accuracy and the rate of convergence. On the S-FEM, however, the compatible strains are subjected to smoothing operations (that is an orthogonal projection, the Theorem 4.1 in [5]). The jumping stresses on the original element interfaces are smoothed out in many S-FEM models. This helped to reduce the error in stresses.

It is worthwhile, however, to emphasize that the study on G space and W^2 formulation is relatively new and the work is far from perfect and complete. As engineers, we hope our preliminary studies can inspire more profound studies of G space and W^2 mathematical formulations, which can provide a solid theoretical basis for even more effective computational methods.

5 Applications

The original applications of S-FEM were in linear elasticity, including basic elastostatics [11, 18, 20], and free and forced vibration analysis [14, 22]. Because of the capability, robustness and versatility of S-FEM, it has been further developed and applied to a large range of problems. This section will review the major application areas of

S-FEM in several aspects: material nonlinearity, fracture mechanics, plates/shells/membranes and composite structures, vibration analysis and acoustic problems, piezoelectric structures and photonic devices, heat transfer and thermo-mechanical problems, and fluid–structure interaction (FSI) simulations. Some special treatments for different problems will also be briefly introduced.

5.1 Nonlinear Material Behavior

In the past 30 years, there has been considerable interest in the computational area of the material behaviors under extreme environments, especially computational material nonlinearity [231–233]. Though grid based methods, particularly the FEM approaches, have made achievements in numerous problems, some numerical difficulties still exist, which limit their applications in some aspects [234–239]. Most of these numerical issues mainly result from large deformation and/or incompressibility of materials. Because of the insensitivity of mesh distortion and locking-free characteristics of some S-FEM models, they can achieve more accurate solutions in modeling nonlinear materials and/or provide simple and effective tools for overcoming the severe volumetric locking in simulating deformation behavior of incompressible or nearly incompressible materials.

5.1.1 Elastic–Plastic Analysis, Shakedown and Limit Analysis

Cui et al. [23] presented the ES-FEM formulations for elastic–plastic problems based on Hencky's deformation theory. Three material models, elastic-perfectly plastic material, work-hardening material and Ramberg–Osgood model, are used and compared with ABAQUS quadrilateral elements to verify the numerical implementations. Cui and Li [64] extended the ES-FEM to simulate metal forming processes with contact algorithms. Liu et al. [240] utilized the selective ES/NS-FEM to treat volumetric locking problems in large-deformation plasticity analysis. The CS-FEM has been applied on two-dimensional elasto-plastic deformations by Bordas et al. [241]. Lee et al. [62] extended the 3D CS-FEM for elasto-plastic finite deformation with emphasis on variable-node elements. Through modifying the volumetric strain in some fashion consistent with the B-bar approach in CS-FEM, the volumetric locking arising from nearly incompressible behavior of elastic–plastic deformations is avoided.

The ES-FEM is firstly extended by Tran et al. [116] for limit and shakedown analysis of structures with elastic-perfectly plastic material. The numerical procedure involves a primal–dual algorithm based on the von Mises yield criterion and a non-linear optimization procedure for the evaluation of the upper and lower bounds of the plastic collapse limit and the shakedown limit. Similar application combined with a primal–dual algorithm by NS-FEM was presented in [118] and a selective ES-FEM of kinematic theorem was introduced in [172] for plastic collapse analysis of structures. Through incorporating the CS-FEM with second-order cone programming (SOCP), Le et al. [117] proposed a numerical procedure of kinematic limit analysis for plane problems.

5.1.2 Visco-elastoplastic Analysis

Nguyen-Thoi et al. extended the ES-FEM and FS-FEM for visco-elastoplastic analyses with the von-Mises yield function and the Prandtl–Reuss flow rule, based on the work of the standard FEM by Carstensen and Klose [242]. They investigated the material behavior of perfect visco-elastoplasticity, and visco-elastoplasticity with isotropic hardening and linear kinematic hardening in a dual model [24, 28]. They found the ES-FEM in 2D and FS-FEM in 3D performed more efficiently (computation time for the same accuracy) than the FEM. A similar study has been carried out in [51] for visco-elastoplasticity by the NS-FEM using both triangular (NS-FEM-T3) and tetrahedral (NS-FEM-T4) meshes.

5.1.3 Hyperelasticity and Applications in Biomechanics

Since the NS-FEM has the properties of strong softening effects and volumetric locking free, it is attractive to deal with volumetric locking, especially for hyperelastic materials. However, pure NS-FEM-T3 shows oscillation phenomena, which leads to the divergent iterative solving process [204]. This instability during large deformation can be explained by eigenvalue analysis for the tangent stiffness, which is essentially the same as the temporal instability with spurious non-zero eigenmodes for dynamics problems [144]. Therefore, the combination of edge-based smoothing techniques or even FEM with the NS-FEM has been proposed to stabilize the system, such as the selective ES/NS-FEM or FS/NS-FEM, αFEM, and βFEM. In [204], Zhang and Liu formulated the nonlinear forms for NS-FEM, ES-FEM and αFEM based on the total Lagrangian formulation. The performances of these methods are compared by numerical examples of compressible Neo-Hookean materials. Later on Jiang et al. extended and implemented the selective FS/NS-FEM and 3D-ES/NS-FEM under the framework of explicit time integration for analysis of extremely large deformation of incompressible isotropic materials and anisotropic incompressible bio-tissues [35, 205, 207].

Figure 8 shows the deformed configurations of a bonded rubber block with nearly-incompressible Mooney–Rivlin hyperelastic material model under torsion. The analysis procedure automatically stops while $J = \det(\mathbf{F}) \leq 0$

appears, which will yield unphysical strain energy due to the excessively element distortion. The second order FEM-T10 with reduced integration (FEM-T10-SRI) stops when the torsion reaches $\theta = 1.14\pi$ shown in Fig. 8a, while the FS/NS-FEM-T4 reaches much larger torsion deformation with $\theta = 2.15\pi$ as illustrated in Fig. 8b. Figure 9 plots the displacement and Von Mises stress distributions of a left rabbit ventricle filled with 30 mmHg blood pressure. The rabbit ventricles with anisotropic Holzapfel–Gasser–Ogden (H–G–O) model was meshed with 19,677 elements and 4328 nodes and the results show the FS/NS-FEM-T4 matches well with the FEM-T10-SRI.

Onishi and Amaya [206] proposed a locking-free selective smoothed finite element method with adaptive mesh rezoning (2D ES/NS-FEM-T4 and 3D FS/NS-FEM-T4) for static implicit analysis of large deformation problems based on the total Lagrangian formulation. Similar to [35, 205, 207], the μ/λ split formulation in the original selective S-FEM [16] was updated by the split of deviatoric and volumetric parts, in order to avoid locking issues in modeling nonlinear materials. In the example shown in Fig. 10, a displacement controlled tensioning along the horizontal direction is performed on a filler particle composite. The selective ES/NS-FEM-T3 with mesh rezoning

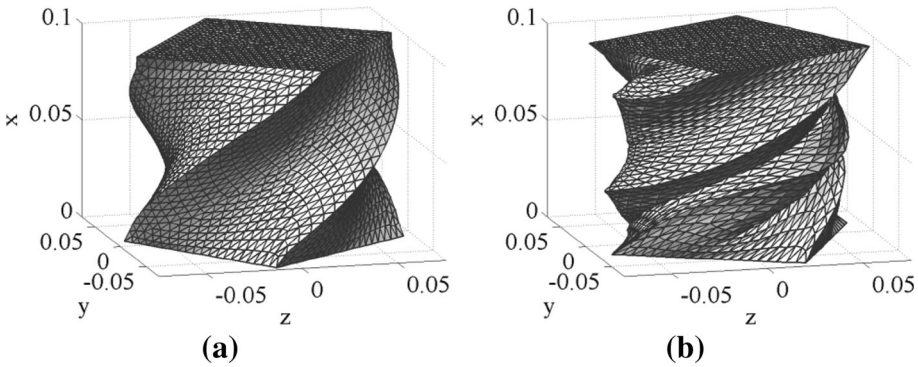

Fig. 8 Final deformed configurations for modeling of a bonded rubber block with 65,224 elements under torsion: **a** the torsion reaches $\theta = 1.14\pi$ obtained by FEM-T10-SRI and **b** the torsion reaches $\theta = 2.15\pi$ obtained by FS/NS-FEM-T4 (from [205])

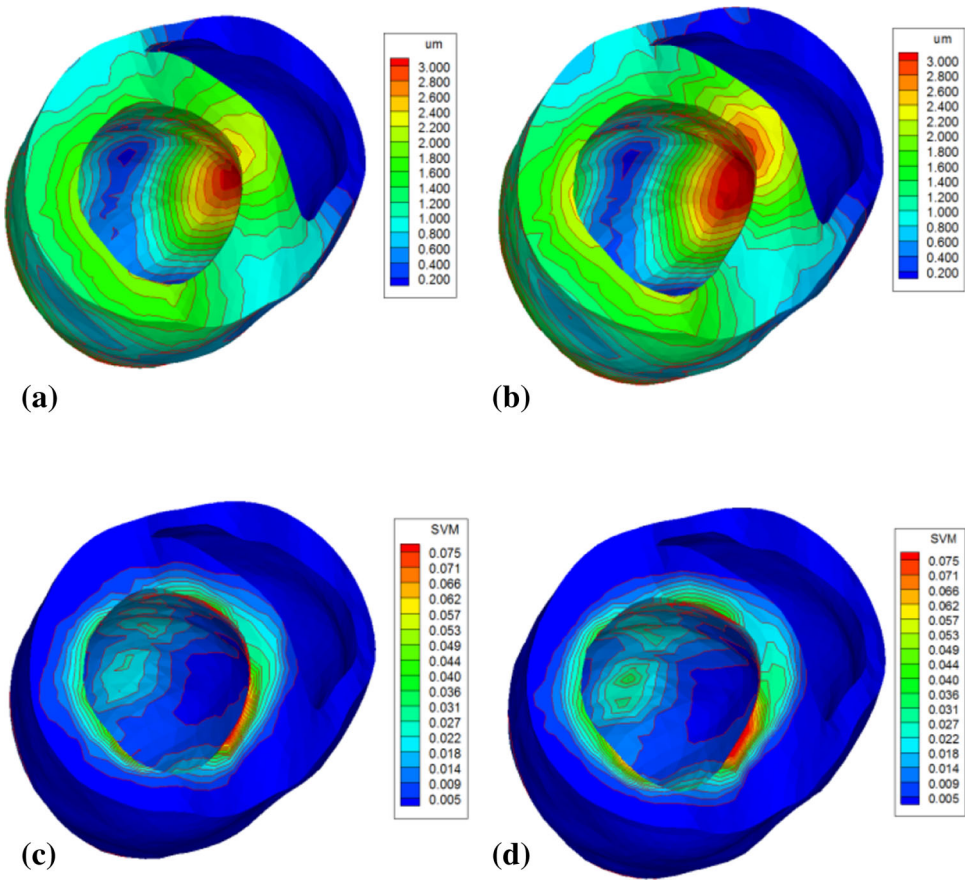

Fig. 9 Simulation of rabbit ventricles in diastole (30 mmHg LV pressure): **a** contour of displacement obtained by FS/NS-FEM-T4 (max value: 3.146 mm), **b** contour of displacement obtained by FEM-T10-SRI (max value: 3.526 mm), **c** contour of von Mises stress (MPa) obtained by FS/NS-FEM-T4 (max value: 0.0778 MPa) and **d** contour of von Mises stress (mPa) obtained by FEM-T10-SRI (max value: 0.0906 MPa) (from [207])

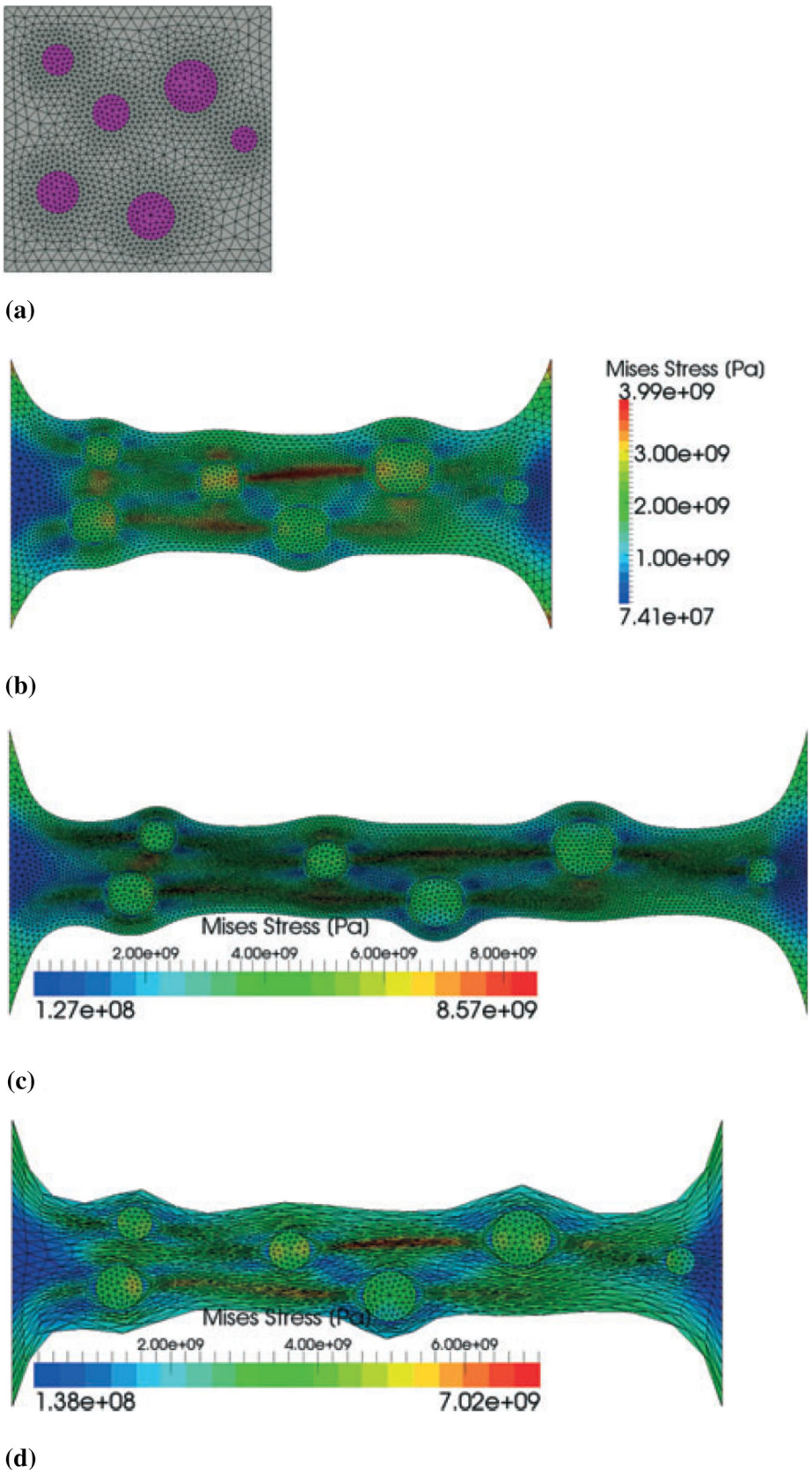

Fig. 10 Contours of von Mises stress on deformed configurations of the filler particle composite tension analysis. The analysis with mesh rezoning in (**b**) and (**c**) lasted further with 4-times and 8-times mesh rezonings, respectively. In (**d**), the computation fails due to excessively element distortion without mesh rezoning (from [206]). **a** Initial mesh: *gray area* represents soft matrix, *pink area* represents hard filler particles. **b** 100% nominal stretch through 4 times of mesh rezoning. **c** 180% nominal stretch through 8 times mesh rezoning. **d** 147% nominal stretch without any mesh rezoning. (Color figure online)

is compared with the analysis without mesh rezoning. Onishi et al. [208] also combined the *F*-bar method with ES-FEM-T4 to formulate a method named "*F*-barES-FEM-T4" to suppress pressure oscillation for nearly incompressible solids.

Duong [225] employed the FS-FEM for simulation of stress-driven isotropic and transversely isotropic growth for soft tissues. Li et al. applied S-FEM models into analyses of elastography problems [210] and modeling multi-layer biomaterial systems [209], such as human tooth, mucosal tissue and spinal disk. These applications utilized some good numerical features of different S-FEM models, including the promising accuracy when using T-mesh to capture the anatomical details of bio-structures and immunity of volumetric locking for incompressible soft tissues.

5.1.4 Crystal Plasticity Modeling

In view of the plastic incompressibility of single crystals, it is very necessary to use appropriate numerical approaches to resolve the volumetric locking issue. Because of the poor performance of the standard FEM in treating large strain problems of nearly incompressible solid, the S-FEM models become a potential tool for modeling crystal plasticity. On the other hand, to generate meshes for polycrystalline samples with a large collection of grains in arbitrary complex shapes, triangular and tetrahedral elements are the best option for mesh generation. Therefore, the S-FEM models with T-meshes are very appealing in crystal plasticity simulations.

Zeng et al. [65] developed a computational framework of S-FEM for modeling crystalline plasticity at finite strains. The conceived βFEM with mixed smoothing techniques was also applied to modeling crystal plasticity [36]. The single crystalline strain localization and shear band development are consistent with literature, in which special elements such as *Q1E4* elements or *F*-bar elements are utilized. Figure 11 shows the application of βFEM in the necking and asymmetrical localization of an f.c.c. single crystal under vertical tension. The proposed numerical algorithms have been also implemented to

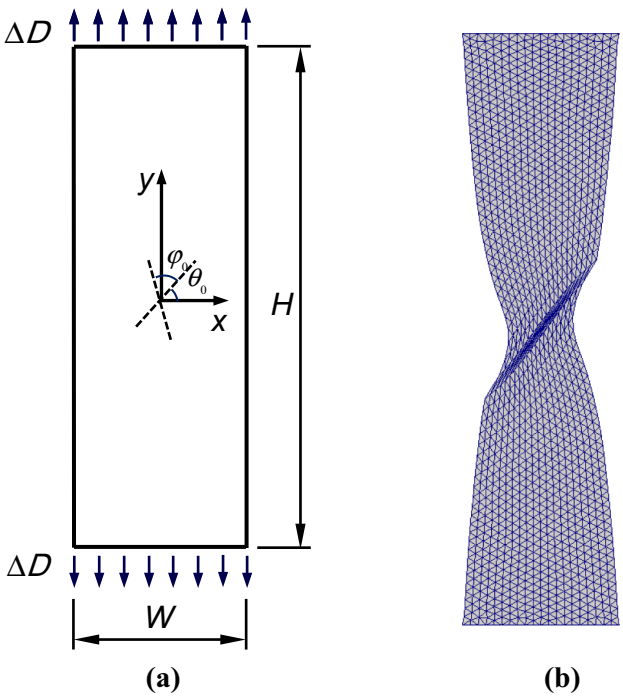

Fig. 11 Asymmetrical localization of a crystalline strip ($W/H = 20$ mm/60 mm) under vertical tension: **a** geometrical dimensions and initial crystal orientations ($\theta_0 = 45.0°$ and $\phi_0 = 60.0°$) and **b** final deformed configuration at $\Delta D = 8.0$ mm (from [36])

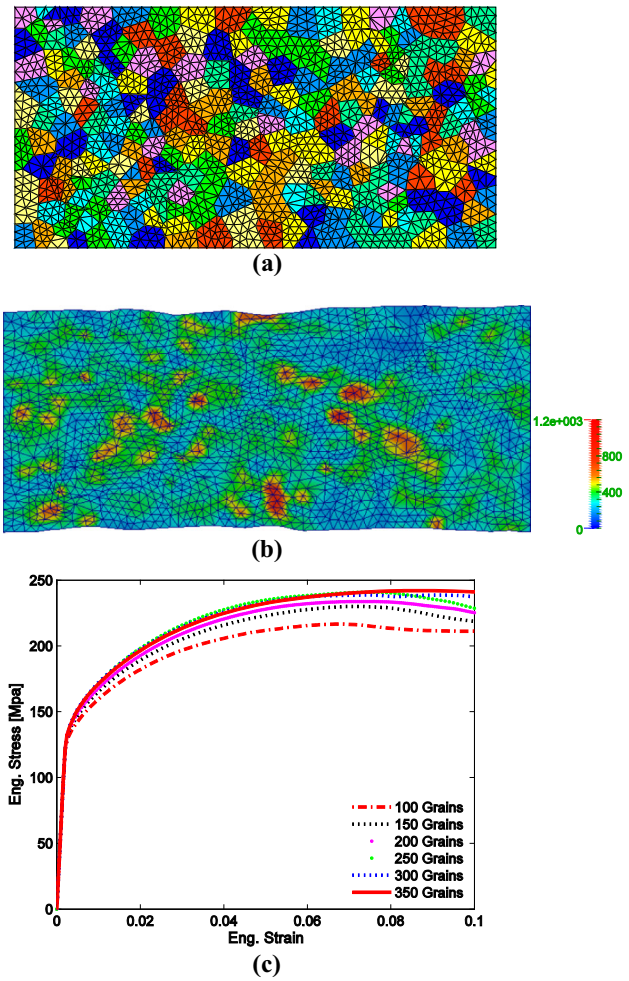

Fig. 12 Simulation of polycrystalline stretch using S-FEM: **a** a representative grain structure with 250 cells generated by Voronoi Tessellation, **b** the equivalent stress (MPa) distribution on the deformed configuration and **c** the equivalent stress–strain curves of different grain structures with 100, 150, 200, 250, 300 and 350 grain cells, respectively (from [65])

simulate the mechanical behavior of polycrystalline aggregates through modeling the synthetic microstructure constructed by Voronoi tessellation technique [65]. In Fig. 12, a specimen with the dimension $W = 800$ μm and $H = 400$ μm is constrained on the left edge and stretched up to 10% total length in the horizontal direction. Figure 12a illustrates a representative microstructure with 250 random grain cells, where varied color shows a number of randomly distributed grains with different initial lattice orientations. The local equivalent stresses are up to almost 500% of macroscopic nominal equivalent stress in Fig. 12b. The equivalent stress–strain curves with six different virtual grain microstructures in Fig. 12c shows the convergence of macroscopic response.

5.2 Fracture Mechanics and Fatigue Behavior

The exploitation of S-FEM in fracture mechanics was mainly based on its higher accuracy than standard FEM, especially when making use of the T-mesh for domain discretization. To capture the singularity feature without the loss of the essential properties, some singular triangular or tetrahedral elements can be formulated within the framework of T-mesh based S-FEM models. This can be completed in a number of ways Chen et al. [121] created a five-node singular crack tip element, which sets an additional node on each of two edges of elements connected directly to the crack tip while linear T3 element mesh was preserved. The approach combined with the ES-FEM was firstly applied to solve problems with mix-mode interface cracks between two dissimilar isotropic materials [121, 128] and then updated to evaluate the stress intensity factors or energy release rates of anisotropic materials [126]. Liu and his co-workers have carried out the concept of singular elements [136] in fracture mechanics for better accuracies in several aspects: (1) combining with the NS-FEM for calculation of the upper bound solutions for fracture parameters [122]; (2) quasi-static crack growth simulation [125] and fatigue analysis with adaptive re-meshing procedure [130, 131, 134]; (3) seven-node singular element, which had a displacement field containing the HRR term and the 2nd-order term, for plastic fracture mechanics [127]; (4) three dimensional elastic fracture mechanics [34]; (5) stationary dynamic crack problems in 2D linear elastic solids [132]; (6) thermoelastic crack problems [140]. Figure 13 shows the crack propagation in a cruciformplate with a corner crack under thermal and mechanical loading conditions. It is evident that the thermal and mechanical conditions boundary/loading conditions affect the trajectories of crack growth.

The S-FEM has also been incorporated with extended finite element method (X-FEM) for analyzing fracture problems. Chen et al. introduced the edge-based strain smoothing technique into the context of XFEM to formulate an edge-based smoothed extended finite element method (ES-XFEM [129] or ESm-XFEM [32]). It takes the advantages of both the ES-FEM and XFEM: improves the accuracy for evaluating stress intensity factors and excludes from mesh alignment with the crack line(s) and re-meshing during crack growth.

Similar work, which combines the node-based strain smoothing technique with X-FEM, was presented in [31]. Jiang et al. adopted the ES-XFEM to analyze the delamination of the composite plate under compression [133] and also extended the idea into 3D fracture problems (termed as FS-XFEM) for linear elastic solids [138]. Wu et al. [141] applied the ES-XFEM for dynamic fracture analysis of 2D elastic media. In addition, Zeng et al. [139] proposed an effective fracture analysis method for stress intensity factor evaluation and prediction of crack propagation, which is based on the virtual crack closure-integral technique implemented in CS-FEM. Figure 14 shows the predicted crack propagation path of a polymethy methacrylate (PMMA) beam with three rivet holes subjected to a concentrated loading on the middle of the upper edge. Vu-Bac et al. [135] combined the ES-FEM with a phantom-node method for 2D linear elastic fracture mechanics.

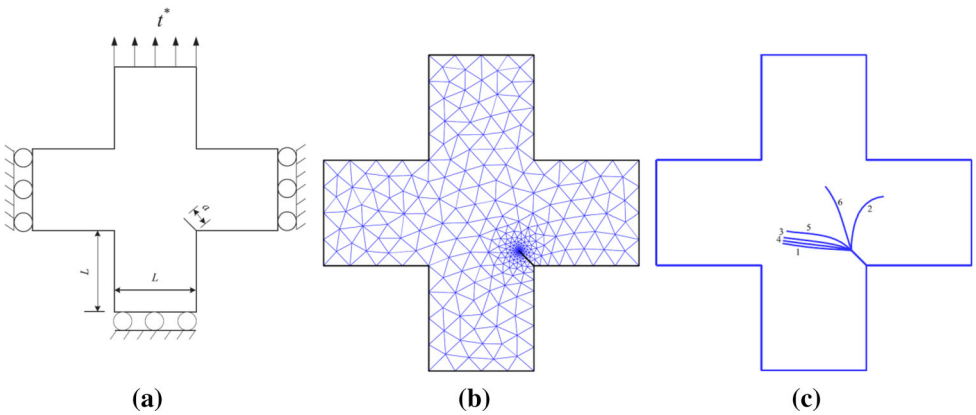

Fig. 13 Cruciform plate with a corner crack under thermal and mechanical loading conditions: **a** geometry and boundary conditions, **b** initial mesh and **c** the final crack paths referred to different boundary/loading conditions (from [140])

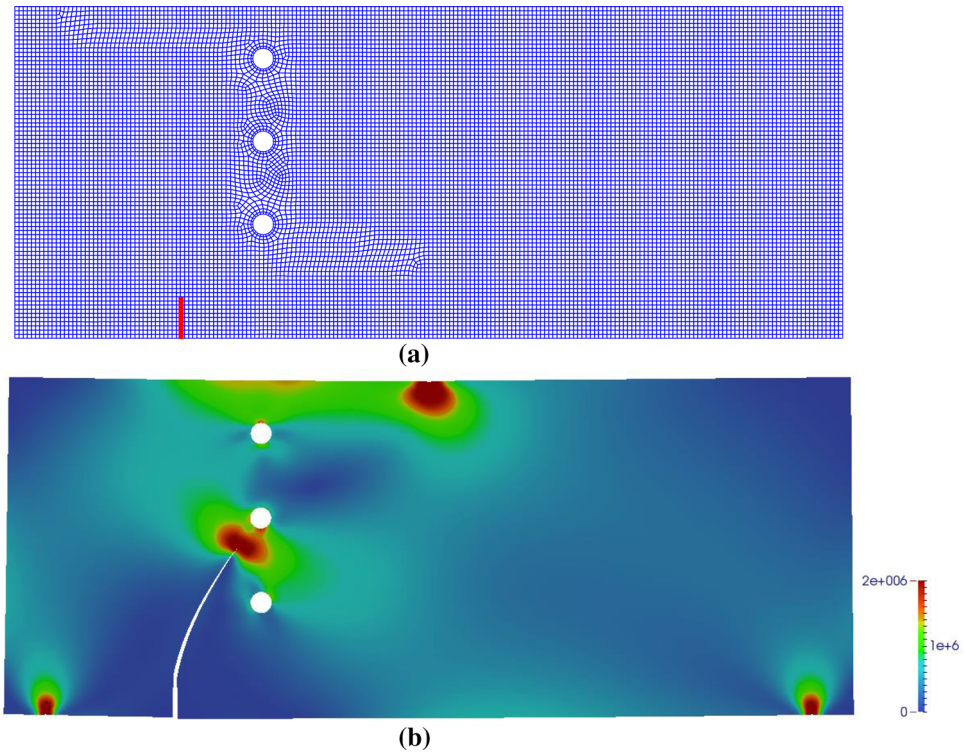

Fig. 14 Crack propagation modeling for PMMA beam: **a** initial mesh with edge crack (from [139]) and **b** final crack path and von Mises stress field with zoomed deformation

5.3 Plates, Shells, Membranes and Composite Structures

The lower-order Mindlin–Reissner plate and shell finite elements have often been preferred and intensively used because of their simplicity and efficiency. It is well known that the shear locking phenomena exist as the plate thickness decreases. In order to alleviate or eliminate this issue and increase accuracy and stability, a number of approaches and formulations have been proposed [84]: (1) strongly enforcing the Kirchhoff constraint by the high-order *p* or *hp* methods [243]; (2) weakly enforcing the Kirchhoff constraint implemented through a modified variational formulation, including the mixed formulation/hybrid elements [8, 244, 245], the assumed natural strain (ANS) method [246–248], enhanced assumed strain (EAS) method [249, 250] and the discrete shear gap (DSG) technique [251]; (3) reduced and selective integration elements [252–254].

A few kinds of S-FEM models were recently developed to overcome transverse shear locking and membrane locking due to mesh distortion. Firstly, Nguyen-Xuan et al. [66] proposed a quadrilateral plate element for static and free vibration analysis of plates. It was named as mixed interpolation and smoothed curvature (MISCk) element [68], which was inspired by the cell-based smoothing technique and MITC (mixed interpolation of tensorial components) or Bathe–Dvorkin element [66, 147]. Then they introduced a four-node quadrilateral shell element with smoothed membrane strain and bending strains based on Mindlin–Reissner theory [67, 76]. Baiz et al. [73] demonstrated a linear bucking analysis of cracked plates by a quadrilateral element with smoothed curvatures and X-FEM, which also utilized the MITC approach to eliminate shear locking. Meanwhile, Cui et al. [19] investigated the linear and geometrically nonlinear behaviors of plates and shells through employing the elements using fewer smoothing cells in the shear term than those in the bending and membrane terms. Later on Cui et al. incorporated the discrete shear gap (DSG) technique with the ES-FEM to mitigate the shear locking effect in statics of arbitrary thin to moderately thick plates and shells [69, 105]. Zheng et al. [75] presents an ES-FEM shell element with DSG technique for material nonlinear analysis of shell structures using an updated Lagrangian explicit algorithm. A similar study was presented for free vibration and buckling analyses of plates in [70]. Figure 15 compares the computational cost of different methods for a square plate clamped along four edges. It has reference solutions for the normalized deflection and the normalized moment at the center of square. Though the computation time of ES-DSG3 is little larger than other three methods, its efficiency of computation (CPU time vs. relative error in energy norm) is obviously the best in all these methods. After that, the DSG technique together with a stabilization technique is incorporated into the NS-FEM [71], alternative alpha FEM (AαFEM) [74], CS-FEM [77] with triangular elements. A number of applications by combinations or

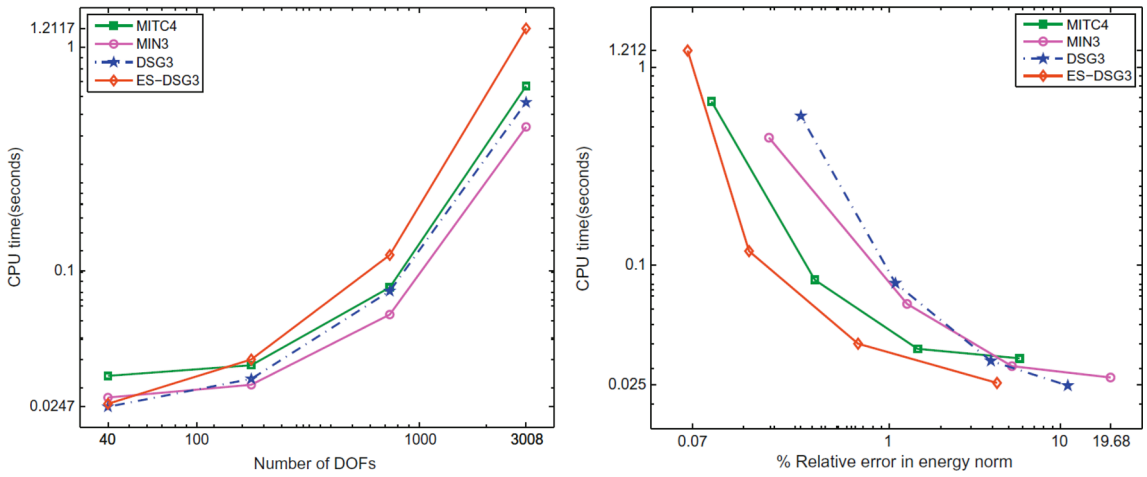

Fig. 15 The computational cost of different methods for clamped square plate: **a** CPU time and **b** computation efficiency in terms of relative energy error norm (from [70])

variations of these approaches have been carried out by Nguyen-Xuan, Nguyen-Thoi and their co-workers [79–83, 87, 88, 91–93, 96–99, 102, 106–109, 111, 112, 255], including stiffened plates, flat shells, composite plates, FGM plates, piezoelectricity plates, and dynamic responses of plates resting on the viscoelastic foundation. Zhang and Liu [72] analyzed 3D spatial membrane structures under large deflection, rotation, and strain, by performing the edge-based gradient smoothing for T3 membrane element in global coordinates.

Additionally, to improve the accuracy of the solutions for the static, dynamic and geometrically nonlinear responses of plates, Nguyen-Thoi and co-investigators formulated a smoothed three-node Mindlin plate element by cell-based strain smoothing operation (CS-MIN3) [78, 85, 86, 90, 95, 101, 103] and edge-based strain smoothing operation (ES-MIN3) [89]. Natarajan et al. [110] studied the static bending and the free vibration of laminated plates by the Carrera's unified formulation (CUF) implemented in CS-FEM. It was further extended by Rodrigues et al. [113] through combination of the 4-noded MITC to improve the accuracy. Herath et al. [114] presented a genetic algorithm (GA) optimization scheme by CS-FEM to design composite marine propeller blades. Élie-Dit-Cosaque et al. [94] applied the cell based smoothing operation into eight node resultant solid-shell element for evaluation of the membrane and bending element stiffness during geometrical linear analysis. Li et al. [115, 256] applied the selective S-FEM to alleviate the volumetric locking issues for numerical homogenization of incompressible base materials with multi-material domain.

5.4 Vibration Analysis and Acoustic Problems

The original SFEM (termed as CS-FEM later) and alternative alpha finite element method (AαFEM) were applied to analyze free and forced vibrations and they were reported to generate more accurate results and higher convergence rate than the standard FEM [14]. Yang et al. [152] presented a novel integration scheme for calculating consistent mass matrix implemented in CS-FEM for free and forced vibration analysis. To alleviate the temporal instability of vibration analysis existed in NS-FEM, a stabilization technique for the NS-FEM was proposed by Zhang and Liu [144] and extended for 3D free vibrations in [151]. A smoothed squared-residual of the equilibrium equation as a stabilization term is added into the smoothed potential energy functional for the original NS-FEM [144]. They also utilized the αFEM to evaluate the upper and lower bounds of the natural frequencies for free vibration problems [145]. The ES-FEM was also proposed to eliminate the temporal instability of vibration analysis in NS-FEM and it performs stable and significantly more accurate than the FEM using quadrilateral elements [22]. For 3D modal analysis, the FS-FEM and 3D ES-FEM was applied to more accurately predict eigenfrequencies and mode stress [52, 148]. Besides, the n-sided polygonal cell-based smoothed finite element method (*n*CS-FEM) was extended to 2D free and forced vibration analyses in [150]. A modified S-FEM using Q4 elements, similar to the idea of CS-FEM using a single cell, was recently proposed by Cui et al. [153] for solving free vibration problems with lower computation costs.

For acoustic problems governed by the Helmholtz equation, it often suffers from the "pollution effect" with

increasing non-dimensional wave number k [257, 258], which is directly related to the "numerical dispersion" errors and accuracy deterioration of the solutions. Much work has been carried out to reduce the dispersion error, including the Galerkin/least-squares FEM [259, 260], quasi-stabilized FEM [261], partition of unity finite element method (PUFEM) [262], the wave envelope method [263], the residual-free finite element method (RFFEM) [264], ultra weak variational formulation (UWVF) [265], element-free Galerkin method (EFGM) [266], the discontinuous enrichment method [267], p-version FEM [268, 269], and the coupled Element-Free Galerkin method with a modified conjugated infinite element (EFGM–CIE) [270]. Though these approaches can reduce or eliminate numerical dispersion error caused by overly-rigid stiffness, their computation costs are relatively expensive. Since the ES-FEM and FS-FEM can provide desired softening effect of stiffness and higher accuracy than standard FEM, they have been employed to acoustic analysis for reduction of the numerical dispersion error, especially in the problems with high wave numbers.

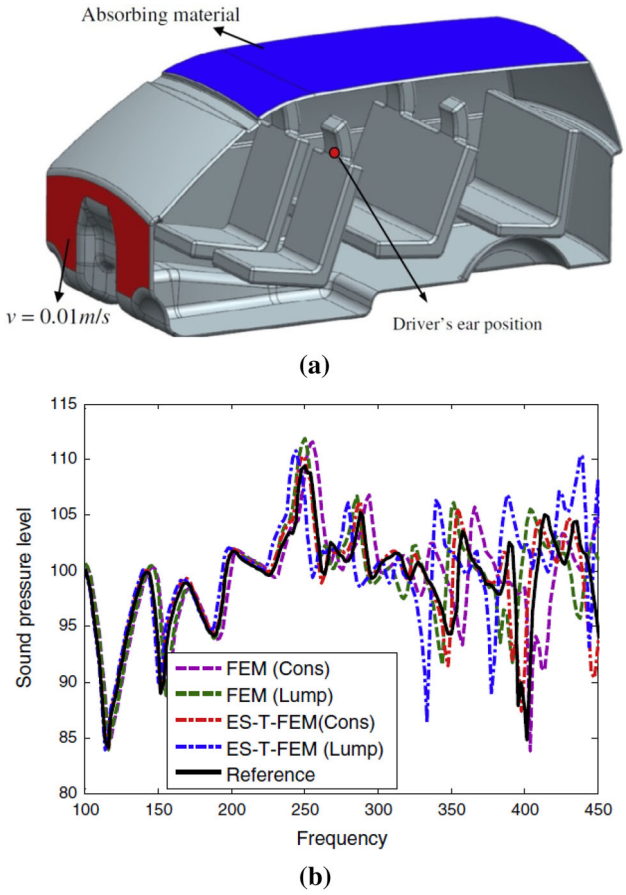

Fig. 16 Predictions of acoustic frequency response at the location of driver's ear for a 3D minivan: **a** problem domain and boundaries and **b** acoustic frequency response (sound pressure level) obtained by ES-T-FEM and FEM using consistent mass matrix or lump mass matrix (from [161])

He et al. [21] applied ES-FEM for solving both 2D and 3D acoustic problems, in which the ES-FEM behaves less sensitive to the wave number and mesh quality and predicts frequency response much better than the standard FEM. He et al. and Li et al. [159] utilized ES-FEM and FS-FEM (or FEM) to structural–acoustic analysis, in which a 2D flexible plate (solved by ES-FEM with DSG technique) is interacted with the 3D acoustic fluid (solved by FS-FEM [29] or FEM [155]). Similar work was extended to the structural–acoustic coupling analysis of shells [166]. To reduce dispersion errors, a few studies employed CS-FEM [156, 271], αFEM [154, 164], ES-FEM [157] NS-FEM [165] and mass-redistribution technique [161, 163] for acoustics, including the 3D mid-frequency acoustic problems [158]. In Fig. 16, the mid-frequency range acoustic response at the location of driver's ear in a minivan was studied [161]. It showed the most accurate result of sound pressure level was achieved by the ES-T-FEM (i.e., 3D ES-FEM) with consistent mass matrix, especially for the frequency >300 Hz. Some hybrid approaches based on smoothing techniques have also been proposed for solving acoustic problems. For example, Li et al. and Chai et al. presented a similar Hybrid S-FEM (HS-FEM) for acoustic analysis for structural–acoustic interaction [160], 2D under water acoustic scattering [167] and 2D acoustic radiation problems [168]. However, the idea of their strain smoothing technique was the same as the αFEM. Wu et al. proposed a hybrid FS-FEM/statistical energy analysis (FS-FEM/SEA) approach and a hybrid FS-FEM/statistical energy analysis (ES-FE-SEA) approach to improve the accuracy of solving the vibro-acoustic system [162] and prediction of transmission loss [169] in the mid-frequency regime, respectively.

5.5 Piezoelectric Structures and Photonic Devices

Because of the features of insensitivity to mesh distortion and higher accuracy even using T-mesh, the S-FEM has been formulated for piezoelectric materials. Nguyen-Van et al. [186] presented a four-node quadrilateral piezoelectric element SPQ4 for linear analysis of 2D piezoelectric problems, which is essentially the same as the CS-FEM. They also studied similar piezoelectric problems by NS-FEM using both triangular and quadrilateral elements [187]. Nguyen-Xuan et al. [188] extended the edge-based smoothing technique for mechanical strains and electric fields for more accurate analysis of 2D piezoelectric structures. To pursue higher computational efficiency and accuracy, Olyaie et al. employed the CS-FEM in reliability based topology optimization of a linear piezoelectric microactuator [189] and deterministic topology

optimization (DTO) for a linear piezoelectric micromotor [190]. The stabilization technique utilized in [144] was extended to NS-FEM for frequency analyses of piezoelectric structures by adding terms to stabilize both mechanical stress equilibrium and electric displacement equilibrium [191]. The hybrid S-FEM (same as αFEM) was used for piezoelectric structures in [192]. In addition, the ES-FEM was adopted with the time domain beam propagation method (TD-BPM) to analyze photonic devices in time domain, which showed the ES-FEM has comparable accuracy to the second order FEM [193].

5.6 Heat Transfer and Thermo-mechanical Problems

The primary field variable for heat transfer problems is temperature (scalar field), which is different from the vector fields (displacements) for solid mechanics. Li et al. [174] formulated bioheat transfer models using 2D ES-FEM and 3D FS-FEM to predict the temperature field of tissue for hyperthermia treatment of breast cancer. Compared to FEM, the S-FEM results have higher accuracy, especially at high temperature gradient region. Kazemzadeh-Parsi and Daneshmand [173] presented a smoothed fixed grid FEM using cell-based smoothing technique. It solves the nonlinear inverse geometry heat transfer problems with known temperatures along the external boundary and un-knowns of the location and shape of a cavity inside the domain. In [175], a fixed grid αFEM formulation is introduced to model phase change and temperature field in cryosurgery of liver tumor. A general formulation of the S-FEM for thermal problems in different dimensions was summarized in [177]. Li et al. [183] used the hybrid S-FEM for accurate modeling of temperature distribution for 2D heat conduction and 3D heat convection and radiation problems. Later on, a generalized mass formulation by changing integration points for evaluating mass matrix was formed with S-FEM in the explicit framework of transient heat and mass transport analysis [272]. Cui et al. [185] performed steady and transient heat transfer analysis by a stable NS-FEM (SNS-FEM). As both the smoothed temperature gradient and the variance of temperature gradient in each smoothing domain are considered, it eliminates the "under-integration" of the weak form and temporal instability of the NS-FEM.

Kumar [176] studied the thermo-mechanical impact problems using CS-FEM by implementation with a visco-plastic constitutive model. Feng et al. utilized the 2D ES-FEM and 3D FS-FEM for analysis of transient thermo-elastic problems with better accuracy and higher convergence, in which both the stress field and its input of the transient temperature field were evaluated by the S-FEM [178–180, 182, 184]. In [181], the 3D ES-FEM was also employed for heat transfer and thermos-mechanical problems. It showed the 3D ES-FEM could provide better accuracy and computational efficiency than FEM and FS-FEM.

5.7 Fluid–Structure Interaction Simulations

The study of fluid–structure interaction (FSI) problems with movable or deformable structures stands as a challenging and rapidly evolving part of engineering sciences because of their strong nonlinearity and multidisciplinary nature [273]. Compared with analytical models, numerical simulation becomes indispensable for sophisticated and complicated FSI problems, along with the continuous development of computational capacities and numerical techniques. Based on the treatment of meshes, the FSI problems can be classified into two types: moving-mesh method (e.g., arbitrary Lagrangian–Eulerian methods (ALE) and spacetime (ST) method) and the immersed-type methods. As a class of non-conforming mesh methods, the fluid–structure interface in the immersed-type methods is allowed to cut cross the fluid grid/mesh. Thus they have been extensively used for investigating a wide variety of FSI problems.

As inspired by the immersed boundary (IB) method and immersed FEM (IFEM) methods, Zhang et al. proposed an immersed smoothed FEM (IS-FEM) for both 2D and 3D FSI problems with largely deformable nonlinear solids placed within the incompressible viscous fluid governed by Navier–Stokes equations [30, 195, 197]. For the fluid flows, the IS-FEM utilized the semi-implicit characteristic-based split scheme. The transient responses of nonlinear solids were solved by S-FEM under the framework of explicit time integration. The proposed algorithm can provide second-order spatial convergence with independence of a wide range of mesh size ratio. Figure 17 shows the contours of the fluid velocity in vertical direction and the fluid pressure in neutral slice plane ($x_1 = 0$) for a solid sphere falling into a cylinder tank filled with incompressible viscous fluid. Three cases with different boundary and initial conditions are considered (the details can be checked in [161]). Yao et al. [196] used the IS-FEM for FSI simulation of aortic valves with idea shapes, in which the blood is considered to be incompressible viscous flow and leaflets of aortic valve were assumed as Mooney–Rivlin hyperelastic material. The simulation results (velocity, pressure and configurations) on a symmetry plane of the leaflets within fluid were captured at three time moments, as depicted in Fig. 18.

He et al. [194] introduced a coupled ES-FEM/BEM formulation for analysis of acoustic fluid–structure interaction problems, in which the plate structure is solved by the ES-FEM and the acoustic fluid is solved using

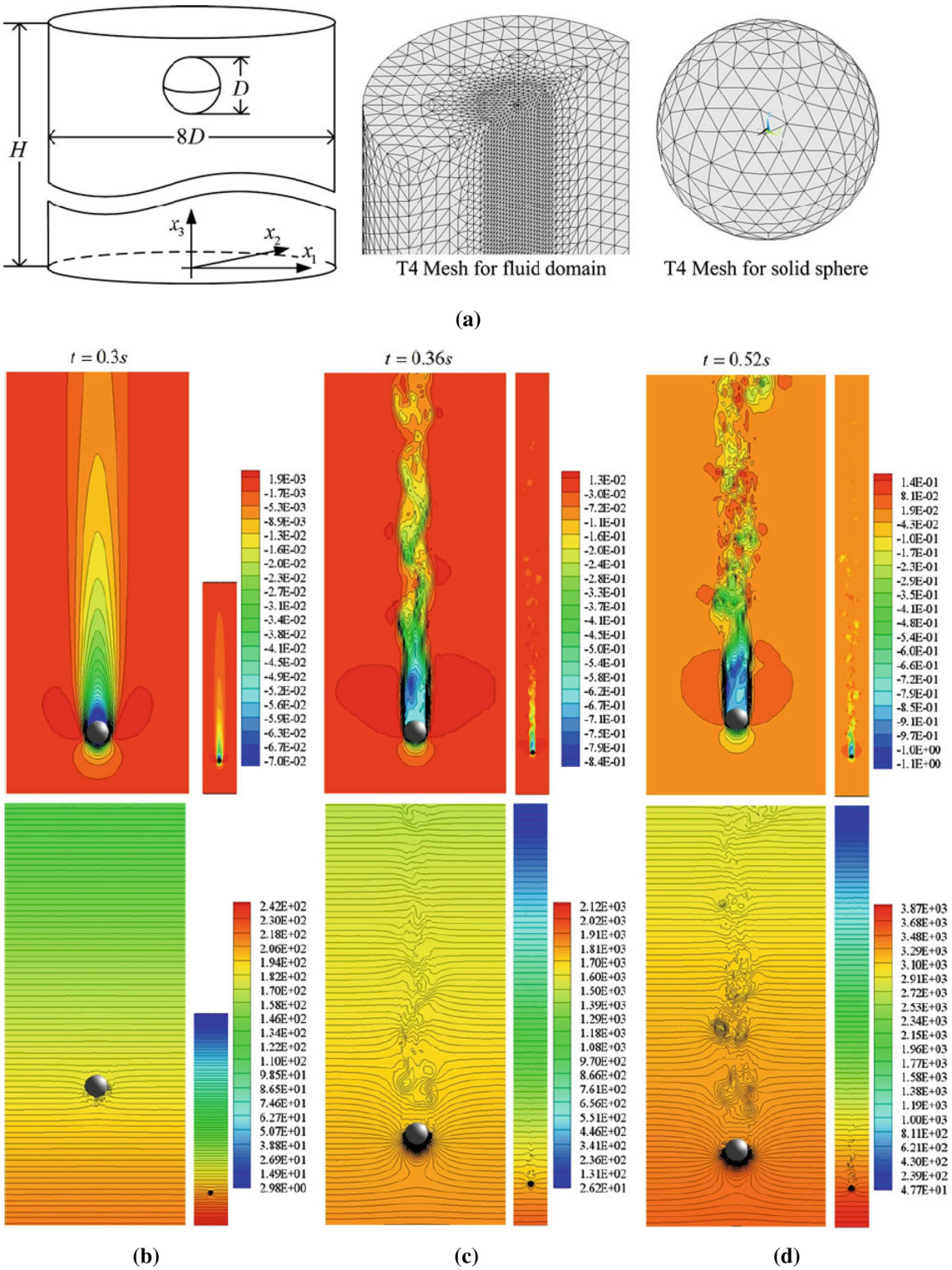

Fig. 17 A sphere falling inside the viscous fluid medium under gravity: sketch of geometry and mesh (**a**), and contours of the fluid velocity in vertical direction (*top view*) and the fluid pressure distributions (*bottom view*) in neutral slice plane $x_1 = 0$ for the three different cases (**b–d**) (from [195])

boundary element method (BEM). Nguyen-Thoi et al. studied 2D FSI problems based on the pressure–displacement formulation, using the ES-FEM for the structure and the FEM [198] or ES-FEM [274] for the fluid media. They also proposed a coupled NS/*n*ES-FEM for dynamic analysis of 2D FSI problems, which utilizes the *n*-sided

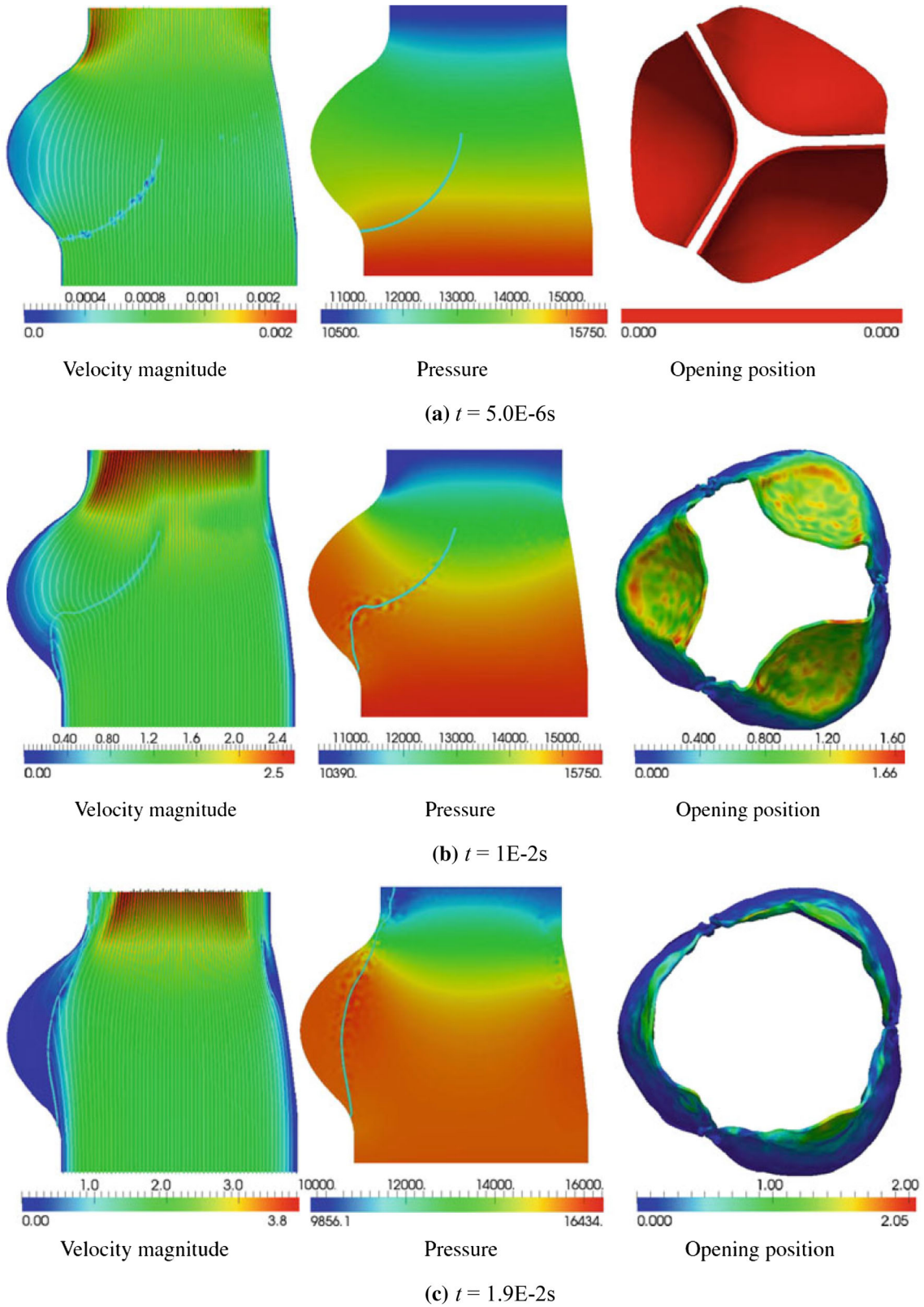

Fig. 18 Snapshots of FSI simulation using IS-FEM for aortic valves: distribution of velocity (with stream lines on slice) and pressure on a symmetry plane of the valve and corresponding configurations of leaflets opening at different time moments (from [196])

polygonal ES-FEM (*n*ES-FEM) to smooth the gradient of displacement for solid and the NS-FEM-T3 to smooth the gradient of pressure for fluid domain [200]. Similar applications were implemented using αFEM-T3 ($\alpha = 0.6$) with both the gradient of pressure and gradient of displacement smoothed by αFEM technique [201]. Based on the weak coupling algorithm, Wang et al. [199] coupled the arbitrary Lagrangian–Eulerian gradient smoothing method (GSM/ALE, for fluid) and the ES-FEM-T3 (for solid) to solve fluid–deformable solid interaction problems. The benchmark examples have shown that results are more sensitive to the mesh size of solid than fluid, thus it recommends that finer mesh should be adopted for the solid domain, especially near the FSI interface region. He introduced some coupling algorithms with CS-FEM and FEM for FSI between a geometrically nonlinear solid and the incompressible fluid media, where the CS-FEM was used for solving the geometrically nonlinear solid [202, 203].

6 Summary and Concluding Remarks

In the field of numerical analysis, mesh or grid based approaches, especially the displacement FEM models, are the most popular and successful computational tools for mechanics and engineering problems. However, it has been found that the standard FEM has some limitations or inherent drawbacks which limit its capability such as the overestimation of stiffness matrix and resultant inaccuracies. Also, the generation of appropriate mesh is a burdensome task, which may need sophisticated preprocessors for problems with complex geometry. The class of S-FEM models reviewed in this work provides an option to reduce both numerical and meshing errors during approximation, since most of S-FEM models works well with T-mesh.

The general formulations, such as the gradient smoothing operation and techniques for strain smoothing, have been briefly summarized. As shown in Sect. 2, based upon the different strain smoothing approaches, these S-FEM models can be generally divided into a few categories: CS-FEM, NS-FEM, ES-FEM, FS-FEM, Selective S-FEM, αFEM, βFEM, and other variations. The features and properties of these different types of models are discussed, in which some of these models with coupling features have been proposed due to the complementary properties of different strain smoothing approaches, i.e., for the purpose of strengthening some advantages and avoiding related drawbacks. In addition to the general formations a few theoretical aspects of S-FEM have been recapitulated in Sect. 4. The emphasis was specifically given to the G space theory, key inequalities, and the weakened weak form.

In general, S-FEM has great potential in numerous problems in engineering and science [275–277]. Compared with the standard FEM, it has many advantages in creating different models in treating nonlinear material behavior, fracture mechanics, plates and shells, vibration analysis, piezoelectric structures, heat transfer and thermo-mechanical problems, as well as FSI problems. This paper is a first review paper on the overview and developments of S-FEM in the past decade. In authors' opinion, the S-FEM has already been proven to be an effective and robust numerical tool for a wide class of problems. As a valuable addition to FEM, it deserves special attention in view of the present trends in the next generation of computational methods for modeling and simulations to more complex systems in engineering and sciences.[1]

Acknowledgements This work is partially supported by US NSF Grant under the Award No. DMS-1214188.

Compliance with Ethical Standards

Conflict of interest The authors declare that they have no conflict of interest.

Ethical Approval This work does not contain any studies with human participants or animals performed by any of the authors.

Informed Consent For this type of study formal consent is not required..

References

1. Hughes TJR (1987) The finite element method: linear static and dynamic finite element analysis. Prentice-Hall, Englewood Cliffs
2. Belytschko T, Liu WK, Moran B, Elkhodary KI (2014) Nonlinear finite elements for continua and structures, 2nd edn. Wiley, West Sussex
3. Liu GR, Quek SS (2013) The finite element method: a practical course, 2nd edn. Butterworth-Heinemann, Oxford
4. Turner MJ (1959) The direct stiffness method of structural analysis, structural and materials panel paper. In: AGARD meeting—1959, Aachen, Germany
5. Liu GR (2009) Meshfree methods: moving beyond the finite element method, 2nd edn. CRC Press, Boca Raton
6. Liu GR, Zhang GY (2013) The smoothed point interpolation methods—G space theory and weakened weak forms. World Scientific, New Jersey
7. Bathe KJ (1996) Finite element procedures. Prentice-Hall, Englewood Cliffs
8. Pian THH, Wu CC (2006) Hybrid and incompatible finite element methods. CRC Press, Boca Raton
9. Liu GR (2016) An overview on meshfree methods: for computational solid mechanics. Int J Comput Methods 13(05):1630001

[1] Some basic S-FEM source code can be found at www.ase.uc.edu/~liugr.

10. Chen JS, Wu CT, Yoon S, You Y (2001) A stabilized conforming nodal integration for Galerkin mesh-free methods. Int J Numer Methods Eng 50(2):435–466
11. Liu GR, Dai KY, Nguyen-Thoi T (2007) A smoothed finite element method for mechanics problems. Comput Mech 39:859–877
12. Dai KY, Liu GR (2007) Smoothed finite element method, CE006. http://hdl.handle.net/1721.1/35825
13. Liu GR, Nguyen TT, Dai KY, Lam KY (2007) Theoretical aspects of the smoothed finite element method (SFEM). Int J Numer Methods Eng 71(8):902–930
14. Dai KY, Liu GR (2007) Free and forced vibration analysis using the smoothed finite element method (SFEM). J Sound Vib 301(3–5):803–820
15. Dai KY, Liu GR, Nguyen-Thoi T (2007) An n-sided polygonal smoothed finite element method (nSFEM) for solid mechanics. Finite Elem Anal Des 43:847–860
16. Nguyen-Thoi T, Liu GR, Dai KY, Lam KY (2007) Selective smoothed finite element method. Tsinghua Sci Technol 12(5):497–508
17. Liu GR (2008) A generalized Gradient smoothing technique and the smoothed bilinear form for Galerkin formulation of a wide class of computational methods. Int J Comput Methods 5(2):199–236
18. Liu GR, Nguyen-Thoi T, Lam KY (2008) A novel alpha finite element method (αFEM) for exact solution to mechanics problems using triangular and tetrahedral elements. Comput Methods Appl Mech Eng 197(45–48):3883–3897
19. Cui XY, Liu GR, Li GY, Zhao X, Nguyen TT, Sun GY (2008) A smoothed finite element method (SFEM) for linear and geometrically nonlinear analysis of plates and shells. CMES: Comput Model Eng Sci 28:109–125
20. Liu GR, Nguyen-Thoi T, Nguyen-Xuan H, Lam KY (2009) A node-based smoothed finite element method (NS-FEM) for upper bound solutions to solid mechanics problems. Comput Struct 87:14–26
21. He ZC, Liu GR, Zhong ZH, Wu SC, Zhang GY, Cheng AG (2009) An edge-based smoothed finite element method (ES-FEM) for analyzing three-dimensional acoustic problems. Comput Methods Appl Mech Eng 199:20–33
22. Liu GR, Nguyen-Thoi T, Lam KY (2009) An edge-based smoothed finite element method (ES-FEM) for static, free and forced vibration analyses of solids. J Sound Vib 320:1100–1130
23. Cui XY, Liu GR, Li GY, Zhang GY, Sun GY (2009) Analysis of elastic–plastic problems using edge-based smoothed finite element method. Int J Press Vessel Pip 86:711–718
24. Nguyen-Thoi T, Liu GR, Vu-Do HC, Nguyen-Xuan H (2009) An edge-based smoothed finite element method for visco-elastoplastic analyses of 2D solids using triangular mesh. Comput Mech 45(1):23–44
25. Liu GR, Nguyen-Xuan H, Nguyen-Thoi T, Xu X (2009) A novel Galerkin-like weakform and a superconvergent alpha finite element method (SαFEM) for mechanics problems using triangular meshes. J Comput Phys 228:4055–4087
26. Liu GR, Nguyen-Thoi T, Lam KY (2009) A novel FEM by scaling the gradient of strains with factor alpha (αFEM). Comput Mech 43(3):369–391
27. Nguyen-Thoi T, Liu GR, Lam KY, Zhang GY (2009) A face-based smoothed finite element method (FS-FEM) for 3D linear and geometrically non-linear solid mechanics problems using 4-node tetrahedral elements. Int J Numer Methods Eng 78(3):324–353
28. Nguyen-Thoi T, Liu GR, Vu-Do HC, Nguyen-Xuan H (2009) A face-based smoothed finite element method (FS-FEM) for visco-elastoplastic analyses of 3D solids using tetrahedral mesh. Comput Methods Appl Mech Eng 198:3479–3498
29. He ZC, Liu GR, Zhong ZH, Cui XY, Zhang GY, Cheng AG (2010) A coupled edge-/face-based smoothed finite element method for structural acoustic problems. Appl Acoust 71:955–964
30. Zhang ZQ, Yao J, Liu GR (2011) An immersed smoothed finite element method for fluid–structure interaction problems. Int J Comput Methods 8(04):747–757
31. Vu-Bac N, Nguyen-Xuan H, Chen L, Bordas S, Kerfriden P, Simpson RN, Liu GR, Rabczuk T (2011) A node-based smoothed XFEM for fracture mechanics. CMES: Comput Model Eng Sci 73:331–356
32. Chen L, Rabczuk T, Bordas SPA, Liu GR, Zeng KY, Kerfriden P (2012) Extended finite element method with edge-based strain smoothing (ESm-XFEM) for linear elastic crack growth. Comput Methods Appl Mech Eng 209:250–265
33. Nguyen-Xuan H, Liu GR (2013) An edge-based smoothed finite element method softened with a bubble function (bES-FEM) for solid mechanics problems. Comput Struct 128:14–30
34. Zeng W, Liu GR, Kitamura Y, Nguyen-Xuan H (2013) A three-dimensional ES-FEM for fracture mechanics problems in elastic solids. Eng Fract Mech 114:127–150
35. Jiang C, Zhang Z-Q, Liu GR, Han X, Zeng W (2015) An edge-based/node-based selective smoothed finite element method using tetrahedrons for cardiovascular tissues. Eng Anal Bound Elem 59:62–77
36. Zeng W, Liu GR, Li D, Dong XW (2016) A smoothing technique based beta finite element method (βFEM) for crystal plasticity modeling. Comput Struct 162:48–67
37. Liu GR (2009) On G space theory. Int J Comput Methods 06(02):257–289
38. Liu GR, Nguyen-Thoi T, Nguyen-Xuan H, Dai KY, Lam KY (2009) On the essence and the evaluation of the shape functions for the smoothed finite element method (SFEM) (Letter to Editor). Int J Numer Methods Eng 77:1863–1869
39. Liu GR, Zhang GY (2009) A normed G space and weakened weak (W2) formulation of a cell-based smoothed point interpolation method. Int J Comput Methods 6(1):147–179
40. Nguyen-Thoi T, Liu GR, Nguyen-Xuan H (2009) Additional properties of the node-based smoothed finite element method (NS-FEM) for solid mechanics problems. Int J Comput Methods 6(4):633–666
41. Nguyen-Thoi T (2009) Development of smoothed finite element method (SFEM). Ph.D. thesis, National University of Singapore
42. Liu GR, Nguyen-Xuan H, Nguyen-Thoi T (2010) A theoretical study on the smoothed FEM (S-FEM) models: properties, accuracy and convergence rates. Int J Numer Methods Eng 84(10):1222–1256
43. Liu GR (2010) A G space theory and a weakened weak (W2) form for a unified formulation of compatible and incompatible methods: part I theory. Int J Numer Methods Eng 81:1093–1126
44. Liu GR (2010) A G space theory and a weakened weak (W2) form for a unified formulation of compatible and incompatible methods: part II applications to solid mechanics problems. Int J Numer Methods Eng 81:1127–1156
45. Liu GR, Nguyen-Thoi T (2010) Smoothed finite element methods. CRC Press, Boca Raton
46. Hung N-X, Bordas SPA, Hung N-D (2008) Smooth finite element methods: convergence, accuracy and properties. Int J Numer Methods Eng 74(2):175–208
47. Hung N-X, Bordas SPA, Hung N-D (2009) Addressing volumetric locking and instabilities by selective integration in smoothed finite elements. Commun Numer Methods Eng 25(1):19–34
48. Bordas SPA, Natarajan S (2010) On the approximation in the smoothed finite element method (SFEM). Int J Numer Methods Eng 81(5):660–670

49. Bordas SPA, Rabczuk T, Hung N-X, Nguyen VP, Natarajan S, Bog T, Quan DM, Hiep NV (2010) Strain smoothing in FEM and XFEM. Comput Struct 88(23–24):1419–1443
50. Nguyen-Xuan H, Nguyen HV, Bordas S, Rabczuk T, Duflot M (2012) A cell-based smoothed finite element method for three dimensional solid structures. KSCE J Civ Eng 16(7):1230–1242
51. Nguyen-Thoi T, Vu-Do HC, Rabczuk T, Nguyen-Xuan H (2010) A node-based smoothed finite element method (NS-FEM) for upper bound solution to visco-elastoplastic analyses of solids using triangular and tetrahedral meshes. Comput Methods Appl Mech Eng 199:3005–3027
52. He ZC, Li GY, Zhong ZH, Cheng AG, Zhang GY, Liu GR, Li E, Zhou Z (2013) An edge-based smoothed tetrahedron finite element method (ES-T-FEM) for 3D static and dynamic problems. Comput Mech 52(1):221–236
53. Nguyen-Thanh N, Rabczuk T, Nguyen-Xuan H, Bordas SPA (2010) An alternative alpha finite element method (AαFEM) for free and forced structural vibration using triangular meshes. J Comput Appl Math 233(9):2112–2135
54. Liu GR, Nguyen-Xuan H, Nguyen-Thoi T (2011) A variationally consistent αFEM (VCαFEM) for solution bounds and nearly exact solution to solid mechanics problems using quadrilateral elements. Int J Numer Methods Eng 85(4):461–497
55. Xiangyang C, Guangyao L, Gang Z, Suzhen W (2010) NS-FEM/ES-FEM for contact problems in metal forming analysis. Int J Mater Form 3(1):887–890
56. Li Y, Liu GR, Zhang GY (2011) An adaptive NS/ES-FEM approach for 2D contact problems using triangular elements. Finite Elem Anal Des 47(3):256–275
57. Xu X, Gu YT, Liu GR (2013) A hybrid smoothed finite element method (H-SFEM) to solid mechanics problems. Int J Comput Methods 10(01):1340011
58. Zhao X, Bordas SPA, Qu J (2013) A hybrid smoothed extended finite element/level set method for modeling equilibrium shapes of nano-inhomogeneities. Comput Mech 52:1417–1428
59. Wu F, Liu GR, Li GY, He ZC (2014) A new hybrid smoothed FEM for static and free vibration analyses of Reissner-Mindlin Plates. Comput Mech 54(3):1–26
60. Cui XY, Chang S, Li GY (2015) A two-step Taylor Galerkin smoothed finite element method for Lagrangian dynamic problem. Int J Comput Methods 12(04):1540004
61. Li E, He ZC, Xu X, Liu GR, Gu YT (2015) A three-dimensional hybrid smoothed finite element method (H-SFEM) for nonlinear solid mechanics problems. Acta Mech 226(12):4223–4245
62. Lee K, Son Y, Im S (2015) Three-dimensional variable-node elements based upon CS-FEM for elastic–plastic analysis. Comput Struct 158:308–332
63. Li Y, Zhang GY, Liu GR, Huang YN, Zong Z (2013) A contact analysis approach based on linear complementarity formulation using smoothed finite element methods. Eng Anal Bound Elem 37(10):1244–1258
64. Cui XY, Li GY (2013) Metal forming analysis using the edge-based smoothed finite element method. Finite Elem Anal Des 63:33–41
65. Zeng W, Larsen JM, Liu GR (2015) Smoothing technique based crystal plasticity finite element modeling of crystalline materials. Int J Plast 65:250–268
66. Nguyen-Xuan H, Rabczuk T, Bordas SPA, Debongnie JF (2008) A smoothed finite element method for plate analysis. Comput Methods Appl Mech Eng 197(2):1184–1203
67. Nguyen-Thanh N, Rabczuk T, Nguyen-Xuan H, Bordas SPA (2008) A smoothed finite element method for shell analysis. Comput Methods Appl Mech Eng 198(2):165–177
68. Nguyen-Xuan H, Nguyen-Thoi T (2009) A stabilized smoothed finite element method for free vibration analysis of Mindlin–Reissner plates. Commun Numer Methods Eng 25(8):882–906
69. Cui XY, Liu GR, Li GY, Zhang GY, Zheng G (2010) Analysis of plates and shells using an edge-based smoothed finite element method. Comput Mech 45:141–156
70. Nguyen-Xuan H, Liu GR, Thai-Hoang C, Nguyen-Thoi T (2010) An edge-based smoothed finite element method (ES-FEM) with stabilized discrete shear gap technique for analysis of Reissner–Mindlin plates. Comput Methods Appl Mech Eng 199:471–489
71. Nguyen-Xuan H, Rabczuk T, Nguyen-Thanh N, Nguyen-Thoi T, Bordas SPA (2010) A node-based smoothed finite element method with stabilized discrete shear gap technique for analysis of Reissner–Mindlin plates. Comput Mech 46(5):679–701
72. Zhang ZQ, Liu GR (2011) An edge-based smoothed finite element method (ES-FEM) using 3-node triangular elements for 3D non-linear analysis of spatial membrane structures. Int J Numer Methods Eng 86(2):135–154
73. Baiz PM, Natarajan S, Bordas SPA, Kerfriden P, Rabczuk T (2011) Linear buckling analysis of cracked plates by SFEM and XFEM. J Mech Mater Struct 6(9–10):1213–1238
74. Nguyen-Thanh N, Rabczuk T, Nguyen-Xuan H, Bordas S (2011) An alternative alpha finite element method with discrete shear gap technique for analysis of isotropic Mindlin–Reissner plates. Finite Elem Anal Des 47(5):519–535
75. Zheng G, Cui X, Li G, Wu S (2011) An edge-based smoothed triangle element for non-linear explicit dynamic analysis of shells. Comput Mech 48(1):65–80
76. Thai-Hoang C, Nguyen-Thanh N, Nguyen-Xuan H, Rabczuk T, Bordas S (2011) A cell-based smoothed finite element method for free vibration and buckling analysis of shells. KSCE J Civ Eng 15(2):347–361
77. Nguyen-Thoi T, Phung-Van P, Nguyen-Xuan H, Thai-Hoang C (2012) A cell-based smoothed discrete shear gap method using triangular elements for static and free vibration analyses of Reissner–Mindlin plates. Int J Numer Methods Eng 91(7):705–741
78. Nguyen-Thoi T, Phung-Van P, Luong-Van H, Nguyen-Van H, Nguyen-Xuan H (2013) A cell-based smoothed three-node Mindlin plate element (CS-MIN3) for static and free vibration analyses of plates. Comput Mech 51(1):65–81
79. Nguyen-Thoi T, Luong-Van H, Phung-Van P, Rabczuk T, Tran-Trung D (2013) Dynamic responses of composite plates on the Pasternak foundation subjected to a moving mass by a cell-based smoothed discrete shear gap (CS-FEM-DSG3) method. Int J Compos Mater 3(A):19–27
80. Nguyen-Thoi T, Phung-Van P, Thai-Hoang C, Nguyen-Xuan H (2013) A cell-based smoothed discrete shear gap method (CS-DSG3) using triangular elements for static and free vibration analyses of shell structures. Int J Mech Sci 74:32–45
81. Nguyen-Thoi T, Bui-Xuan T, Phung-Van P, Nguyen-Xuan H, Ngo-Thanh P (2013) Static, free vibration and buckling analyses of stiffened plates by CS-FEM-DSG3 using triangular elements. Comput Struct 125:100–113
82. Phung-Van P, Nguyen-Thoi T, Le-Dinh T, Nguyen-Xuan H (2013) Static and free vibration analyses and dynamic control of composite plates integrated with piezoelectric sensors and actuators by the cell-based smoothed discrete shear gap method (CS-FEM-DSG3). Smart Mater Struct 22(9):095026
83. Phung-Van P, Nguyen-Thoi T, Tran LV, Nguyen-Xuan H (2013) A cell-based smoothed discrete shear gap method (CS-DSG3) based on the C 0-type higher-order shear deformation theory for static and free vibration analyses of functionally graded plates. Comput Mater Sci 79:857–872
84. Wu CT, Wang HP (2013) An enhanced cell-based smoothed finite element method for the analysis of Reissner–Mindlin plate bending problems involving distorted mesh. Int J Numer Methods Eng 95(4):288–312

85. Luong-Van H, Nguyen-Thoi T, Liu GR, Phung-Van P (2014) A Cell-based smoothed finite element method using mindlin plate element (CS-FEM-MIN3) for dynamic response of composite plates on viscoelastic foundation. Eng Anal Bound Elem 42:8–19
86. Phung-Van P, Nguyen-Thoi T, Luong-Van H, Lieu-Xuan Q (2014) Geometrically nonlinear analysis of functionally graded plates using a cell-based smoothed three-node plate element (CS-MIN3) based on the C 0-HSDT. Comput Methods Appl Mech Eng 270:15–36
87. Phung-Van P, Nguyen-Thoi T, Luong-Van H, Thai-Hoang C, Nguyen-Xuan H (2014) A cell-based smoothed discrete shear gap method (CS-FEM-DSG3) using layerwise deformation theory for dynamic response of composite plates resting on viscoelastic foundation. Comput Methods Appl Mech Eng 272:138–159
88. Phung-Van P, Thai CH, Nguyen-Thoi T, Nguyen-Xuan H (2014) Static and free vibration analyses of composite and sandwich plates by an edge-based smoothed discrete shear gap method (ES-DSG3) using triangular elements based on layer-wise theory. Compos B 60:227–238
89. Nguyen-Thoi T, Bui-Xuan T, Phung-Van P, Nguyen-Hoang S, Nguyen-Xuan H (2014) An edge-based smoothed three-node Mindlin plate element (ES-MIN3) for static and free vibration analyses of plates. KSCE J Civ Eng 18(4):1072–1082
90. Luong-Van H, Nguyen-Thoi T, Liu GR, Phung-Van P (2014) A cell-based smoothed finite element method using three-node shear-locking free Mindlin plate element (CS-FEM-MIN3) for dynamic response of laminated composite plates on viscoelastic foundation. Eng Anal Bound Elem 42:8–19
91. Phung-Van P, Nguyen-Thoi T, Dang-Trung H, Nguyen-Minh N (2014) A cell-based smoothed discrete shear gap method (CS-FEM-DSG3) using layerwise theory based on the C 0-HSDT for analyses of composite plates. Compos Struct 111:553–565
92. Phung-Van P, Luong-Van H, Nguyen-Thoi T, Nguyen-Xuan H (2014) A cell-based smoothed discrete shear gap method (CS-FEM-DSG3) based on the C0-type higher-order shear deformation theory for dynamic responses of Mindlin plates on viscoelastic foundations subjected to a moving sprung vehicle. Int J Numer Methods Eng 98(13):988–1014
93. Nguyen-Thoi T, Rabczuk T, Lam-Phat T, Ho-Huu V, Phung-Van P (2014) Free vibration analysis of cracked Mindlin plate using an extended cell-based smoothed discrete shear gap method (XCS-DSG3). Theor Appl Fract Mech 72:150–163
94. Élie-Dit-Cosaque XJ, Gakwaya A, Naceur H (2015) Smoothed finite element method implemented in a resultant eight-node solid-shell element for geometrical linear analysis. Comput Mech 55(1):105–126
95. Phung-Van P, Nguyen-Thoi T, Bui-Xuan T, Lieu-Xuan Q (2015) A cell-based smoothed three-node Mindlin plate element (CS-FEM-MIN3) based on the C 0-type higher-order shear deformation for geometrically nonlinear analysis of laminated composite plates. Comput Mater Sci 96:549–558
96. Nguyen-Thoi T, Phung-Van P, Nguyen-Thoi MH, Dang-Trung H (2015) An upper-bound limit analysis of Mindlin plates using CS-DSG3 method and second-order cone programming. J Comput Appl Math 281:32–48
97. Nguyen-Thoi T, Nguyen-Thoi MH, Vo-Duy T, Nguyen-Minh N (2015) Development of the cell-based smoothed discrete shear gap plate element (CS-FEM-DSG3) using three-node triangles. Int J Comput Methods 12(04):1540015
98. Le-Anh L, Nguyen-Thoi T, Ho-Huu V, Dang-Trung H, Bui-Xuan T (2015) Static and frequency optimization of folded laminated composite plates using an adjusted differential evolution algorithm and a smoothed triangular plate element. Compos Struct 127:382–394
99. Nguyen-Minh N, Nguyen-Thoi T, Bui-Xuan T, Vo-Duy T (2015) Static and free vibration analyses of stiffened folded plates using a cell-based smoothed discrete shear gap method (CS-FEM-DSG3). Appl Math Comput 266:212–234
100. Nguyen-Thoi MH, Le-Anh L, Ho-Huu V, Dang-Trung H, Nguyen-Thoi T (2015) An extended cell-based smoothed discrete shear gap method (XCS-FEM-DSG3) for free vibration analysis of cracked Reissner–Mindlin shells. Front Struct Civ Eng 9(4):341–358
101. Dang-Trung H, Luong-Van H, Nguyen-Thoi T, Ang KK (2016) Analyses of stiffened plates resting on viscoelastic foundation subjected to a moving load by a cell-based smoothed triangular plate element. Int J Struct Stab Dyn 2016:1750011
102. Ho-Huu V, Do-Thi TD, Dang-Trung H, Vo-Duy T, Nguyen-Thoi T (2016) Optimization of laminated composite plates for maximizing buckling load using improved differential evolution and smoothed finite element method. Compos Struct 146:132–147
103. Nguyen-Thoi T, Rabczuk T, Ho-Huu V, Le-Anh L, Dang-Trung H, Vo-Duy T (2016) An extended cell-based smoothed three-node Mindlin plate element (XCS-MIN3) for free vibration analysis of cracked FGM plates. Int J Comput Methods 2016:1750011
104. Nguyen-Hoang S, Phung-Van P, Natarajan S, Kim HG (2016) A combined scheme of edge-based and node-based smoothed finite element methods for Reissner–Mindlin flat shells. Eng Comput 32(2):267–284
105. Cui XY, Liu GR, Li GY (2011) Bending and vibration responses of laminated composite plates using an edge-based smoothing technique. Eng Anal Bound Elem 35(6):818–826
106. Nguyen-Xuan H, Tran LV, Nguyen-Thoi T, Vu-Do HC (2011) Analysis of functionally graded plates using an edge-based smoothed finite element method. Compos Struct 93(11):3019–3039
107. Thai-Hoang C, Nguyen-Thanh N, Nguyen-Xuan H, Rabczuk T (2011) An alternative alpha finite element method with discrete shear gap technique for analysis of laminated composite plates. Appl Math Comput 217(17):7324–7348
108. Nguyen-Xuan H, Tran LV, Thai CH, Nguyen-Thoi T (2012) Analysis of functionally graded plates by an efficient finite element method with node-based strain smoothing. Thin Wall Struct 54:1–18
109. Hoang CT, Tran VL, Trung DT, Trung NT, Hung NX (2012) Analysis of laminated composite plates using higher-order shear deformation theory and node-based smoothed discrete shear gap method. Appl Math Model 36(11):5657–5677
110. Natarajan S, Ferreira AJM, Bordas SPA, Carrera E, Cinefra M (2013) Analysis of composite plates by a unified formulation-cell based smoothed finite element method and field consistent elements. Compos Struct 105:75–81
111. Phan-Dao HH, Nguyen-Xuan H, Thai-Hoang C, Nguyen-Thoi T, Rabczuk T (2013) An edge-based smoothed finite element method for analysis of laminated composite plates. Int J Comput Methods 10(01):1340005
112. Natarajan S, Ferreira AJM, Bordas S, Carrera E, Cinefra M, Zenkour AM (2014) Analysis of functionally graded material plates using triangular elements with cell-based smoothed discrete shear gap method. Math Probl Eng 2014:247932
113. Rodrigues JD, Natarajan S, Ferreira AJM, Carrera E, Cinefra M, Bordas SPA (2014) Analysis of composite plates through cell-based smoothed finite element and 4-noded mixed interpolation of tensorial components techniques. Comput Struct 135:83–87
114. Herath MT, Natarajan S, Prusty BG, John NS (2014) Smoothed finite element and genetic algorithm based optimization for shape adaptive composite marine propellers. Compos Struct 109:189–197

115. Li E, Zhang Z, Chang CC, Liu GR, Li Q (2015) Numerical homogenization for incompressible materials using selective smoothed finite element method. Compos Struct 123:216–232
116. Tran TN, Liu GR, Nguyen-Xuan H, Nguyen-Thoi T (2010) An edge-based smoothed finite element method for primal-dual shakedown analysis of structures. Int J Numer Methods Eng 82(7):917–938
117. Le CV, Nguyen-Xuan H, Askes H, Bordas S, Rabczuk T, Nguyen-Vinh H (2010) A cell-based smoothed finite element method for kinematic limit analysis. Int J Numer Methods Eng 83(12):1651–1674
118. Nguyen-Xuan H, Rabczuk T, Nguyen-Thoi T, Tran TN, Nguyen-Thanh N (2012) Computation of limit and shakedown loads using a node-based smoothed finite element method. Int J Numer Methods Eng 90(3):287–310
119. Le CV, Nguyen-Xuan H, Askes H, Rabczuk T, Nguyen-Thoi T (2013) Computation of limit load using edge-based smoothed finite element method and second-order cone programming. Int J Comput Methods 10(01):1340004
120. Nguyen-Xuan H, Rabczuk T (2015) Adaptive selective ES-FEM limit analysis of cracked plane-strain structures. Front Struct Civ Eng 9(4):478–490
121. Chen L, Liu GR, Nourbakhsh N, Zeng K (2010) A singular edge-based smoothed finite element method (ES-FEM) for bimaterial interface cracks. Comput Mech 45(2–3):109–125
122. Liu GR, Chen L, Nguyen-Thoi T, Zeng K, Zhang GY (2010) A novel singular node-based smoothed finite element method (NS-FEM) for upper bound solutions of fracture problems. Int J Numer Methods Eng 83(11):1466–1497
123. Liu GR, Nourbakhshnia N, Chen L, Zhang YW (2010) A novel general formulation for singular stress field using the ES-FEM method for the analysis of mixed-mode cracks. Int J Comput Methods 7(01):191–214
124. Liu GR, Nourbakhshnia N, Zhang YW (2011) A novel singular ES-FEM method for simulating singular stress fields near the crack tips for linear fracture problems. Eng Fract Mech 78(6):863–876
125. Nourbakhshnia N, Liu GR (2011) A quasi-static crack growth simulation based on the singular ES-FEM. Int J Numer Methods Eng 88(5):473–492
126. Chen L, Liu GR, Jiang Y, Zeng K, Zhang J (2011) A singular edge-based smoothed finite element method (ES-FEM) for crack analyses in anisotropic media. Eng Fract Mech 78(1):85–109
127. Jiang Y, Liu GR, Zhang YW, Chen L, Tay TE (2011) A singular ES-FEM for plastic fracture mechanics. Comput Methods Appl Mech Eng 200(45):2943–2955
128. Chen L, Liu GR, Zeng K, Zhang J (2011) A novel variable power singular element in G space with strain smoothing for bi-material fracture analyses. Eng Anal Bound Elem 35(12):1303–1317
129. Chen L, Liu GR, Zeng K (2011) A combined extended and edge-based smoothed finite element method (ES-XFEM) for fracture analysis of 2D elasticity. Int J Comput Methods 8(04):773–786
130. Nourbakhshnia N, Liu GR (2012) Fatigue analysis using the singular ES-FEM. Int J Fatigue 40:105–111
131. Nguyen-Xuan H, Liu GR, Nourbakhshnia N, Chen L (2012) A novel singular ES-FEM for crack growth simulation. Eng Fract Mech 84:41–66
132. Liu P, Bui TQ, Zhang C, Yu TT, Liu GR, Golub MV (2012) The singular edge-based smoothed finite element method for stationary dynamic crack problems in 2D elastic solids. Comput Methods Appl Mech Eng 233:68–80
133. Jiang Y, Tay TE, Chen L, Sun XS (2013) An edge-based smoothed XFEM for fracture in composite materials. Int J Fatigue 179(1–2):179–199
134. Nguyen-Xuan H, Liu GR, Bordas S, Natarajan S, Rabczuk T (2013) An adaptive singular ES-FEM for mechanics problems with singular field of arbitrary order. Comput Methods Appl Mech Eng 253:252–273
135. Vu-Bac N, Nguyen-Xuan H, Chen L, Lee CK, Zi G, Zhuang X, Liu GR, Rabczuk T (2013) A phantom-node method with edge-based strain smoothing for linear elastic fracture mechanics. J Appl Math 2013:978026
136. Liu GR, Chen L, Li M (2014) S-FEM for fracture problems, theory, formulation and application. Int J Comput Methods 11(03):1343003
137. Jiki PN, Agber JU (2014) Damage evaluation in gap tubular truss 'K' bridge joints using SFEM. J Constr Steel Res 93:135–142
138. Jiang Y, Tay TE, Chen L, Zhang YW (2015) Extended finite element method coupled with face-based strain smoothing technique for three-dimensional fracture problems. Int J Numer Methods Eng 102(13):1894–1916
139. Zeng W, Liu GR, Jiang C, Dong XW, Chen HD, Bao Y, Jiang Y (2016) An effective fracture analysis method based on the virtual crack closure-integral technique implemented in CS-FEM. Appl Math Model 40(5):3783–3800
140. Chen H, Wang Q, Liu GR, Wang Y, Sun J (2016) Simulation of thermoelastic crack problems using singular edge-based smoothed finite element method. Int J Mech Sci 115:123–134
141. Wu L, Liu P, Shi C, Zhang Z, Bui TQ, Jiao D (2016) Edge-based smoothed extended finite element method for dynamic fracture analysis. Appl Math Model 40(19–20):8564–8579
142. Liu GR, Zeng W, Nguyen-Xuan H (2013) Generalized stochastic cell-based smoothed finite element method (GS_CS-FEM) for solid mechanics. Finite Elem Anal Des 63:51–61
143. Hu XB, Cui XY, Feng H, Li GY (2016) Stochastic analysis using the generalized perturbation stable node-based smoothed finite element method. Eng Anal Bound Elem 70:40–55
144. Zhang ZQ, Liu GR (2010) Temporal stabilization of the node-based smoothed finite element method and solution bound of linear elastostatics and vibration problems. Comput Mech 46(2):229–246
145. Zhang ZQ, Liu GR (2010) Upper and lower bounds for natural frequencies: a property of the smoothed finite element methods. Int J Numer Methods Eng 84(2):149–178
146. Nguyen-Thanh N, Thai-Hoang C, Nguyen-Xuan H, Rabczuk T (2010) A smoothed finite element method for the static and free vibration analysis of shells. J Civ Eng Archit 4(9):34
147. Wang L, Han D, Liu GR, Cui X (2011) Free vibration analysis of double-walled carbon nanotubes using the smoothed finite element method. Int J Comput Methods 8(04):879–890
148. He Z, Li G, Zhong Z, Cheng A, Zhang G, Li E (2013) An improved modal analysis for three-dimensional problems using face-based smoothed finite element method. Acta Mech Solida Sin 26(2):140–150
149. Cui XY, Li GY, Liu GR (2013) An explicit smoothed finite element method (SFEM) for elastic dynamic problems. Int J Comput Methods 10(01):1340002
150. Nguyen-Thoi T, Phung-Van P, Rabczuk T, Nguyen-Xuan H, Le-Van C (2013) Free and forced vibration analysis using the n-sided polygonal cell-based smoothed finite element method (*n*CS-FEM). Int J Comput Methods 10(01):1340008
151. Feng H, Cui XY, Li GY, Feng SZ (2014) A temporal stable node-based smoothed finite element method for three-dimensional elasticity problems. Comput Mech 53(5):859–876
152. Yang G, Hu D, Ma G, Wan D (2016) A novel integration scheme for solution of consistent mass matrix in free and forced vibration analysis. Meccanica 51(8):1897–1911
153. Cui XY, Hu X, Li GY, Liu GR (2016) A modified smoothed finite element method for static and free vibration analysis of

solid mechanics. Int J Comput Methods. doi:10.1142/S0219876216500432
154. He ZC, Liu GR, Zhong ZH, Zhang GY, Cheng AG (2010) Dispersion free analysis of acoustic problems using the alpha finite element method. Comput Mech 46(6):867–881
155. He ZC, Liu GR, Zhong ZH, Zhang GY, Cheng AG (2010) Coupled analysis of 3D structural–acoustic problems using the edge-based smoothed finite element method/finite element method. Finite Elem Anal Des 46(12):1114–1121
156. Yao LY, Yu DJ, Cui XY, Zang XG (2010) Numerical treatment of acoustic problems with the smoothed finite element method. Appl Acoust 71(8):743–753
157. He ZC, Cheng AG, Zhang GY, Zhong ZH, Liu GR (2011) Dispersion error reduction for acoustic problems using the edge-based smoothed finite element method (ES-FEM). Int J Numer Methods Eng 86:1322–1338
158. He ZC, Li GY, Zhong ZH, Cheng AG, Zhang GY, Li E, Liu GR (2012) An ES-FEM for accurate analysis of 3D mid-frequency acoustics using tetrahedron mesh. Comput Struct 106:125–134
159. Li W, Chai Y, Lei M, Liu GR (2014) Analysis of coupled structural-acoustic problems based on the smoothed finite element method (S-FEM). Eng Anal Bound Elem 42:84–91
160. Li E, He ZC, Xu X, Liu GR (2015) Hybrid smoothed finite element method for acoustic problems. Comput Methods Appl Mech Eng 283:664–688
161. He ZC, Li GY, Liu GR, Cheng AG, Li E (2015) Numerical investigation of ES-FEM with various mass re-distribution for acoustic problems. Appl Acoust 89:222–233
162. Wu F, Liu GR, Li GY, Cheng AG, He ZC, Hu ZH (2015) A novel hybrid FS-FEM/SEA for the analysis of vibro-acoustic problems. Int J Numer Methods Eng 102(12):1815–1829
163. He Z, Li G, Zhang G, Liu G, Gu Y, Li E (2015) Acoustic analysis using a mass-redistributed smoothed finite element method with quadrilateral mesh. Eng Comput 32(8):2292–2317
164. He ZC, Li E, Li GY, Wu F, Liu GR, Nie X (2015) Acoustic simulation using α-FEM with a general approach for reducing dispersion error. Eng Anal Bound Elem 61:241–253
165. Wang G, Cui XY, Feng H, Li GY (2015) A stable node-based smoothed finite element method for acoustic problems. Comput Methods Appl Mech Eng 297:348–370
166. Wang G, Cui XY, Liang ZM, Li GY (2015) A coupled smoothed finite element method (S-FEM) for structural-acoustic analysis of shells. Eng Anal Bound Elem 61:207–217
167. Chai Y, Li W, Gong Z, Li T (2016) Hybrid smoothed finite element method for two-dimensional underwater acoustic scattering problems. Ocean Eng 116:129–141
168. Chai Y, Li W, Gong Z, Li T (2016) Hybrid smoothed finite element method for two dimensional acoustic radiation problems. Appl Acoust Part A 103:90–101
169. Wu F, He ZC, Liu GR, Li GY, Cheng AG (2016) A novel hybrid ES-FE-SEA for mid-frequency prediction of transmission losses in complex acoustic systems. Appl Acoust 111:198–204
170. Kumar V, Metha R (2013) Impact simulations using smoothed finite element method. Int J Comput Methods 10(4):1350012
171. Nguyen-Thoi T, Liu GR, Nguyen-Xuan H, Nguyen-Tran C (2011) Adaptive analysis using the node-based smoothed finite element method (NS-FEM). Int J Numer Method Biomed Eng 27(2):198–218
172. Nguyen-Xuan H, Wu CT, Liu GR (2016) An adaptive selective ES-FEM for plastic collapse analysis. Eur J Mech A-Solid 58:278–290
173. Kazemzadeh-Parsi MJ, Daneshmand F (2009) Solution of geometric inverse heat conduction problems by smoothed fixed grid finite element method. Finite Elem Anal Des 45(10):599–611
174. Li E, Liu GR, Tan V (2010) Simulation of hyperthermia treatment using the edge-based smoothed finite-element method. Numer Heat Transf A-Appl 57(11):822–847
175. Li E, Liu GR, Tan V, He ZC (2010) An efficient algorithm for phase change problem in tumor treatment using αFEM. Int J Therm Sci 49(10):1954–1967
176. Kumar V (2013) Smoothed finite element methods for thermo-mechanical impact problems. Int J Comput Methods 10(1):13400100
177. Xue BY, Wu SC, Zhang WH, Liu GR (2013) A smoothed FEM (S-FEM) for heat transfer problems. Int J Comput Methods 10(01):1340001
178. Feng SZ, Cui XY, Li GY (2013) Analysis of transient thermo-elastic problems using edge-based smoothed finite element method. Int J Therm Sci 65:127–135
179. Feng SZ, Cui XY, Li GY, Feng H, Xu FX (2013) Thermo-mechanical analysis of functionally graded cylindrical vessels using edge-based smoothed finite element method. Int J Pres Ves Pip 111:302–309
180. Feng SZ, Cui XY, Li GY (2013) Transient thermal mechanical analyses using a face-based smoothed finite element method (FS-FEM). Int J Therm Sci 74:95–103
181. Li E, He ZC, Xu X (2013) An edge-based smoothed tetrahedron finite element method (ES-T-FEM) for thermomechanical problems. Int J Heat Mass Transf 66:723–732
182. Feng S, Cui X, Li G (2014) Thermo-mechanical analyses of composite structures using face-based smoothed finite element method. Int J Appl Mech 6(02):1450020
183. Li E, Zhang Z, He ZC, Xu X, Liu GR, Li Q (2014) Smoothed finite element method with exact solutions in heat transfer problems. Int J Heat Mass Transf 78:1219–1231
184. Feng S, Cui X, Li G (2014) Thermo-mechanical analysis of composite pressure vessels using edge-based smoothed finite element method. Int J Comput Methods 11(06):1350089
185. Cui XY, Li ZC, Feng H, Feng SZ (2016) Steady and transient heat transfer analysis using a stable node-based smoothed finite element method. Int J Therm Sci 110:12–25
186. Nguyen-Van H, Mai-Duy N, Tran-Cong T (2008) A smoothed four-node piezoelectric element for analysis of two-dimensional smart structures. CMES: Comput Model Eng Sci 23(3):209–222
187. Nguyen-Van H, Mai-Duy N, Tran-Cong T (2008) A node-based element for analysis of planar piezoelectric structures. CMES: Comput Model Eng Sci 36(1):65–95
188. Nguyen-Xuan H, Liu GR, Nguyen-Thoi T, Nguyen-Tran C (2009) An edge-based smoothed finite element method for analysis of two-dimensional piezoelectric structures. Smart Mater Struct 18(6):065015
189. Olyaie MS, Razfar MR, Kansa EJ (2011) Reliability based topology optimization of a linear piezoelectric micromotor using the cell-based smoothed finite element method. CMES: Comput Model Eng Sci 75(1):43–87
190. Olyaie MS, Razfar MR, Wang S, Kansa EJ (2011) Topology optimization of a linear piezoelectric micromotor using the smoothed finite element method. CMES: Comput Model Eng Sci 82(1):55–81
191. Chen L, Zhang YW, Liu GR, Nguyen-Xuan H, Zhang ZQ (2012) A stabilized finite element method for certified solution with bounds in static and frequency analyses of piezoelectric structures. Comput Methods Appl Mech Eng 241:65–81
192. Li E, He ZC, Chen L, Li B, Xu X, Liu GR (2015) An ultra-accurate hybrid smoothed finite element method for piezoelectric problem. Eng Anal Bound Elem 50:188–197
193. Atia KSR, Heikal AM, Obayya SSA (2015) Efficient smoothed finite element time domain analysis for photonic devices. Opt Express 23(17):22199–22213

194. He ZC, Liu GR, Zhong ZH, Zhang GY, Cheng AG (2011) A coupled ES-FEM/BEM method for fluid–structure interaction problems. Eng Anal Bound Elem 35(1):140–147
195. Zhang ZQ, Liu GR, Khoo BC (2012) Immersed smoothed finite element method for two dimensional fluid–structure interaction problems. Int J Numer Methods Eng 90(10):1292–1320
196. Yao J, Liu GR, Narmoneva DA, Hinton RB, Zhang ZQ (2012) Immersed smoothed finite element method for fluid–structure interaction simulation of aortic valves. Comput Mech 50(6):789–804
197. Zhang ZQ, Liu GR, Khoo BC (2013) A three dimensional immersed smoothed finite element method (3D IS-FEM) for fluid–structure interaction problems. Comput Mech 51(2):129–150
198. Nguyen-Thoi T, Phung-Van P, Rabczuk T, Nguyen-Xuan H, Le-Van C (2013) An application of the ES-FEM in solid domain for dynamic analysis of 2D fluid–solid interaction problems. Int J Comput Methods 10(01):1340003
199. Wang S, Khoo BC, Liu GR, Xu GX, Chen L (2014) Coupling GSM/ALE with ES-FEM-T3 for fluid–deformable structure interactions. J Comput Phys 276:315–340
200. Nguyen-Thoi T, Phung-Van P, Nguyen-Hoang S, Lieu-Xuan Q (2014) A smoothed coupled NS/*n*ES-FEM for dynamic analysis of 2D fluid–solid interaction problems. Appl Math Comput 232:324–346
201. Nguyen-Thoi T, Phung-Van P, Nguyen-Hoang S, Lieu-Xuan Q (2014) A coupled alpha-FEM for dynamic analyses of 2D fluid–solid interaction problems. J Comput Appl Math 271:130–149
202. He T (2015) On a partitioned strong coupling algorithm for modeling fluid–structure interaction. Int J Appl Mech 7(2):1550021
203. He T (2015) Semi-implicit coupling of CS-FEM and FEM for the interaction between a geometrically nonlinear solid and an incompressible fluid. Int J Comput Methods 12(5):1550025
204. Zhang ZQ, Liu GR (2014) Solution bound and nearly exact solution to nonlinear solid mechanics problems based on the smoothed FEM concept. Eng Anal Bound Elem 42:99–114
205. Jiang C, Zhang ZQ, Han X, Liu GR (2014) Selective smoothed finite element methods for extremely large deformation of anisotropic incompressible bio-tissues. Int J Numer Methods Eng 99(8):587–610
206. Onishi Y, Amaya K (2014) A locking-free selective smoothed finite element method using tetrahedral and triangular elements with adaptive mesh rezoning for large deformation problems. Int J Numer Methods Eng 99(5):354–371
207. Jiang C, Liu GR, Han X, Zhang ZQ, Zeng W (2015) A smoothed finite element method for analysis of anisotropic large deformation of passive rabbit ventricles in diastole. Int J Numer Method Biomed Eng 31(1):1–25
208. Onishi Y, Iida R, Amaya K (2016) F-bar aided edge-based smoothed finite element method using tetrahedral elements for finite deformation analysis of nearly incompressible solids. Int J Numer Methods Eng. doi:10.1002/nme.5337
209. Li E, Chen J, Zhang Z, Fang J, Liu GR, Li Q (2016) Smoothed finite element method for analysis of multi-layered systems—applications in biomaterials. Comput Struct 168:16–29
210. Li E, Liao WH (2016) An efficient finite element algorithm in elastography. Int J Appl Mech 8(3):1650037
211. de Souza Neto EA, Pires FMA, Owen DRJ (2005) F-bar-based linear triangles and tetrahedra for finite strain analysis of nearly incompressible solids. Part I: formulation and benchmarking. Int J Numer Methods Eng 62(3):353–383
212. Natarajan S, Bordas S, Ooi ET (2015) Virtual and smoothed finite elements: A connection and its application to polygonal/polyhedral finite element methods. Int J Numer Methods Eng 104(13):1173–1199
213. Sohn D, Jin S (2015) Polyhedral elements with strain smoothing for coupling hexahedral meshes at arbitrary nonmatching interfaces. Comput Methods Appl Mech Eng 293:92–113
214. Francis A, Ortiz-Bernardin A, Bordas S, Natarajan S (2016) Linear smoothed polygonal and polyhedral finite elements. Int J Numer Methods. doi:10.1002/nme.5324
215. Nguyen-Thoi T, Liu GR, Nguyen-Xuan H (2011) An n-sided polygonal edge-based smoothed finite element method (nES-FEM) for solid mechanics. Int J Numer Method Biomed Eng 27(9):1446–1472
216. Wang S (2014) An ABAQUS implementation of the cell-based smoothed finite element method using quadrilateral elements. Master thesis, University of Cincinnati
217. Bordas S, Natarajan S, Kerfriden P, Augarde CE, Mahapatra DR, Rabczuk T, Pont SD (2011) On the performance of strain smoothing for quadratic and enriched finite element approximations (XFEM/GFEM/PUFEM). Int J Numer Methods Eng 86:637–666
218. Ong TH, Heaney CE, Lee CK, Liu GR, Nguyen-Xuan H (2015) On stability, convergence and accuracy of bES-FEM and bFS-FEM for nearly incompressible elasticity. Comput Methods Appl Mech Eng 285:315–345
219. Wu CT, Hu W, Liu GR (2014) Bubble-enhanced smoothed finite element formulation: a variational multi-scale approach for volume-constrained problems in two-dimensional linear elasticity. Int J Numer Methods Eng 100(5):374–398
220. Leonetti L, Garcea G, Nguyen-Xuan H (2016) A mixed edge-based smoothed finite element method (MES-FEM) for elasticity. Comput Struct 173:123–138
221. Liu GR, Zhang GY, Dai KY, Wang YY, Zhong ZH, Li GY, Han X (2005) A linearly conforming point interpolation method (LC-PIM) for 2D solid mechanics problems. Int J Comput Methods 2(4):645–665
222. Zhang GY, Liu GR, Wang YY, Huang HT, Zhong ZH, Li GY, Han X (2007) A linearly conforming point interpolation method (LC-PIM) for three-dimensional elasticity problems. Int J Numer Methods Eng 72:1524–1543
223. Liu GR, Zhang GY (2008) Upper bound solution to elasticity problems: a unique property of the linearly conforming point interpolation method (LC-PIM). Int J Numer Methods Eng 74(7):1128–1161
224. Liu GR, Li Y, Dai KY, Luan MT, Xue W (2006) A linearly conforming radial point interpolation method for solid mechanics problems. Int J Comput Methods 3(4):401–428
225. Duong MT (2014) Hyperelastic modeling and soft-tissue growth integrated with the smoothed finite element method—SFEM. Ph.D. thesis, RWTH Aachen University
226. Duong MT, Nguyen-Nhu H, Staat M (2015) Modeling and simulation of a growing mass by the smoothed finite element method (SFEM). In: 3rd ECCOMAS Young Investigators Conference. July 20–23, Aachen, Germany
227. Zeng W, Liu GR, Jiang C, Nguyen-Thoi T, Jiang Y (2016) A generalized beta finite element method with coupled smoothing techniques for solid mechanics. Eng Anal Bound Elem 73:103–119
228. Liu GR (2016) On partitions of unity property of nodal shape functions: rigid-body-movement reproduction and mass conservation. Int J Comput Methods 13(02):1640003
229. Yue JH, Li M, Liu GR, Niu RP (2016) Proofs of the stability and convergence of a weakened weak method using PIM shape functions. Comput Math Appl 72(4):933–951
230. Liu GR, Zhang GY, Wang YY, Zhong ZH, Li GY, Han X (2007) A nodal integration technique for meshfree radial point interpolation method (NI-RPCM). Int J Solids Struct 44:3840–3860

231. Chakrabarty J (2006) Theory of plasticity. Butterworth-Heinemann, Burlington
232. Holzapfel G (2000) Nonlinear solid mechanics: a continuum approach for engineering. Wiley, New York
233. de Souza Neto EA, Peric D, Owen DRJ (2008) Computational methods for plasticity: theory and applications. Wiley, Hoboken
234. Belytschko T, Krongauz Y, Organ D, Fleming M, Krysl P (1996) Meshless methods: an overview and recent developments. Comput Methods Appl Mech Eng 139(1–4):3–47
235. Liu GR, Liu MB (2003) Smoothed particle hydrodynamics: a meshfree particle method. World Scientific, Singapore
236. Barth T, Ohlberger M (2004) Finite volume methods: foundation and analysis. In: Stein E, de Borst R, Hughes TJR (eds) Fundamentals, encyclopedia of computational mechanics, vol 1. Wiley, New York
237. Onate E, Idelsohn SR, Del Pin F, Aubry R (2004) The particle finite element method. An overview. Int J Comput Methods 1(2):267–307
238. Liu MB, Liu GR (2010) Smoothed particle hydrodynamics (SPH): an overview and recent developments. Arch Comput Methods Eng 17(1):25–76
239. Liu MB, Liu GR, Zhou LW, Chang JZ (2015) Dissipative particle dynamics (DPD): an overview and recent developments. Arch Comput Methods Eng 17(1):25–76
240. Liu J, Zhang ZQ, Zhang GY (2015) A smoothed finite element method (S-FEM) for large-deformation elastoplastic analysis. Int J Comput Methods 12(4):1–26
241. Bordas S, Nguyen-Dang H, Phan-Phuong Q, Nguyen-Xuan H, Natarajan S, Duflot M (2009) Smoothed finite element method for two-dimensional elastoplasticity. Vietnam J Mech VAST 31(3–4):293–312
242. Carstensen C, Klose R (2002) Elastoviscoplastic finite element analysis in 100 lines of matlab. J Numer Math 10:157–192
243. Suri M (1996) Analytic and computational assessment of locking in the hp finite element method. Comput Methods Appl Mech Eng 133:347–371
244. Zienkiewicz OC, Lefebvre D (1988) A robust triangular plate bending element of Reissner–Mindlin type. Int J Numer Methods Eng 26:1169–1184
245. Pian THH, Chen D-P, Kang D (1983) A new formulation of hybrid/mixed finite element. Comput Struct 16(1–4):81–87
246. Hughes TJR, Tezduyar T (1981) Finite elements based upon Mindlin plate theory with particular reference to the four-node isoparametric element. J Appl Mech 48(3):587–596
247. Bathe KJ, Dvorkin EN (1985) A four-node plate bending element based on Mindlin/Reissner plate theory and a mixed interpolation. Int J Numer Methods Eng 21:367–383
248. Bathe KJ, Dvorkin EN (1986) A formulation of general shell elements. The use of mixed interpolation of tensorial components. Int J Numer Methods Eng 22(3):697–722
249. Simo JC, Rifai MS (1990) A class of mixed assumed strain methods and the method of incompatible modes. Int J Numer Methods Eng 29(8):1595–1638
250. César de Sá JMA, Natal Jorge RM, Fontes Valente RA, Almeida Areias PM (2002) Development of shear locking-free shell elements using an enhanced assumed strain formulation. Int J Numer Methods Eng 53:1721–1750
251. Bletzinger K, Bischoff M, Ramm E (2000) A unified approach for shearlocking-free triangular and rectangular shell finite elements. Comput Struct 75:321–334
252. Zienkiewicz OC, Taylor RL, Too JM (1971) Reduced integration technique in general analysis of plates and shells. Int J Numer Methods Eng 3:275–290
253. Hughes TJR, Taylor RL, Kanoknukulchai W (1977) Simple and efficient element for plate bending. Int J Numer Methods Eng 11:1529–1543
254. Hughes TJR, Cohen M, Haroun M (1978) Reduced and selective integration techniques in finite element analysis of plates. Nucl Eng Des 46:203–222
255. Tran LV, Nguyen-Thoi T, Thai CH, Nguyen-Xuan H (2015) An edge-based smoothed discrete shear gap method using the C0-type higher-order shear deformation theory for analysis of laminated composite plates. Mech Adv Mater Struc 22(4):248–268
256. Li E, Zhang Z, Chang CC, Zhou S, Liu GR, Li Q (2015) A new homogenization formulation for multifunctional composites. Int J Comput Methods 13(2):1640002
257. Ihlenburg F, Babuška I (1995) Dispersion analysis and error estimation of Galerkin finite element methods for the Helmholtz equation. Int J Numer Methods Eng 38:3745–3774
258. Deraemaeker A, Babuška I, Bouillard P (1999) Dispersion and pollution of the FEM solution for the Helmholtz equation in one, two and three dimensions. Int J Numer Methods Eng 46:471–499
259. Harari I, Hughes TJR (1992) Galerkin/least-squares finite element methods for the reduced wave equation with nonreflecting boundary conditions in unbounded domains. Comput Methods Appl Mech Eng 98(3):411–454
260. Thompson LL, Pinsky PM (1995) A Galerkin least-squares finite element method for the two-dimensional Helmholtz equation. Int J Numer Methods Eng 38:371–397
261. Babuška I, Ihlenburg F, Paik ET, Sauter SA (1995) A generalized finite element method for solving the Helmholtz equation in two dimensions with minimal pollution. Comput Methods Appl Mech Eng 128(3–4):325–359
262. Melenk JM, Babuška I (1996) The partition of unity finite element method: basic theory and applications. Comput Methods Appl Mech Eng 139(1–4):289–314
263. Chadwick EA, Bettess P (1997) Modelling of progressive short waves using wave envelopes. Int J Numer Methods Eng 40:3229–3246
264. Franca L, Farhat C, Macedo A, Lessoine M (1997) Residual-free bubbles for the Helmholtz equation. Int J Numer Methods Eng 40:4003–4009
265. Cessenat O, Despres B (1998) Application of an ultra weak variational formulation of elliptic PDES to the two-dimensional Helmholtz problem. SIAM J Numer Anal 35(1):255–299
266. Bouillard P, Suleau S (1998) Element-free Galerkin solutions for Helmholtz problems: formulation and numerical assessment of the pollution effect. Comput Methods Appl Mech Eng 162(1):317–335
267. Farhat C, Harari I, Franca LP (2001) The discontinuous enrichment method. Comput Methods Appl Mech Eng 190:6455–6479
268. Dey S, Datta DK, Shirron JJ, Shephard MS (2006) P-version FEM for structural acoustics with a posteriori error estimation. Comput Methods Appl Mech Eng 195:1946–1957
269. Petersen S, Dreyer D, Ov Estorff (2006) Assessment of finite and spectral element shape functions or efficient iterative simulations of interior acoustics. Comput Method Appl Mech Eng 195:6463–6478
270. Kireeva O, Mertens T, Bouillard Ph (2006) A coupled EFGM–CIE method for acoustic radiation. Comput Struct 84(29–30):2092–2099
271. Yao L, Li Y, Li L (2015) Dispersion error reduction for acoustic problems using the smoothed finite element method (SFEM). Int J Numer Methods Fluids 80:343–357
272. Li E, He ZC, Zhang Z, Liu GR, Li Q (2016) Stability analysis of generalized mass formulation in dynamic heat transfer. Numer Heat Transf B-Fund 69(4):287–311
273. Sigrist JF (2015) Fluid-structure interaction: an introduction to finite element coupling. Wiley, West Sussex

274. Nguyen-Thoi T, Phung-Van P, Ho-Huu V, Le-Anh L (2015) An edge-based smoothed finite element method (ES-FEM) for dynamic analysis of 2D fluid–solid interaction problems. KSCE J Civ Eng 19(3):641–650
275. Zeng W (2015) Advanced development of smoothed finite element method (S-FEM) and its applications. Ph.D. thesis, University of Cincinnati
276. Jiang Y (2013) Smoothed methods for fracture problems and application to composite materials. Ph.D. thesis, National University of Singapore
277. Nourbakhshnia N (2012) A new singular S-FEM for the linear elastic fracture mechanics. Ph.D. thesis, National University of Singapore